ISTANBUL TECHNICAL UNIVERSITY ★ GRADUATE SCHOOL

CORROSION AND CORROSION PROTECTION PROPERTIES OF BINARY Fe-Al ALLOYS-INTERMETALLICS

M.Sc. THESIS

Burcu EROĞLU

Department of Metallurgical and Materials Engineering

Materials Engineering Programme

FEBRUARY 2021

ISTANBUL TECHNICAL UNIVERSITY ★ GRADUATE SCHOOL

CORROSION AND CORROSION PROTECTION PROPERTIES OF BINARY Fe-Al ALLOYS-INTERMETALLICS

M.Sc. THESIS

Burcu EROĞLU
(506181409)

Department of Metallurgical and Materials Engineering

Materials Engineering Programme

Thesis Advisor: Prof. Dr. Mustafa Kamil ÜRGEN

FEBRUARY 2021

İSTANBUL TEKNİK ÜNİVERSİTESİ ★ LİSANSÜSTÜ EĞİTİM ENSTİTÜSÜ

İKİLİ Fe-Al ALAŞIMLARININ- İNTERMETALİKLERİNİN KOROZYON VE KOROZYONDAN KORUMA ÖZELLİKLERİ

YÜKSEK LİSANS TEZİ

Burcu EROĞLU
(506181409)

Metalurji ve Malzeme Mühendisliği Anabilim Dalı

Malzeme Mühendisliği Programı

Tez Danışmanı: Prof. Dr. Mustafa Kamil ÜRGEN

ŞUBAT 2021

Burcu EROĞLU, a M.Sc. student of İTU Graduate School student ID 506181409, successfully defended the thesis entitled "CORROSION AND CORROSION PROTECTION PROPERTIES OF BINARY Fe-Al ALLOYS-INTERMETALLICS", which she prepared after fulfilling the requirements specified in the associated legislations, before the jury whose signatures are below.

Thesis Advisor :	**Prof. Dr. Mustafa Kamil ÜRGEN** Istanbul Technical University	.....
Jury Members :	**Prof. Dr. M. Kürşat KAZMANLI** Istanbul Technical University	.....
	Asst. Prof. Dr. Fatma BAYATA Istanbul Bilgi University	.....

Date of Submission : 25 January 2021
Date of Defense : 10 February 2021

To my lovely Limon,

FOREWORD

Firstly, I would like to express my sincere gratitude to my supervisor Prof. Dr. Mustafa Kamil ÜRGEN, for his invaluable support, encouragement, inspiration and for sharing his immense knowledge during my M.Sc. study.

I am also thankful to the rest of my M.Sc. thesis committee members, Prof. Dr. Muhammet Kürşat KAZMANLI and Asst. Prof. Dr. Fatma BAYATA for their interest and support.

I express my gratitude to Erkan KAÇAR, who helped me in each theoretical and practical stages of my M.Sc. study, for never ceasing to believe me, and for being there for me with his everlasting vivacious.

I am also grateful to Çağatay YELKARASI and Burçak AVCI for their valuable contributions to my thesis study.

I am indebted to my family, mother, father, and sister for their trust in me, material and spiritual support throughout my M.Sc. study, and for being there for me along with my life.

February 2021

Burcu EROĞLU
(Metallurgical and Material Engineer)

TABLE OF CONTENTS

Page

ABBREVIATIONS

SEM	**:** Scanning Electron Microscopy
EDS	**:** Energy Dispersive Spectroscopy
BSEi	**:** Back Scattered Electron Image
SEi	**:** Seconder Electron Image
XRD	**:** X-Ray Diffraction
CVD	**:** Chemical Vapor Deposition
PVD	**:** Physical Vapor Depositon
CA-PVD	**:** Cathodic Arc Physical Vapor Deposition
CA-EMIT	**:** Cathodic Arc Electron Metal Ion Treatment
FCC	**:** Face Centered Cubic
BCC	**:** Body Centered Cubic
IF-Steel	**:** Interstitial Free Steel
DC	**:** Direct Current
AC	**:** Alternative Current
Vrms	**:** Root Mean Square Voltage

SYMBOLS

at.%	**:** Atomic Percent
wt.%	**:** Weight Percent
M	**:** Molarity
N	**:** Normality
ρ	**:** Density
Tc	**:** Cruie Temperature
α-Fe(Al)	**:** Disordered Solid solution
γ-Fe(Al)	**:** Disordered Solid solution
A2	**:** Strukturbericht symbol of Disordered Solid Solution (α-Fe(Al))
B2	**:** Strukturbericht symbol of Ordered Solid Solution (FeAl)
$D0_3$	**:** Strukturbericht symbol of Ordered Solid Solution (Fe_3Al)
E_{corr}	**:** Corrosion Potential
E_{pp}	**:** Primary Passivation Potential
E_{cp}	**:** Complete Passivation Potential
E_b	**:** Breakdown Potential
i_{corr}	**:** Corrosion Current Density
i_{crit}	**:** Critical Current Density
i_p	**:** Passive Current Density
i_o	**:** Exchange Current Density

LIST OF TABLES

Page

LIST OF FIGURES

Page

CORROSION AND CORROSION PROTECTION PROPERTIES OF BINARY Fe-Al ALLOYS-INTERMETALLICS

SUMMARY

It is well known that corrosion and corrosion protection properties of Fe-rich iron aluminides and Al-rich intermetallics which are the major constituents of aluminized steel, depend on the phases formed on the substrate, the sequences of the phases, the nature of the hostile environment and the extent of damage on the surface. This study aims to investigate the corrosion resistance and simultaneous corrosion protection properties of binary Fe-Al compounds that constitute the aluminized layer. For this purpose, both Fe-rich and Al-rich Fe-Al phases, produced by the CA-EMIT process, were used to determine their electrochemical corrosion behaviors in both acidic (0.5M H_2SO_4) and chloride (200ppm Cl^- with pH4 adjusted by H_2SO_4) containing media. Electrochemical experiments were performed, as Open Circuit Potential (OCP) and Potentiodynamic Polarization measurements. Considered the electrochemical corrosion potential of each phase, a galvanic series was created in chloride-containing media. To be examined the reliability of the galvanic series in terms of corrosion protection provided, galvanic pairs were created by forming cracks on the surface of samples. These samples treated such that the relevant phase was exposed to the media while the IF-steel remained the substrate exposed through cracks. Aluminizing was realized on IF-steel substrates with selected temperatures by varying the AC substrate voltages in a cathodic arc physical deposition unit. Treated surfaces were tested using electrochemical potentiodynamic polarization experiments in both sulfuric acid and chloride containing media. The samples surfaces were examined by X-Ray Diffractometer (XRD), Scanning Electron Microscopy (SEM), Electron Dispersive Spectroscopy (EDS) and Optical profilometer. Accordingly, Al-rich phases (Fe_2Al_5-Fe_4Al_{13}, Fe_2Al_5) and Fe-rich phases (Fe_3Al-FeAl) were formed on the substrates at the processing temperature of 1100, 1150, and 1200^oC, respectively. In 0.5M H_2SO_4, Fe-rich phases produced by the CA-EMIT method exhibited corrosion resistance similar to Fe-rich bulk iron aluminides in terms of improved passivation behavior in the presence of Al in the alloy. The increasing Al contents of the layers improved passivation behavior. Some cracks that occurred during electrochemical experiments in 0.5M H_2SO_4 were interpreted as an indication of their susceptibility to environmentally induced cracking. In the simulated acid rain environment (200ppm Cl^- adjusted pH 4 by H_2SO_4), a galvanic series was created in the nobility order: Fe_3Al-FeAl>IF-steel>Fe_2Al_5-Fe_4Al_{13}>Fe_2Al_5. The Al-rich intermetallic layers provided, to IF-steel substrate, both barrier corrosion protection by exhibiting passive behavior up to breakdown potential and cathodic protection by sacrificing themselves in the event of cracks. On the other hand, the Fe-rich intermetallic layer with the lack of passivation failed to act as a protective barrier, and in the presence of paths that allows electrolytic conduct between the substrate, it may create a problem of accelerating the corrosion of steel with galvanic action.

İKİLİ Fe-Al ALAŞIMLARININ-İNTERMETALİKLERİNİN KOROZYON VE KOROZYONDAN KORUMA ÖZELLİKLERİ

ÖZET

Demirce zengin Fe-Al alaşım grubu (demir alüminitler), ticari ve yaygın kullanımda önemli bir başarıya sahip olmayan ancak en çok araştırılan alaşım gruplarından biridir. Bu alaşımlara olan ilgi, alaşımların yer kabuğunda en çok bulunan iki metalden meydana gelmeleri sayesinde kolay ulaşılabilirlikleri ve maliyetleri; paslanmaz çelik ve nikel esaslı alaşımlara alternatif olmaları; ikili sistemde iki düzenli yapının ($D0_3$ and B2) bulunması; ve özellikle kükürt içeren yüksek sıcaklıktaki atmosferlere karşı gösterdikleri yüksek sıcaklık korozyon direncinden kaynaklanmaktadır. Demir alüminitlerle ilgili çalışmalar, 1930'larda Oak Ridge Ulusal Laboratuvarı'nda (ORNL), bu alaşımların mükemmel yüksek sıcaklık oksidasyon dirençlerinin keşfinden sonra ilerletildi. Ancak alaşımların zayıf mekanik özellikleri, 1960'larda bu çalışmaların durdurulmasına neden oldu. 1980'lerde, alaşımlama veya üretim yöntemlerinde modifikasyonlar yoluyla mekanik özellikleri iyileştirme çabalarıyla yeniden başlatılan çalışmlar, 2000 yılında, oda sıcaklığında zayıf süneklik/tokluk, paslanmaz çeliklere kıyasla zayıf sulu ortam korozyon direnci, ve özellikle klorür iyonları içeren ortamlarda hidrojen gevrekliği sorunlarının üstesinden gelinemediği için terk edildi. Bugün, özellikle Avrupa'da bu sorunların aşılması için çabalar (alaşımlama ve tane boyutu küçültme ile) devam etmektedir. Bu geliştirilmiş alaşımlar ticari olarak kitlesel formda, kömür gazlaştırma sistemleri, yüksek güçlü dizel motorları, türbin kanatları ve nükleer reaktörlerde ısı yüklü parçalarda kullanılmaktadırlar.

Kitlesel olarak üretilen Fe-Al alaşımları, çeşitli altlıklar üzerine kaplama olarak da üretilmektedirler. Demir alüminitlerin kaplama olarak üretimi doğrudan kaplama veya difüzyon ile mümkündür. Fiziksel buhar biriktirme (PVD), termal sıçratma, ticari doğrudan üretim yöntemlerindendir. Fe-Al alaşımlarının Fe esaslı malzemeler üzerine kaplanmasında en yaygın kullanılan yöntem, alüminyumlama olarak bilinen difüzyon esaslı işlemdir. Paket sementasyonu, sıcak daldırma, kimyasal buhar biriktirme (CVD) ve çamur füzyonu, ticarileştirilmiş çeşitli difüzyon esaslı kaplama yöntemleridir. Yakın zamanda geliştirilen katodik ark plazma destekli difüzyon yöntemi (Katodik Ark Electron/Metal İyon İşlemi-CA-EMIT), araştırma grubumuzda çeliklerin kontrollü alüminyumlanmasında başarılı bir şekilde uygulanmıştır. Bu yöntemde, altlığa uygulanan çevrimsel AC hızlandırma gerilimi sayesinde, kaplama ve ısıtma işlemleri aynı anda uygulanır. Bu sayede, altlığın üzerinde istenilen kalınlık ve sırada, hem demirce hem de alüminyumca zengin fazların geniş bir bileşim aralığında elde edilmesi sağlanır.

Kitlesel ve kaplama demir alüminitlerin literatürde var olan yüksek sıcaklık korozyon özelliklerinin yanı sıra, genişleyen kullanım alanları ile beraber yaş (elektrokimyasal) korozyon davranışlarının anlaşılması gerekliliği ortaya çıkmıştır. Kitlesel demir alüminitlerin elektrokimyasal korozyon davranışları üzerine yapıla çalışmlar, içerdiği alüminyum miktarı %40 Al' a (aksi söylenmedikçe atomik oran kabul edilecektir) kadar olan demirce zengin fazlar üzerine yoğunlaşmış ve çoğunlukla sülfürik asit

ortamında gerçekleştirilmiştir. Bileşen elementlerin, alaşımın elektrokimyasal davranışı üzerindeki etkisini incelemek amacıyla çeşitli çalışmlar yapılmıştır. Bu kapsamda yapılan çalışmalarda demirin alüminyum ile alaşımlanması, sülfürik asit ortamında, alaşımın pasifleşme özelliğini iyileştirmektedir. Pasifleşme davranışındaki bu iyileşme, artan alüminyum içeriği ile daha da gelişmektedir. Yüzeyde koruyucu pasif film tabakasının oluşumunu desteklemek için Al içeriğinin %10' u, uygun korozyon direncini kazandırmak için %19' u aşması gerekmektedir. Ancak %19 sınırına ulaşıldıktan sonra artan Al içeriği korozyon davranışında %19 Al içeriğine kıyasla belirgin bir gelişme sağlamamaktadır. Demir alümintlerin aktif korozyon bölgesinde sergiledikleri elektrokimyasal davranışları üzerine yapılan çalışmlara göre, aktif korozyon hızı demirin yüzeyden çözeltiye çözünmesi tarafından yönetilir. Pasif bölgede sergilenen davranış için önerilen mekanizmalar farklı olsa da ortak kanı, tam pasifleşmenin hem demir oksit/hidroksitlerin hem de alüminyum oksit/hidroksitlerin birlikte var olması ile gerçekleştiği yönündedir. Alaşım elementlerinin demir alümintlerin elektrokimyasal davranışı üzerine etkisine ilişkin çalışmalara göre, alaşıma C eklenmesi sonucu oluşacak karbür fazlarının etrafının seçici çözünmesi alaşımın korozyon direncinde gerilemeye neden olur. Demirce zengin demir alüminitlerin klorür içeren ortamlardaki elektrokimyasal davranışları üzerine yapılan sınırlı sayıdaki çalışmalarda, alaşıma Mo ve Cr eklenmesi sonucu oluşan, koruyucu Al_2O_3 filmini destekler nitelikte olan Cr_2O_3/MoO_3 filmleri, daha pozitif kırılma potansiyeline dolayısıyla daha iyi korozyon direncine imkan verirler.

Demirce zengin demir alüminidlerin aksine alüminize çeliğin ana bileşenleri olan alüminyumca zengin intermetaliklerin yaş korozyon davranışına ilişkin çalışmalar sınırlıdır. Çeliği elektrokimyasal bozulmadan korumak için uygulanan yüzey kaplamalarının bir sonucu olan alüminize çeliğin sıcak damgalama, pişirme kazanları gibi uygulamalarda mükemmel yüksek sıcaklık oksidasyon direnci sergilemesi, alüminize çeliklerin yaş korozyona karşı performanslarını ele almayı da gerektirir. Bu kapsamda yapılan çalışmlarda, alüminize çeliğin korozyon davranışı; altlığa sağlanan bariyer koruması ve altlık-kaplama arayüzeyine elektrolitin nüfuz etmesine sebep olan bir hasarın varlığında sağlanan katotik koruma olmak üzere iki bakımdan incelenmiştir. Yapılan çalışmalar, atmosferik ortamı temsil etmek için genellikle Cl^- içeren ortamlarda gerçekleştirilmiştir. Şimdiye kadar yapılan çalışmalarda, alüminize çeliklerin elektrokimyasal korozyon davranışlarını, dış yüzeyde oluşan saf Al tabakası ve altındaki alüminyumca zengin fazların davranışı belirler. Yüzeydeki saf Al tabakası sağlam olduğu sürece korozyon davranışı bu tabaka tarafından belirlenir. Ancak bu katmanın hasara uğraması durumunda, yüzeydeki saf alüminyum tabakasının altındaki tabakaların niteliği ve bunların aralarındaki etkileşim önem kazanır.

Genel olarak alüminize çeliğin korozyon ve korozyondan koruma özellikleri, altlığın üzerinde oluşan fazlara, bu fazların sırasına, korozif ortama, ve yüzeyde meydana gelen hasarın boyutuna bağlıdır. Ancak demirce zengin ve yüzeyinde saf Al katmanı bulundurmayan alüminyumca zengin fazların korozyondan korunma davranışları hakkında doğrudan tahminde bulunmak mümkün değildir.

Bu çalışmada, alüminize tabakayı oluşturan, hem demirce hem de alüminyumca zengin fazların korozyon ve eş zamanlı korozyondan koruma özelliklerinin incelenmesi amaçlanmıştır. Bu amaç doğrultusunda, CA-EMIT yöntemi ile üretilen demirce ve alüminyumca zengin Fe-Al fazları, elektrokimyasal korozyon davranışlarının incelenebilmesi için hem asidik (0.5M H_2SO_4) hem de asit yağmurunu temsil etmek için klorür içeren ortamlarda (200ppm Cl^-) elektrokimyasal deneye tabi tutulmuştur.

Alüminyumlama işlemi, sıcaklığını ayarlamak için AC hızlandırma voltajı uygulanan IF-çeliği üzerine, Ar ortamında gerçekleştirilmiştir. İşlem süresince katot akımı sabit (90A) tutulmuştur. İşlem gören numuneler, açık devre potansiyelleri ölçüldükten sonra elektrokimyasal potansiyodinamik polarizasyon deneyine tabi tutulmuştur. Deney öncesinde ve sonrasında nihai yüzeylerin mikroyapıları, taramalı elektron mikroskopu (SEM) ile incelenmiş, X-ışını difraksiyonu (XRD), enerji dağılımlı X-ışını spektroskopisi (EDS) analizleri yapılmış ve optik profilometrede üç boyutlu görüntüleri alınmıştır. Altlığa ulaşan olası bir hasar varlığında sergilenecek olan elektrokimyasal korozyon ve korozyondan koruma davranışını incelemek amacıyla klorür içeren ortamdaki korozyon potansiyellerine göre bir galvanik seride sıralanan numunlerin yüzeylerinde altlığa ulaşacak çatlaklar oluşturulmuş ve elektrokimyasal deneyler tekrarlanmıştır.

Buna göre, işlem sıcaklığının 1100 ve 1150^{o}C' de 90 dakika boyunca tutulduğu numunelerin yüzeyinde alüminyumca zengin fazlar (sırasıyla Fe_2Al_5-Fe_4Al_{13} ve Fe_2Al_5) oluşurken, 1200^{o}C' de 30 dakilada alüminyumca zengin fazların kararlı olduğu sıcaklığın üzerine çıkıldığı için demirce zengin fazlar (Fe_3Al-FeAl) oluşmuştur. Sıcaklığın 1100 ^{o}C'de tutulduğu işlemde, yüzeyden altlığa doğru sırasıyla Fe_2Al_5-Fe_4Al_{13}, Fe_2Al_5+$FeAl_2$, $FeAl_2$+FeAl, Fe_3Al+FeAl, Fe_3Al+α-Fe(Al), α-Fe(Al) fazları oluşmuştur. Sıcaklığın 1150^{o}C'de tutulduğu işlemde bu sıralama: Fe_2Al_5, Fe_2Al_5+$FeAl_2$, Fe_3Al+FeAl, Fe_3Al+α-Fe(Al), α-Fe(Al) olmuştur. Sıcaklığın 1200 ^{o}C'de tutulduğu işlemde ise sıralama şöyledir: Fe_3Al+FeAl, FeAl-α-Fe(Al), α-Fe(Al).

CA-EMIT yöntemiyle üretilen demirce zengin faz, 0.5M H_2SO_4' te, demirce zengin kitlesel demir alüminitlere benzer korozyon direnci sergilemiştir. Alaşımda Al bulunması, alaşımın sülfürik asit çözeltisindeki pasivasyon davranışını iyileştirmitir. Alüminyumca zengin intermetalikler, daha yüksek Al içerikleri sayesinde sergiledikleri daha düşük pasif akım yopunlukları bakımından daha iyi pasifleşme davranışı sergilemişlerdir. Artan Al miktarı ile pasif akım yoğunluğu azalma eğilimi göstermektedir. Aktif korozyon bölgesinde (anodik çözünme) alaşımların korozyon potansiyeli artan Al miktarı ile daha aktif bölgeye doğru kaymış olup demir ve alüminyumun potansiyel değerleri arasında kalmıştır. Fe-Al fazlarının bu bölgedeki korozyon hızları ise IF-çeliğininkinden daha fazla olup artan alüminyum miktarı ile artmaktadır. Bununla birlikte, korozyon deneyi sırasında bir miktar çatlama meydana gelmiştir. Bu durum, fazların çevresel olarak desteklenen çatlamalara karşı hassasiyetlerinin bir göstergesi olabilir.

Temsili asit yağmuru ortamında (200ppm Cl^- pH4 H_2SO_4 ile ayarlanmış), numunelerin korozyon potansiyellerinin sıralanmasıyla üretilen galvanik seride asalet sırası: Fe_3Al-FeAl> IF-steel> Fe_2Al_5-Fe_4Al_{13}> Fe_2Al_5 olarak bulunmuştur. Alüminyum ve alüminyumca zengin fazlar pasifleşme davranışına atfedilen oyuklanma potansiyeli değerine sahipken, IF-çeliği ve demirce zengin fazlar için bu değer bulunamamıştır. Alüminyumca zengin intermetalik tabakalar, IF-çelik alt tabakaya, oyuklanma potansiyeline kadar gösterdikleri pasif davranış sayesinde hem bariyer korozyon koruması hem de yüzeyden alt katmana ulaşan kusurlar olması durumunda kendilerini feda ederek katodik koruma sağlamışlardır. Öte yandan, pasifleşme davranışı sergilemeyen demirce zengin intermetalik tabaka, koruyucu bir bariyer görevi göstermediği gibi alt tabaka ile arasında elektrolitik bağlantıya izin veren yolların varlığında, galvanik etki ile çeliğin korozyonunu hızlandırması bakımından bir problem yaratabilir.

1. INTRODUCTION

The iron-rich Fe-Al alloy group (iron aluminides) is one of the most researched groups of alloys without significant success for commercial and widespread use. The interest in these alloys aroused from availability and cost because they are the alloys of the two most redundant metals in the earth crust and potential alternatives to stainless steels and nickel alloys. Additional reasons for this interest are the presence of two ordered structures ($D0_3$ and B2) in this binary system, their lightweight compared to steels and nickel alloys and high-temperature corrosion resistance, especially to sulfur-bearing high-temperature atmospheres. When talking about these alloys, the extensive efforts of (Oakridge National Laboratories, USA) ORNL on the development of Fe-Al alloys should be mentioned. Iron aluminides-related studies were enhanced after their excellent high-temperature oxidation resistance that is discovered at Oak Ridge National Laboratory (ORNL) in the 1930s. However, the poor mechanical properties led to the abandonment of these studies in the 1960s. In the 1980s, studies were resumed with efforts to achieve improved mechanical properties through alloying or modifications in production methods [1]. The studies were also abandoned in 2000 without significant success because the efforts put forth did not overcome the poor ductility/toughness at room temperature and creep behavior, weak wet corrosion resistance compared to stainless steels, especially in chloride-containing media and very high susceptibility towards hydrogen embrittlement problems satisfactorily. Today efforts are still continuing to overcome these problems (alloying and grain refinement based), especially in Europe (Germany, Spain, Poland and Czechia). These improved alloys are commercially available in cast form for coal gasification, high power diesel engines, turbine blades applications. heat loaded pieces in nuclear reactors [2,3]

Another way of producing iron aluminides is to produce these alloys as coatings on different substrates. Production of iron aluminides as a coating is possible with direct overlay coatings or diffusion methods. In direct overlay coating, physical vapor deposition (PVD), thermal spraying, overlay welding (or joining) are commercialized

methods for depositing these alloys on different substrates. The most widely used method for the production of Fe-Al alloys on iron-based materials is the diffusion-based processes known as aluminizing [4,5]. There are several methods commercially available for diffusion-based coatings, such as pack cementation [6], hot dipping [7,8], chemical vapor deposition (CVD) [9], slurry reaction coating [10]. Among these, hot dipping is the only method that is conducted in atmospheric conditions. In all the other methods, substrate and the depositing materials are protected from the atmosphere either by packing or utilization of vacuum. In addition to these a cathodic arc plasma aided diffusion (Cathodic Arc Electron/Metal Ion Treatment-CA-EMIT) method that is recently developed by our research group is successfully used for controlled aluminizing of steels. In this method coating and heating process is applied simultaneously by using AC bias voltages applied to the substrate [11]. This method allowed us to produce phases with a large variation of the composition, i.e. both Fe-rich and Al-rich phases in the desired sequence and thickness on the substrate.

There are many studies in the literature concerning the high-temperature oxidation properties of bulk and coated iron aluminides for determining their potential use in adverse high-temperature environments [12–15]. The extension of the usage of iron aluminides also brought forth the necessity of understanding their wet (electrochemical corrosion) behavior. The studies on electrochemical corrosion of bulk iron aluminides are concentrated on iron-rich phases containing Al up to 40% (will be considered as atomic percent unless otherwise indicated). In the scope of the electrochemical behavior of bulk iron aluminides in sulfuric acid environments, several studies were conducted to interpret the effects of constituent elements on relevant behavior. According to the common remark, alloying Fe with Al improves both passivation and repassivation behavior in the sulfuric acid environments in a trend of further improvement with an increasing amount of Al. It has been revealed that Al content must exceed 10% to promote the formation of the protective passive film and 19% Al to provide proper corrosion resistance. Further increased Al content failed to provide a significant difference in corrosion resistance, compared to 19% Al [16–18]. The studies on the electrochemical behavior of iron aluminides in the active corrosion region demonstrated that the active corrosion rate is governed by the dissolution of iron from the surface to the solution [19]. Although they differ from each other by the

proposed passivation mechanism, the results of overall studies agreed on the fact that complete passivation is provided by both Al oxides/hydroxides and Fe oxides/hydroxides [20–22]. Within the studies on the effect of an alloying element on electrochemical behavior, the addition of C to Fe-rich iron aluminides in a sulfuric acid environment caused a regression in corrosion resistance due to the selective dissolution of carbide phases [23]. In the limited studies conducted in Cl^- containing environments, in which the effect of alloying on the electrochemical behavior of Fe-rich iron aluminides has been investigated, with the addition of Mo and Cr an improved electrochemical behavior by means of nobler breakdown potential (E_b) was obtained due to the cooperation of Al_2O_3-Cr_2O_3/MoO_3 [24,25].

Contrary to Fe-rich iron aluminides, studies on the wet corrosion behavior of Al-rich intermetallics which the major constituents of aluminized steel, are very limited. The widespread use of steel requires surface coatings to protect steel from electrochemical degradation. Aluminized steel ensures excellent high-temperature oxidation resistance in applications such as hot stamping, cooking pans, plates, ovens, heaters etc. Thus their performance against wet corrosion should also be considered. The electrochemical behavior of aluminized steel is examined in terms of provided barrier protection to the substrate and cathodic protection behavior in the presence of a path that allows electrolyte penetration to the coating and substrate interface. Studies conducted within this scope have generally been carried out in environments containing Cl^- in order to simulate the atmospheric environment with chloride contamination. In studies conducted so far, it has been observed that the corrosion behavior of aluminized steels is dominated by the behavior of the free-Al layer formed on the outer surface and the aluminum-rich phases underneath [6,26–32]. As long as the top aluminum layer is intact, the corrosion behavior is governed by this layer. However, in cases where defects extending through the coatings are present, the nature of the layers below the pure top aluminum layer (free Al layer) and the interplay among them should be taken into consideration. In the study of De Graeva et al. [26], a galvanic series is created by measuring the corrosion potentials of pure Al, Fe and Fe-Al alloys and intermetallics. Accordingly, $E_{corr,}Al < E_{corr}steel < E_{corr}FeAl_3 < E_{corr}$ Fe_2Al_5, were obtained. In another study conducted by Maki [28], it is indicated that the additives used in production processes to control the formation mechanism of phases vary corrosion behavior of aluminized steel. Type1 hot-dipped aluminized steel

exhibited worse corrosion protection properties than Type2 hot-dipped aluminized steel due to the fact that in Type1 Al dissolved selectively around acicular Fe_2Al_8Si phases, which are more noble compared to Al, in the atmospheric environment.

Overall, the corrosion protection behavior of aluminized steel depends on the phases formed on the substrate, the sequences of the phases, the nature of the hostile environment (Cl^- content) and the extent of damage on the surface. On the other hand, within the presence of Fe-rich layers and the absence of free-Al layer, it is not possible to straightforward estimation on electrochemical corrosion protection behaviors. There is a need for a deeper investigation on both the corrosion behavior of Fe/Al-rich aluminized steel without the free-Al layer in the atmospheric environment and the Al-rich iron aluminides in the sulfuric acid environment. To obtain the phase sequence in the desired order and controlled thickness is essential to achieve this purpose.

The aim of this study is to investigate the corrosion resistance and simultaneous corrosion protection properties of each binary Fe-Al compounds that constitute the aluminized layer. For this purpose, aluminized samples that are produced by the CA-EMIT technique is used. This technique allows us to produce Fe-Al alloys with the required composition to a large extent because of the precise controlling ability of the diffusion parameters (flux of diffusing species and temperature). Thus within the study, both iron-rich and aluminum-rich Fe-Al phases that are produced by the CA-EMIT process are used for determining their electrochemical corrosion behaviors in both acidic and chloride containing media.

2. IRON ALUMINIDES

At the beginning of the 20th century, ordered intermetallic alloys emerged as a result of the search for new materials to fill the insufficient properties of steel and superalloys [2]. In an intermetallic compound, different atoms settle in specific lattice points and involved strong bonding [33]. Intermetallic compounds have attracted considerable attention due to their superior physical and mechanical properties which arises from their bonding and order properties [34]. Most striking features of these intermetallic compounds are, their high melting temperatures, high thermal conductivities, significant wear and corrosion resistance at elevated temperatures, good tensile and yield strength at high temperatures, higher fatigue resistance than superalloys [35]. On the other hand, Intermetallic compounds suffer from poor ductility at room temperature and a decrease in strength above the critical temperature where deviation from long-range ordering begins. However, by controlling microstructure either by changing production methods, alloying or heat treatment, intermetallic compounds are attempted to stripping off from poor mechanical features and became candidate for structural applications [3]. With their high-temperature corrosion resistance which arises from the protective film formed on their surface, superior to other intermetallics, aluminides are draw attention within intermetallic alloys. Moreover, among these, transition metal aluminides exhibit lower density than superalloys. Another feature of these aluminides is that their favorable magnetic, electrical and optical properties. Iron aluminides attracted substantial interest as an alternative to Ni and Cr based superalloys and other commercial high temperature alloys due to economic concerns such as the fact that they contain the most common elements in nature, ease of production and lack of strategic and rare elements (Ni, Cr, Nb) [3,36]. When oxidation and sulfidation resistance superior to Ni and other Fe based alloys and all given above taken into consideration, iron aluminides have been considered as most promising candidates by researchers [37]. In addition to their high temperature corrosion behaviors, recently, studies on electrochemical behavior of iron aluminides are conducted to compare them with stainless steel. Iron aluminides also exhibit analogous tensile strength with ferritic and austenitic steel. Deviations on stoichiometry to the

Al-rich side of FeAl (B2) give rise to constitutional vacancies (as high as 10^{-2}) on the structure and thus changing on the high temperature strength and creep resistance [33,38]. the studies on iron aluminides started in the 1930s with recognition of their excellent oxidation resistance, have been suspended in the 1960s due to as said ductility and strength drops at ambient and elevated temperatures, respectively. The discontinued studies were resumed in the late 1980s by Oak Ridge National Laboratory (ORNL) as part of a program to conduct studies for fossil fuel conversion [1].

2.1 Iron Aluminum Binary Phase Diagram

The binary iron-aluminum (Fe-Al) phase diagram, which has been studied using different techniques such as dilatometer measurement, measurement of specific heat and electrical resistivity, elastic modulus and magnetic property measurements, X-ray diffraction methods, has recently been studied in depth with TEM. In 1982, the first recognized binary Fe-Al phase diagram was reported [36]. The information gathered about the binary phase diagram were assessed by Kubaschewski [39], and afterward the widely accepted form of the phase diagram was created by Kattner and Burton (Figure 2.1) [40]. Relying on the DTA results, Stein and Palm [41] corrected some invariant reaction temperatures and critical temperatures in the diagram of Kattner and Burton. (Figure 2.2) [37].

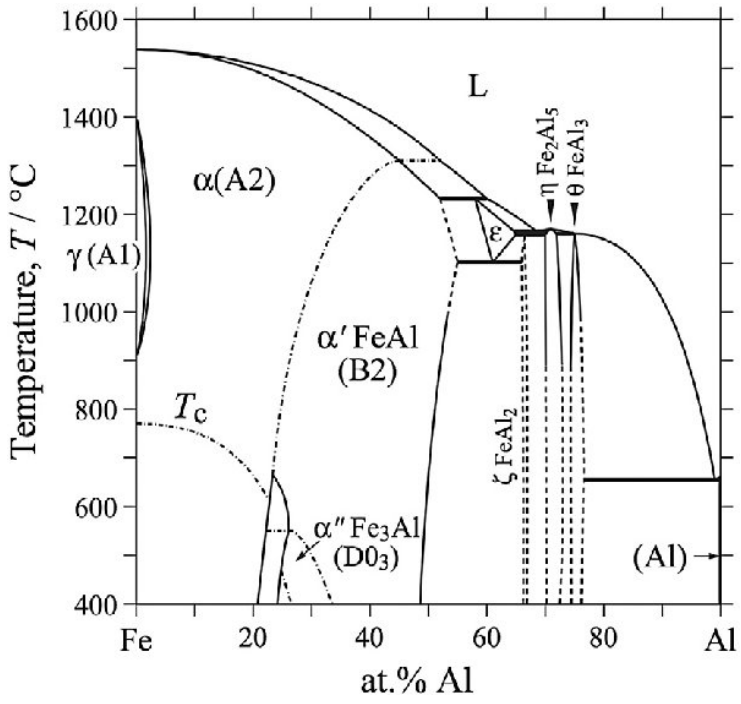

Figure 2.1 : Fe-Al Binary phase diagram assessed by Kattner and Burton [40].

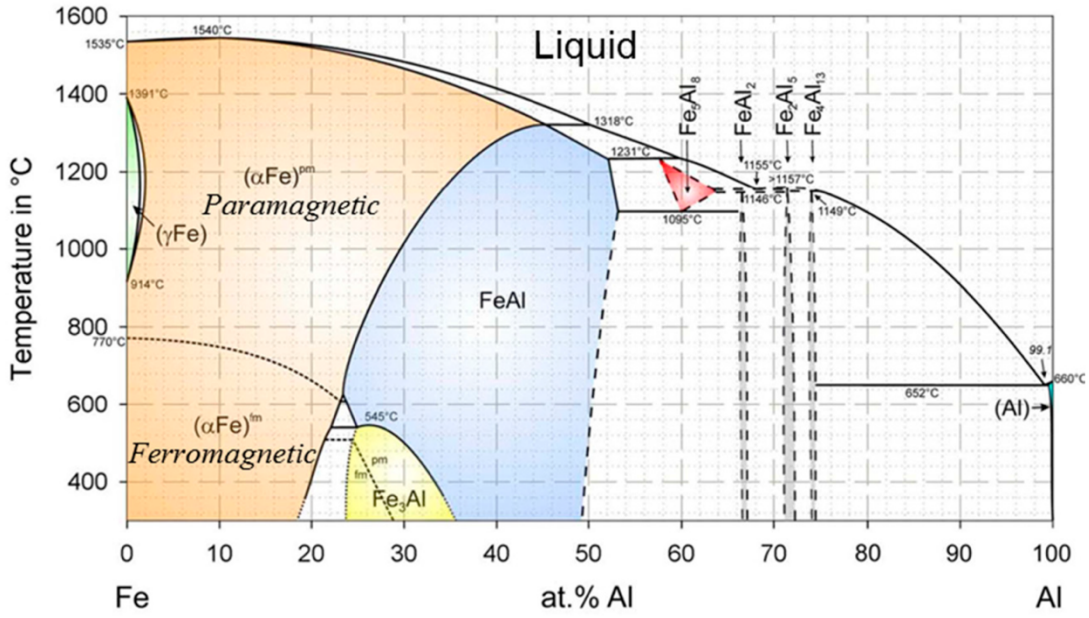

Figure 2.2 : Revised phase diagram by Stein and Palm [41].

The dashed lines in the binary diagram represents the solubility lines that are still not fully determined, first or second-ordered transitions from disordered phases to ordered phases and Curie temperature nominated as Tc [42]. In the Table 2.1, the reaction temperatures revealed by Kattner and Burton are given together with the suggested corrections in the subsequent studies [41,43]

Table 2.1 : Comparison of reaction temperatures data in the literature.

Reactions	Temperature [40]	Temperature [41,43]
$L + FeAl \leftrightarrow Fe_5Al_8$	1232	1231
$L \leftrightarrow Fe_5Al_8 + Fe_2Al_5$	1165	1157
$L + Fe_2Al_5 \leftrightarrow Fe_4Al_{13}$	≈1160	1150
$Fe_5Al_8 + Fe_2Al_5 \leftrightarrow FeAl_2$	1156	1145
$L \leftrightarrow Fe_4Al_{13} + (Al)$	655	654
$Fe_5Al_8 \leftrightarrow FeAl + FeAl_2$	1102	1095
$L \leftrightarrow$ α-Fe(Al)	-	1540±1
$L \leftrightarrow Fe_2Al_5$	1169	≈1158
$\gamma Fe \leftrightarrow$ α-Fe(Al)	912	-
$FeAl \leftrightarrow Fe_3Al$	552.5	545±2
α-Fe(Al) ↔ FeAl	1310	1318±1

There are numerous metastable non-equilibrium phases in the phase diagram of Fe-Al binary system because of the large difference in the atomic radius of Fe and Al, and different crystal structures of Fe (BCC) and Al (FCC) at room temperature.

Accordingly, only 0.04% Fe can be dissolved in Al while solubility of Al may reach to 20% Al in Fe [44]. Stable phase regions in the binary phase diagram are liquid phase (L), A2 disordered solid solution (α-Fe(Al)), γ-Fe(Al), B2 ordered solid solution (FeAl), $D0_3$-ordered solid solution (Fe_3Al), ε phase (Fe_5Al_8) and phases with narrow solubility ranges, $FeAl_2$, Fe_2Al_5, $FeAl_3$, Al solid solution with capacity of dissolving 0.04% Fe. Crystal structures, compositional ranges of all existing phases with their label and stability in the Fe-Al binary system are given in Table 2.2 [36,40,42,43,45,46]. Stabilities of related phases are designated as S (stable till low temperatures), S*(stable from high temperatures to 400°C (unknown below it), HT (stable only at high temperatures), and M (metastable).

Table 2.2 : Crystallographic and compositional data for Fe-Al Phase diagram [36,40,42,43,45,46].

Phases	Label in Figure	Crystal Structure	Composition Range (at%Al)	Prototype	Stability
Liquid	L	-	0-100	-	HT
α-Fe(Al)	αFe (pm)[1] αFe (fm)[2]	BCC/A2	0-45	W	S
γ-Fe(Al)	γFe	FCC	0-1.3	Cu	S-HT
AlFe	FeAl	BCC/B2	23.3-55	CsCl	S
$AlFe_3$	Fe_3Al	BCC/$D0_3$	23-34	BiF3	S
Al_8Fe_5 (ε)	Fe_5Al_8	BCC/D82	56-64.4	Cu_5Zn_8	S-HT
Al_2Fe	$FeAl_2$	Triclinic	65.8-67.1	$FeAl_2$	S*
Al_5Fe_2	Fe_2Al_5	Orthorhombic	70-73	Fe_2Al_5	S*
$Al_{13}Fe_4$ (Al_3Fe)	Fe_4Al_{13}	Monoclinic	74.5-76.6	Fe_4Al_{13}	S
Al	Al	FCC	99.998-100	Cu	S
Metastable Phases					
Al_9Fe_2	-	-	68.5	-	M
Al_6Fe	-	-	74.3	-	M

[1] Paramagnetic
[2] Ferromagnetic

It is possible to consider the Fe-Al phase diagram in two main portions as the iron-rich region up to FeAl and the region rich in aluminum [38]. Figure 2.3 [37] shows the phase diagram of the binary system in the composition range of Fe-rich side.

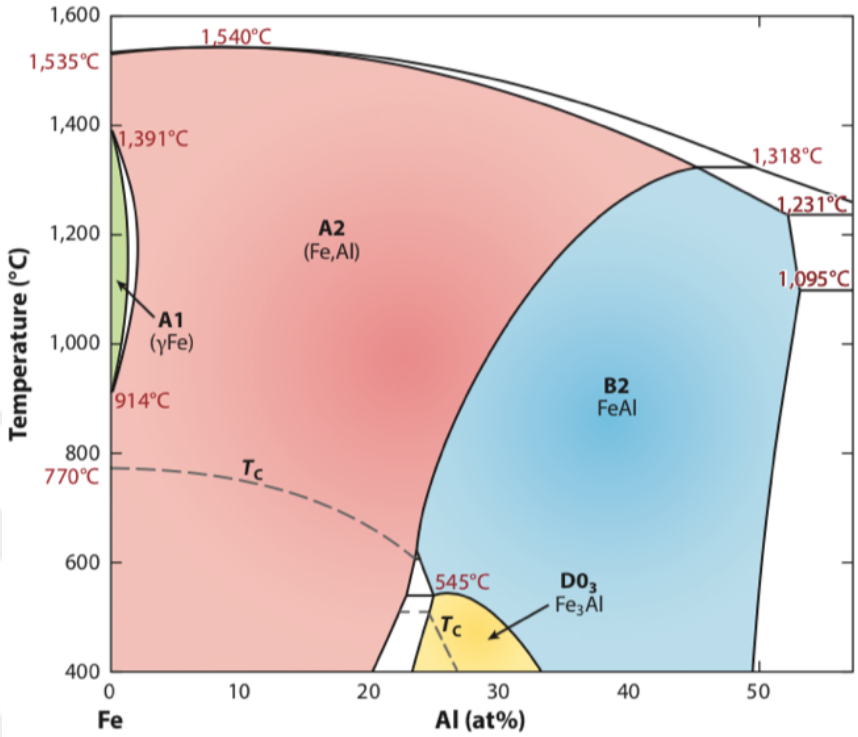

Figure 2.3 : Fe- rich portion of the phase diagram [37].

The phase diagram deduced that disordered α-Fe(Al) solid solution with the Strukturbericht symbol A2, can dissolve different amounts of Al depending on temperature, up to 45% at high temperatures. The phase diagram can be separated into three portions at lower temperatures as follows: The region where the disordered solid solution of α-Fe(Al) stably exists, up to 18.75% Al concentration at room temperature; the zone which Fe_3Al intermetallic phase formed at temperatures below 545°C, at a concentration of approximately 25% Al; the region at the ongoing Al concentrations, in which imperfectly ordered FeAl phase is stable over a wide compositional range [37,38,43]. Figure 2.4 reveals that there are α-Fe(Al)+FeAl and α-Fe(Al)+Fe_3Al dual phase regions, besides α-Fe(Al), FeAl and Fe_3Al single phase regions [47,48].

Crystal structures of disordered solid solution and ordered phases (FeAl-Fe_3Al) are represented in the Figure 2.5 [37] respectively. In the disordered A2 phase (a-Fe(Al)), Fe and Al atoms take places randomly in the BCC crystallographic positions namely, as Al atoms are added Fe atoms are substituted by Al atoms. At increasing Al concentrations, Al atoms settle in BCC lattice sites in two different types of ordering.

In the B2 crystal lattice of ordered FeAl phase which has CsCl type structure, in the $Fe_{50}Al_{50}$ stoichiometric composition, body center of the cell is occupied by the Al atoms, while the Fe atoms are settling the corners of the cubic cell. In the $D0_3$ structure of ordered F_3Al phase which is also BCC based, Wyckoff positions of 8c (1/4,1/4, 1/4) and 4b (1/2,1/2, 1/2) are occupied by Fe atoms whereas Al atoms are positioned at 4a (0, 0, 0) for the ideal stoichiometric composition [37,49–52]. Although the ideal stoichiometric compositions of B2 ordering and $D0_3$ ordering are 50Fe-50Al and 25Fe-75Al respectively, both phases have solubility at wide ranges as seen in the phase diagram. Existence of the lattice defects cause deviation from the ideal stoichiometry [36,42] The perfect ordering of both structures is possible only when they have their stoichiometric composition [53].

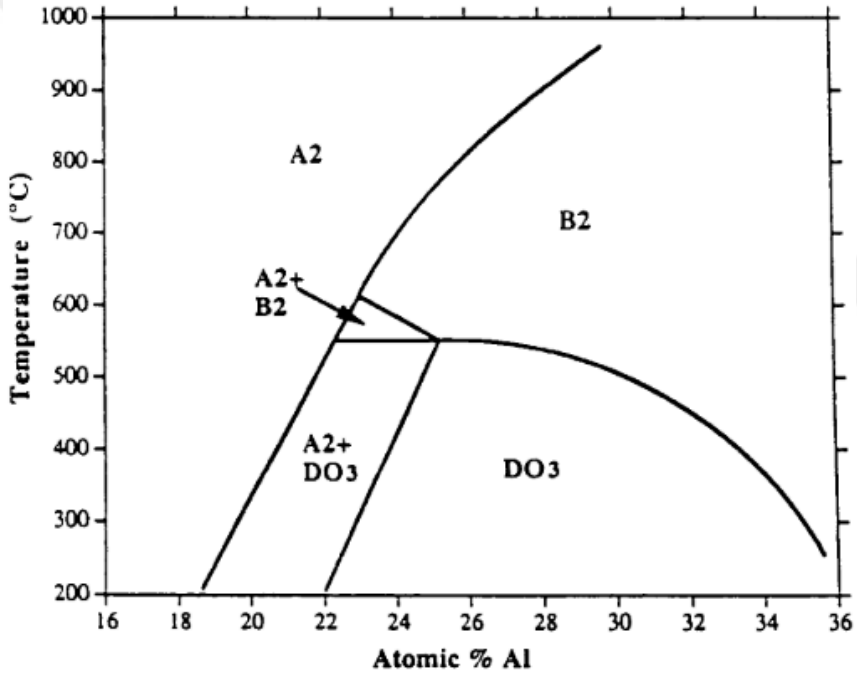

Figure 2.4 : A closer look at the iron-rich part of the binary system at around 25% Al[48].

There are transitions for ordering (A2/B2 and B2/$D0_3$) and magnetic transformations (para/ferro) in the Fe rich portion of the diagram. The transition between disordered A2 and ordered B2 is second ordered in the composition range of 23-45% Al and the transition temperature rises with increasing content. Just before ferromagnetic transition line, the transition of A2/B2 becomes first-ordered. While the Curie temperature decreases with increasing amount of aluminum for both A2 and $D0_3$, this reduction is more striking for $D0_3$ is due to the fact that the ferromagnetic transition temperature decreases significantly by chemical ordering. The transition between $D0_3$

and B2 is second-ordered [41,42,45]. At temperatures above the B2-$D0_3$ ordering transition, where the B2 structure is stable, the Fe_3Al composition has a B2 structure, thus if quenching performed from these temperatures, there would be retained B2 phase at room temperature. At the stoichiometric compositions of Fe_3Al, ~550ºC is the transition temperature (Tc) between B2 and $D0_3$ structures. When the increase in the amount of aluminum that increases the stability of the B2 phase reaches about 36-37%, the $D0_3$ phase disappears. There is a wide range of solubility of imperfectly ordered B2 phase in the Fe_3Al phase at temperatures between 550-700°C, in which stability increases up to the highly ordered FeAl composition [38].

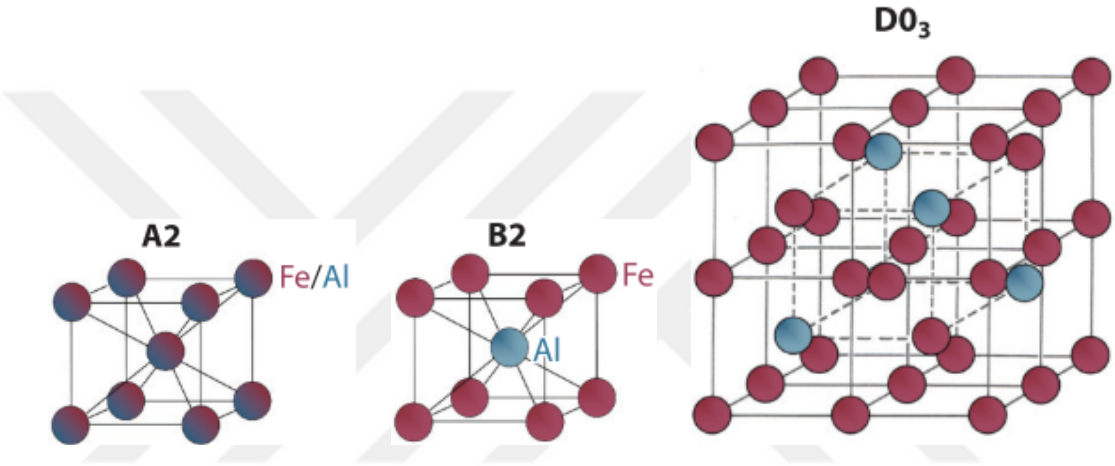

Figure 2.5 : The unit cells of the disordered and ordered structures (Fe, red; Al, blue; Fe or Al, shaded violet) [37].

In the Al-rich portion of the binary diagram, in addition to Fe_5Al_8 (ε), $FeAl_2$, Fe_2Al_5, and Fe_4Al_{13} phases; FeAl phase which is stable in the Fe-rich side of the diagram, has stability region. Besides stable phases Fe_2Al_9 and $FeAl_6$ are two metastable phases take place in the Al-rich portion of the diagram. In contrast to FeAl with the simple cubic crystal structure, triclinic, orthorhombic and monoclinic complex structures are hold by $FeAl_2$, Fe_2Al_5, and Fe_4Al_{13} phases, respectively [43]. The Fe_5Al_8 phase, which was designated as ε phase until it was determined to have a Cu_5Zn_8 type BCC structure, is a high temperature phase [54,55]. In accordance with literature, it is accepted that, Fe_5Al_8 phase formed from liquid and FeAl by peritectic reaction, transforms to FeAl and $FeAl_2$ by eutectoid reaction. The phases in the Al-rich portion of the diagram have an extremely tight homogeneity ranges, that 65.8-67.1% Al for $FeAl_2$, 70-73% Al for Fe_2Al_5, 74.5-76.6% Al for Fe_4Al_{13} [43]. The actual composition of Fe_4Al_{13} phase, which was previously referred to as $FeAl_3$ in the literature, was found by Black [43,56,57].

2.2 Application Areas of Iron Aluminides

Due to their appealing properties as follows: Relatively low density, excellent corrosion, high temperature oxidation and sulfurization resistance, remarkable wear resistance, ease of fabrication, and lightweight relative to stainless steel and Ni-based alloy, higher electrical resistance than commercially available materials used as heating elements [35], aluminides draws attention for industrial applications [58,59]. Iron aluminides can be used as in bulk form or as a coating for applications in various environments and are used in industry sectors such as aviation, automotive, marine and energy. In high temperature and corrosive conditions, metallic compounds are coated with iron aluminides to protect them from environmental damage. [37,60].

Boilers and gas turbines in power generation plants are attractive usage areas for iron aluminides which combine high-temperature corrosion resistance and high-temperature strength. Iron aluminides are appropriate for tools as receptacles and rotating tools used in molten salt applications, pipes and tubes in petrochemical processing, respectively [61]. Turbocharger pieces and exhaust valves in automobile industry [62], tools at sulfur-containing environment [25], radiant-burner tubes operating at temperatures approaching 800–900°C, heat treatment columns of furnaces for carbonization, walking beam furnace rails, porous filtration systems in coal gasification plants, are among functional applications of iron aluminides [58]. Additionally their magnetic permeability, and electrical resistance, makes iron aluminides suitable for magnetic and electronic parts [1].

Although iron aluminides are already used in several areas, they are candidates for numerous applications namely; as cutting blade materials for cutlery or industrial cutting applications [63], arsenic and antimony oxides filtering system at high temperatures [64] catalyst for sodium chlorate electrosynthesis [65]. Furthermore, iron aluminides can be recognized as lunar engineering material because of that they are formed as a by product of the oxygen and silicon production in the moon [66].

In addition to their engaging physical and mechanical properties, iron aluminides have become candidates for use in aqueous environments with and instead of stainless steel due to economic concern and their corrosion resistance in hostile environments. Such applications are pipes and tanks used in seawater disposal, apparatus for nutrition (in place of hazardous heavy metals), artificial body parts in contact with liquid body

substances [17]. Besides, lately, iron aluminides have been involved to hot stamped parts as heat-treated and non-treated aluminized steels, to bring into preferable process efficiency, much better high temperature and wet corrosion properties to process inputs [5].

2.3 Production Methods

Iron aluminides can be produced in bulk or as coatings on the surface of a base material, thus gaining advanced properties with the mechanical properties of the substrate material and the surface properties of iron aluminides. Production of iron aluminides as a coating is possible by directly overlay coating or diffusion [4,5].

2.3.1 Production of bulk iron aluminides

In iron aluminides' bulk production, melting is the traditional method. Induction melting (IM) is the method by which Fe-Al alloys are formed from pure elements. IM-based, Vapor induction melting (VIM), air induction melting (AIM) and electroslag remelting (ESR) methods are utilized in production, the first being at the laboratory scale and latter at the industrial scale [67]. Moreover, there is Exo-Melt^{TM} a process developed industrially to produce particularly nickel and iron [68]. Electron beam melting and arc melting are also among the methods to produce alloys [69].

Although the melting method is economical, it has some difficulties, such as the difference between the melting points of aluminum and iron, voids arise from generated hydrogen, difficult control of the reaction, heat releasing nature of the formation reaction. Mechanical alloying is another method considered to overcome these obstacles [61]. Spark plasma sintering and self-propagating high-temperature process are methods within the powder metallurgy which is widely included in investigations for the synthesis of iron aluminides [37].

2.3.2 Production of iron aluminides by overlay coating

In overlay coating, the base material content is not included in the coating or is included in a negligible amount. As a result, completely different compounds from the substrate can be obtained in the coating layer. Such overlay coating processes are physical vapor deposition (PVD), thermal spraying, overlay welding (or joining) [4,5]. In the literature, overlay welding proses is used by means of laser cladding and

electrospark deposition to obtain relatively thick coatings in the form of stoichiometric and non-stoichiometric Fe_3Al and FeAl phases. Within the scope of the thermal spraying, studies on iron aluminides produced by using high-velocity oxygen fuel and cold spraying methods exist. In addition to studies on oxidation and wet corrosion resistance (in Hank' s solution, NaOH, NaCl and H_2SO_4 solutions) of iron aluminides produced by high-velocity oxygen fuel [70–73] there are studies on the cavitation resistance of Fe-40Al coating produced by cold spraying [5].

2.3.2.1 Physical vapor deposition (PVD)

With the physical vapor deposition (PVD) in which a coating formed by the deposition of atomized or vaporized metal atoms on the substrate material, dense and adherent layers can be obtained. We can divide the PVD method into two groups based on evaporation and sputtering, the first of which are thermal evaporation, e-beam, laser and cathodic arc PVD, while the ones belong to sputtering type are diode, triode, magnetron and ion beam sputtering processes. There are studies on iron aluminides produced by magnetron sputtering and cathodic arc vapor deposition (CA-PVD), which are different PVD methods. In regards to CA-PVD, the vacuum chamber (anode) and the coating source (cathode) are connected to a DC power source that provides low voltage and high current. With sudden short-circuit of the cathode with an anode at higher voltages, triggering is provided. Eventually, the source of coating material is simultaneously vaporized and ionized by the electric arc formed on it [74]. In the study of Paldey and Deevi [75], oxidation resistance of 430C steel is developed after coated by CA-PVD which has Fe-40Al and Fe-45Al cathodes.

2.3.3 Production of iron aluminides by diffusion

There are several diffusion based methods for the production of for iron aluminides: Pack cementation [6], hot dipping [7,8], chemical vapor deposition (CVD) [9], slurry reaction coating [10], CA-EMIT [11].

2.3.3.1 Pack cementation

The pack cementation which is in other saying in-situ CVD method is utilized to coat steel base material with the desired element. In this method, which is one of the most prevalent iron-aluminide coating methods, it is ensured that the steel is aluminized by diffusion. Within the process, the substrate to be coated is embedded in cement which

consists of Al/Al alloys, activators, and an inert filler material (mostly Al_2O_3); after being placed in a sealed crucible, it is heated in a furnace to high temperatures in an inert atmosphere. It was observed that the $FeAl_3$ and Fe_2Al_5 phases formed on the surface of low carbon steel treated with this method improved the aqueous environment corrosion behavior of the steel [6].

2.3.3.2 Hot dipping

The method of coating iron and steel with aluminum or Al-Si alloys by hot dipping is a common way to increase their corrosion resistance. The $FeAl_2$, Fe_2Al_5 and $FeAl_3$ phases formed as a result of immersion of the material to be coated into molten aluminum or aluminum alloy vary depending on the temperature, holding time and the type of alloy [7,8].

2.3.3.3 Slurry reaction coating

Although this method is similar to pack cementation, instead of gas formation, there is an exothermic reaction of the metallic powder melt on the substrate. The method is harmful to health due to Cr^{6+}, which occurs as the product of acidic chromates used as binders. Fe_2Al_5 is the most common phase produced by slurry reaction coating. In the study that iron aluminides produced by this method exhibits significant oxidation resistance in steam environment, there was traces of Kirkendall pores arise from different diffusion rates of constituent elements in FeAl and Fe_2Al_5 [10].

2.3.3.4 Chemical vapor deposition (CVD)

The precursor used in CVD method is $AlCl_3$. This compound in gas form is produced by flowing of halogen gases through heated Al pellets. When the precursor gas is introduced into the chamber with the help of carrier gas, it is reduced on the heated substrate as a result of chemical reaction leaving behind metallic aluminum layer, where the diffusion processes are initiated. CVD method provides a uniform coating of complex shaped parts in a contaminant free manner [9].

2.3.4 Cathodic arc electron/metal ion treatment (CA-EMIT)

CA-EMIT method is a cathodic arc-based method with an acquired supplemental diffusion feature, developed by Öncel and Ürgen [11]. The hardware of the method (Figure2.6) consists of a vacuum chamber, aluminum cathodes and suitable power

supplies for evaporating the target and biasing the substrate. The originality of the process arouses from the usage of an AC bias power supply which allows heating the substrate to the desired processing temperature in a controlled manner. During the positive cycle of the AC bias voltage, emitted electrons are directed to the surface of the target, causing the substrate material to be heated. Contrary to ions, electrons provide heating without sputtering from the surface of the material. By controlling the bias voltage, the temperature of the surface is adjusted. On the other hand, in the negative cycle of the bias voltage, metal ions flow through the target surface and the coating process is performed.

With this procedure which enables coating and heating at a single process, by controlling the temperature of the substrate along with the ionization of coating material, i.e. controlling diffusion, the phases with a wide range composition and in different thicknesses in the desired sequence are obtained. Additional benefits of this method to other diffusion-based methods are as follows: Energy retrenchment as eliminating walls heating subject to heating directly the substrate; eliminating of the need for an additional presence of a heating source as it keeps the temperature of the substrate under control; absence of harmful gas emissions as in methods of pack cementation and CVD [11,74].

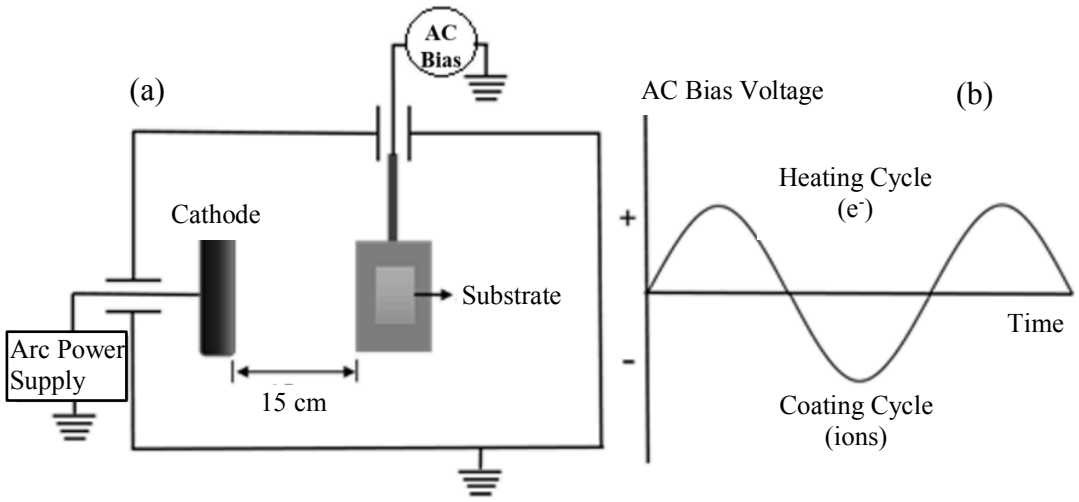

Figure 2.6 : Schematic demonstration of (a) CA-EMIT equipment, and (b) example diagram for Time vs. AC Voltage [76].

2.4 Diffusion in Iron Aluminum Binary System

The understanding of diffusion mechanism between aluminum and iron is essential in order to obtain the desired phases in the desired thickness and order. Some of the

phases that form is more brittle (e.g. Fe_2Al_5), and may cause undesirable effects in the system (such as the onset of cracks in the presence of a possible impact, or corrosion progress).

In the production of iron aluminides by diffusion, depending on the temperature, the solid iron is in contact with aluminum in the solid, liquid or gas state.

The diffusion in which liquid aluminum is contacted with solid iron, such as hot dipping begins with the diffusion of iron atoms towards liquid aluminum and a diffusion dissolution interlayer is formed with the reaction of $2Fe+5Al_{(liq)}=Fe_2Al_5$. In this interlayer, the Fe_2Al_5 phase begins to grow towards iron. This phase, which is in the form of a continuous thin layer on the surface as aluminum diffuses along the direction of [001], grows as a tongue-like structure at the base with the vertical diffusion of the iron due to the crystal structure distortion. This growth prevents further diffusion of iron and dissolution of Fe_2Al_5 into the liquid aluminum takes place. As a result of $Fe_2Al_5+Al_{(liq)}=2FeAl_3$ reaction that takes place. During cooling $FeAl_3$ phase adjacent to Fe_2Al_5 phase begins to form on the surface. In the latter stages of cooling, $FeAl_3$ in the form of proeutectic dots and needle-like begins to precipitate in the aluminum layer [77].

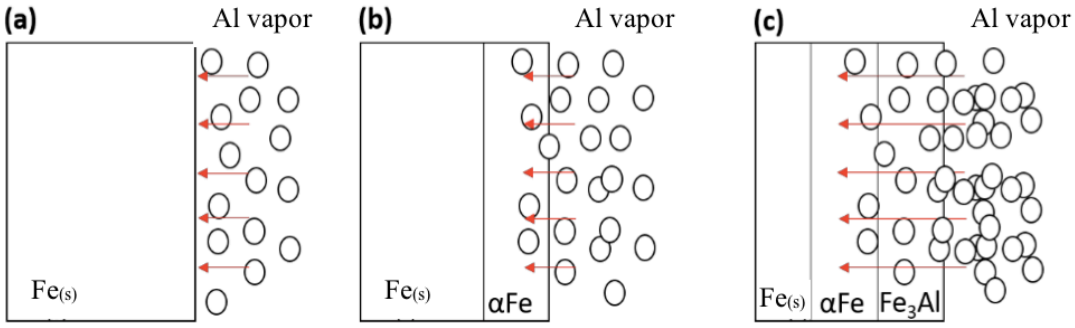

Figure 2.7 : Diffuison in solid iron-gas aluminum system [78].

In solid-gas systems, on the other hand, constant aluminum layer is absent on the surface, instead, aluminum is carried to the surface in vapor form. Thus, formation takes place from phases located at iron rich side of binary phase diagram. In the CA-EMIT process which is used in this thesis study, solid-gas interaction is involved. In systems where this interaction exists, as represented in the Figure 2.7, diffusion controlled by three different mechanisms namely, flowing rate of aluminum vapor to the surface in the first stage, diffusion rate of aluminum in the iron in the second stage, diffusion rate of aluminum in formed Fe-Al phases in the third stage

In the first stage of the process, the aluminum vapor that flows through the surface diffuses into the solid iron and gives rise to the formation of aluminum solid solution (α-Fe(Al)). With progressed diffusion, Fe_3Al and FeAl phases formed respectively depending on aluminum concentration, slows the diffusion rate. Putting it differently, parameters of diffusion controlling are aluminum concentration (activation), temperature, and behavior in formed phases. As the activity of aluminum on the surface of the iron increases, its diffusion increases simultaneously and it becomes independent at a saturation point. With increasing temperature, the activity of aluminum thus diffusion coefficient increases. In the third stage, which involves a transition from disordered to ordered, the aluminum enriched structure causes the diffusion to slow down. It is stated in the study of Hirano and Hishinuma that with the decrease of disorder in the α-Fe(Al) solid solution in the temperature range of 800-1000°C the disorder decreases and as a consequence the activation energy of interdiffusion increases [79].

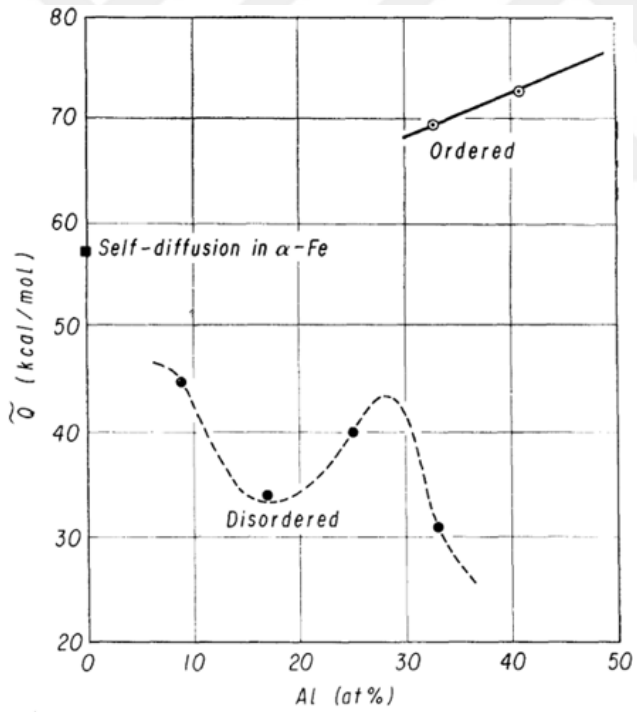

Figure 2.8 : Activation energy for interdiffusion of BCC Fe-Al solid solution in ordered and disordered states [79].

According to Figure 2.8, in disordered states, activation energy for interdiffusion in the range of 30-45 kcal/mol and increases to 70kcal/mol at ordered state. Besides, self-diffusion activation energy of aluminum in α-Fe(Al) solid solution is determined as 40kcal/mol which indicates iron diffusion is significantly slower than aluminum

diffusion in BCC iron. The interdiffusion coefficient, which is affected by the aluminum content at all temperatures, reaches its maximum value at the point where the aluminum content causes the transition from disordered to ordered structure as seen in the Figure 2.9 [79].

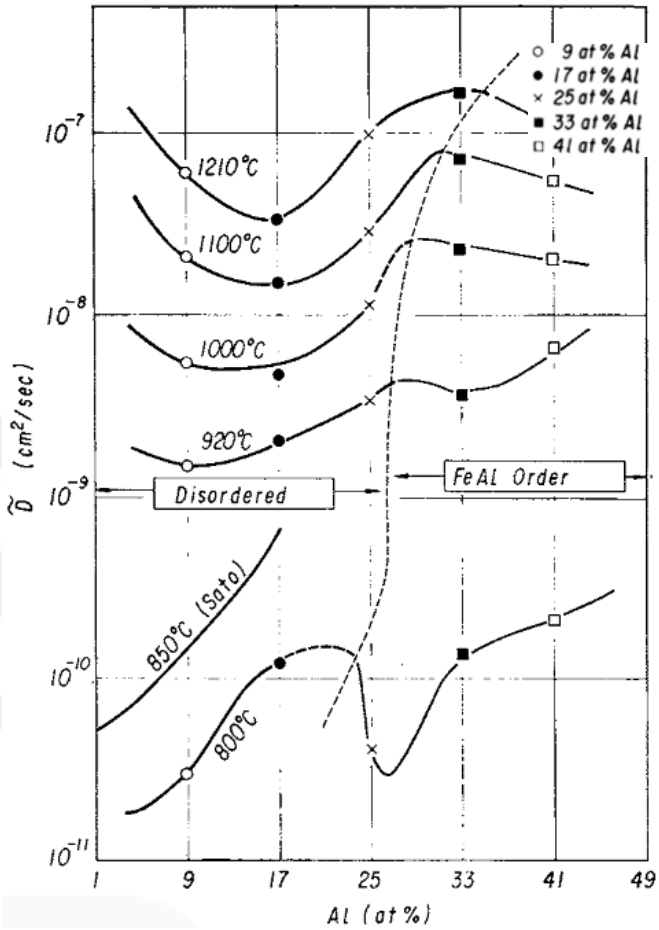

Figure 2.9 : Temperature and composition dependence of diffusion coefficient in Fe-Al solid solution [79].

In the study of Nishida et al. a marker was embed in iron surface before diffusion annealing in aluminum vapor system at the temperature range of 800-1000°C. Upward movement of marker indicated faster diffusion of aluminum than that of iron. Besides as temperature increases, the marker position was found in higher aluminum concentration regions which corresponded to the ordered phases. [80].

3. CORROSION OF IRON ALUMINIDES

Iron aluminides have attracted attention in terms of their mechanical properties and, being cheaper and accessible than strategic elements, as well as forming a protective compact oxide layer on the surface in oxidizing environments and have been used in elevated temperature applications. The use of iron aluminides as structural materials at high temperatures has increased with the prevention of the sudden strength decrease at high temperatures above 550^{o}C, which restricts the industrial use of these materials, and has become a rival to many alloys. Concomitantly these developments, iron aluminides were taken to be utilized widely as structural material or coating in high-temperature applications such as; high-temperature chemical and metallurgical processes; any processes where combustion is embraced in the way that gas turbines, engines, destructors; gasification processes as in coal gasification, heat loaded parts in nuclear reactors. In addition to high temperature corrosion resistance, these materials have started to be used in room temperature applications and aqueous environments by forestalling the ductility drop issue at room temperature, which has given rise to the tendency of iron aluminides to studies on aqueous environment corrosion. With the improvements made, iron aluminides have been a candidate for use in applications with aqueous media contact as in; waterworks parts as pipes and tubes; food industry; biomaterials such as surgical materials or implants [2,17,71,81].

When all these are taken into consideration, it is convenient to approach the corrosion behavior of iron aluminides under the titles of high-temperature corrosion and owing to the developments made in recent decades, the aqueous environment namely electrochemical corrosion.

3.1 High Temperature Corrosion

High temperature corrosion can occur in different ways namely oxidation, carburization and halogen corrosion, sulfidation, molten salt corrosion, depending on the conditions in which the materials are used and the overall corrosion reaction characteristics. Most of the high temperature corrosion reactions depend on the

oxidation reaction in that in the presence of corrosion attack the alloys form an oxide layer on their surfaces which may protect them. Besides, oxygen activities are high enough for oxygen to be involved in the corrosion reaction in most industrial settings [82]. Although it was first stated in 1934 [83] that iron aluminides are a candidate materials showing resistance to oxidation at elevated temperatures, the corrosion behavior of iron aluminides in several different corrosive states is a more recent issue. In recent studies, iron aluminides are considered corrosion resistant alloys for high temperature use in a variety of aggressive environments. [84]. Due to their corrosion resistances in these environments, iron aluminides have a fairly range of commercial operation areas as structural materials or coatings at temperatures range between 600-1300°C [85].

3.1.1 Oxidation

The remarkably resistance of iron aluminides to corrosion is due to the fact that they form a dense, protective and chemically stable alumina scale. Among these alumina scale, α-Al_2O_3, has lowest rate constant relatively even at temperatures as elevated above 1000°C [86]. Alumina sustains its stability even in a lack of oxygen. Furthermore, alumina, contrary to chromia formed on the surface of traditional stainless steel and nickel-based alloys, persists at temperatures above 1000 ° C without evaporation [87].

The equilibrium oxygen partial pressure of some metal oxides and oxygen partial pressures in industrial processes are given in Table 3.1 and Table 3.2, respectively. According to Table 3.1 and Table 3.2, it can clearly be seen that only alumina formers can encounter the required stable oxide scale in goal gasification and petrochemical plants. Based on the data in the table, although there is not much difference between the alumina scales that nickel aluminides and iron aluminides form on their surfaces, iron aluminides have some advantages as given below:

Thermal stability of iron aluminides is higher than nickel aluminides. In iron aluminides, diffusion coefficient of aluminum is higher because of their ferritic structure when compared to austenitic Ni_3Al. The slow diffusion of aluminum in Ni_3Al results in aluminum depletion under the alumina scale and the generation of a nonprotective nickel oxide layer [87].

Table 3.1 : Equilibrium partial pressures of some metal oxides [87].

Oxides	PO_2/P_oO_2
$^2/_3Al_2O_3$	$1.6x10^{-34}$
$^2/_3Cr_2O_3$	$3.4x10^{-22}$
2 NiO	$9x10^{-11}$
½ Fe_3O_4	$4.9x10^{-15}$
$^2/_3Fe_2O_3$	$9.5x10^{-14}$

Table 3.2 : Oxygen partial pressures of some high temperature processes [87].

High temperature processes	Oxygen partial pressure in bar
Petrochemical plants	10^{-25}-10^{-30}
Gas cooled reactors	10^{-25}-10^{-30}
Fluidized bed combustion	10^{0}-10^{-5}
Coal gasification	$\approx10^{-25}$

Although oxidation rate of iron alloys is suppressed by small amount of added aluminum (4%), the minimum aluminum concentration required to impede the overgrowth alumina scale and internal oxidation at 800 °C, is about 14%. Since the affinity of oxygen in aluminum is higher than iron (the standard Gibbs energy of formation of α-Al_2O_3 is -1.582, 260 J/mol and ≈6.5 times higher than which of FeO), aluminum oxide formation occurs preferentially over iron oxide formation [36]. Fe atoms may be oxidized at the beginning of process. It is important to have sufficient aluminum concentration in the alloy to provide protection by forming a Fe-Al spinel layer underneath the outer layer of Fe_2O_3 and Fe_3O_4, and preventing the diffusion of Fe ions to the outward. With the increasing amount of aluminum, firstly Al_2O_3 starts to form instead of spinel and Fe_2O_3 layer, afterwards, external formation of Al_2O_3 takes place [88]. These critical amount of aluminum concentrations can be reduced and increased by adding chromium and nickel respectively [1,89]. Similarly, the oxidation resistance of Fe_3Al was modified with the add-on elements and it was stated that 5% Ti, 10% V and 2.3% Mo added to iron aluminide caused a decrease in oxidation resistance at 1089K [83].

With the formation of the alumina scale, its adhesion to the underlying layer and its strength became the determinants of the high temperature oxidation resistance of the material. It has been observed that the scale contains porous transitional

alumina (γ-Al_2O_3, δ-Al_2O_3 and θ-Al_2O_3) at the temperatures lower than 1200 °C, and α-Al_2O (corundum) in stable form of alumina at higher temperatures [12]. As the temperature increases or as time progresses, metastable phases transform to stable phase. Thus, the existence of Fe_2O_3 contents relies on time, temperature, and Al content in the alloy [36].

3.1.2 Sulfidation

Iron aluminides have an outstanding sufidation resistance in the sulfur bearing environments. Since the sulfidation of iron aluminides at high temperature will differ depending on the sulfur forms and the partial oxygen pressure in the environment [84], the sulfur-containing media will be examined by divided into two titles as sulfur vapor and mixture of H_2-H_2S; mixed-gaseous environments.

3.1.2.1 Sulfur vapor and mixture of H_2-H_2S

In studies conducted by adding aluminum to iron and iron-chromium alloys, it has been observed that the addition of aluminum increases the sulfidation resistance of the alloy remarkably in sulfur vapor or H_2S/H_2 mixtures environments; besides, the increase in the Al/Cr ratio supports this resistance [1]. Strafford and Datta [90] states that preferentially usage of aluminum as an alloying element at these environments arises from the fact that aluminum sulfide has higher thermodynamic stability than iron sulfide (ΔG^o_{298} = -130 kcal/mole and -65kcal/mole respectively), aluminum undergoes sulfidation with a lower rate than iron and chromium do, and aluminum sulfide has a relatively large molecular volume. Strafford and Manifold [91] proposed a mechanism for iron aluminade with 5wt% Al in the sulfur vapor environment (1atm) and temperature range of 500-700°C that, in the first stage of sulfidation which is parabolic stage, a compact layer of iron sulfide is formed by diffusing Fe^{+2} ions to the scale/sufide interface while vacancies flows opposite direction. At this stage, although thermodynamically formation of aluminum sulfide is possible, the diffusional growth rate, which is a kinetic factor, is faster for iron sulfide. The movement of the vacancies causes the formation of gaps at iron sulfide/alloy interface, as a result, the sulfur vapor formed by the dissolution of iron sulfide reacts with the alloy and causes the iron sulfide and aluminum sulfide scale to grow further. At the point where, outer growth of iron sulfide scale becomes dependent on the diffusion of Fe^{+2} ions through inner FeS+Al_2S_3 layer to outer layer, Al_2S_3 particles hinder the movement of Fe^{+2} ions and

outward FeS scale growth becomes linear. However, at the temperatures between 800-1000°C and the sulfur pressures higher than 1 torr, iron sulfide formation is not hindered by Al_2S_3 thus, sulfidation rates increases sharply even though higher aluminum content than 18 at%. Sulfidation resistance disappears with increasing temperature because of the porous scale formation adjoined to alloy and mechanical deformation of the surface of alloy by precipitates of internal sulfides [1]. Setterlund and Prescott [92] revealed that alloying iron with aluminum increases sulfidation resistance at 540°C in H_2/H_2S environment in an empiric manner.

3.1.2.2 Mixed gaseous environments

In many industrial high temperature applications, sulfur coexist with oxygen, carbon, chlorine and/or hydrogen. Flue gases containing SO_2 and high oxygen partial pressure [$p(O_2)$], syngas with high sulfur partial pressure [$p(SO_2)$] and low oxygen partial pressure [$p(O_2)$], which are formed by gasification of coal, are some of them. In these applications, even the low oxygen partial pressure is adequate to form an alumina layer on FeAl and Fe_3Al alloys. The adherence and integrity of the formed alumina layer specify the corrosion behavior of alloys on which it forms. We can see from the studies that in a mixed gas atmosphere containing sulfur and oxygen, the presence of Al_2O_3 layer provides an unrivaled corrosion resistance. In the study of Gesmundo at al., [93], FeCrAl alloy was exposed to a H_2S-CO_2 mixed gas atmosphere of high [$p(SO_2)$] (10^{-6} atm) and low [$p(O_2)$] (10^{-20} atm) at 700 °C, and was able to achieve a corrosion resistance equivalent to FeAl alloy when only pre-oxidized. DeVan [94] supported the claim that FeAl and Fe_3Al alloys has sulifdation resistance better then Fe-Cr-Alloys with the study in same pressure conditions at 800°C. Besides, in the low [$p(O_2)$] and high [$p(SO_2)$] atmospheres, iron aluminides have comparable means of corrosion resistance with major heat resistance alloys as MoSi and TiAl. The corrosion behavior of iron aluminides, in the combustion atmosphere is similar to seen in air and pure oxygen environments with low [$p(SO_2)$] high and [$p(O_2)$] which are contrary to described so far. In the environments of mixed gases with more than 1% SO_2 the oxidation behavior of iron aluminides corresponds to that of pure oxidizing media [84].

3.1.3 Carburization

According to the limited studies on the carburizing of iron aluminides, in order for iron aluminides to be resistant to corrosion as in a sulfur bearing mixed gas atmosphere,

oxygen and carbon partial pressures are required to support the stability and formation kinetics of the alumina layer. In the study of Smith et al, it is claimed that by the reason of the alumina layer as an obstacle to carbide formation, resistance of FeAl alloys to high temperature carburization is above of commercial heat resistant alloys [84]. In applications at temperatures below 815°C, carburization is no longer a problem due to its low kinetic factor, instead the metal dusting becomes a threat. With increasing amount of Al and temperature, metal dusting resistance of iron aluminides, which arises from alumina layer formation, is enhanced, according to literature [95]. Strauß et al. have revealed that deterioration of FeAl arises from metal dusting in high carbon activity conditions can be depressed by alloying 2-4% Cr [96].

3.1.4 Halogen corrosion (gaseous corrosion by chlorine and hydrogen chloride)

According to the systematic literature study conducted by Natesan [97], it has been observed that in a mixed gas atmosphere containing approximately 2% HCl, Fe_3Al has sufficient high temperature corrosion resistance. He also claimed that corrosion resistance of iron aluminides decreases barely in a H_2S-H_2 -H_2O atmosphere with HCl. Contrary to the behavior in H_2S-H_2-H_2O atmosphere, the corrosion resistance of the Fe_3Al alloy containing 5% Cr in the combustion gas atmosphere in the presence of HCl is superior to the alloy containing 2% Cr [84]. In the study of Saunders et al. [98]it is observed that in H_2S-H_2-H_2O-HCl atmosphere at 450 and 500°C, Fe_3Al-Cr alloy exhibits better corrosion resistance then Fe-16%Al-5%Cr alloy. However, although Fe_3Al alloys exhibit good corrosion resistance at high temperatures and these atmospheres, with exposure to acidic condensates with cooling, a significant degradation occurs [99].

3.1.5 Hot corrosion

Hot corrosion arises from deposited salts, on materials in contact with salt melts, can occurs in many industrial environments as in heat-transfer and energy-storage in solar and nuclear energy systems, fuel cells, batteries in high temperature applications, heat treating industry and metallurgical extraction industry [37,82]. Although, there is lack of corrosion resistance of iron aluminates in the presence of molten sufates in SO_2 mixed gas environment, it has been observed in the study conducted by Gleeson et al. [100] that the alloying with Cr will decrease the corrosion rate; however, the studies on alloying in the literature are limited [59]. The moderate corrosion resistance of

Fe_3Al alloys in the environment where melt alkali sufates exist, superior to corrosion resistance in the presence of $CaSO_4$ deposits formed in the fluidized coal combustion atmosphere. During combustion, sulfur and/or chlorine react with other foreign substances in the fuel and feed the salt vapor, and accumulate on the parts during cooling. In many cases, ashes from the combustion of minerals also gathered as the content of these deposits [82]. According to studies on effects of alloying, in the simulated flue gas atmosphere with 0.25-1% SO_2 (14%CO_2-10%H_2O-4%O_2 and balance N_2), in the presence of ashes as Fe_2O_3, K_2SO_4, Na_2SO_4; at 650-700^oC, Fe_3Al-Cr alloy (2% Cr) exhibited lower corrosion resistance whereas Fe_3Al-Cr alloy (5% Cr) had the same resistance with 347 stainless steel. However with increasing exposure time, Fe_3Al-Cr alloy (5% Cr) exhibited best corrosion resistance in all [101]. With regard to the studies at highly oxidizing environment of chemical air separation which involves molten $NaNO_3$-KNO_3-Na_2O_2 (at 650^oC), as amount of aluminum content increased, corrosion resistance increased outstandingly. Furthermore, it is claimed that iron aluminides, especially when they have higher amount of aluminum then 30%, exhibit superior corrosion resistance to stainless steels, nickel-base alloys, refractory metals [102]. At temperatures lower than 600^oC in the $NaNO_3$-KNO_3-Na_2O_2 atmosphere in the absence of Na_2O_2 which accelerates corrosion rate , it is expected that iron aluminides exhibit remarkable corrosion resistance [82].

3.2 Electrochemical Corrosion of Bulk Iron Aluminides

Iron aluminides are become more widely used since progress was made on their room temperature mechanical properties through addition alloying elements and achieved microstructural control by modifications in production methods [17,81,103]. Iron aluminides are exposed to several different aqueous environments including their common use in sulfur-containing applications; chlorine-containing seawater atmosphere; in liquid body substances as being biomaterials, replacing stainless steels; and in the food industry, replacing crucial metals such as Cr and Ni [17]. With respect to the systematic literature researches, studies have been carried out on the electrochemical corrosion behavior of different compositions of iron aluminides in various electrolytes such as acidic, basic, chloride and sulfur-compound solutions with different approaches and the effect of alloying elements on this corrosion behavior has been investigated [16–25,70–73,103–131]. In Table 3.3, the studies on the

electrochemical corrosion behavior of iron aluminides in the aqueous environment are listed, each with references, as the environment in which they are examined, the composition of the alloy, and the applied approaches. Below, respectively; the mechanism of electrochemical corrosion resistance of iron aluminides; the electrochemical behavior of iron aluminides; the effect of alloying elements on this behavior; and the comparison of iron aluminides with rival stainless steel and aluminum rich steels are included.

Table 3.3 : Studies on the electrochemical corrosion behaviour of iron aluminides in aqueous environments.

Alloy (at.%)	Electrolyte	Approach	Method	Ref
Fe-25Al	0.25M H_2SO_4	Repassivation kinetics and mechanism	Rapid scratched electrode technique	[104]
Fe-25Al	0.25M H_2SO_4	Effect of alloying with C	Potentiodynamic polarization	[107]
Fe-24.4Al	0.5 M H_2SO_4,	Passive film formation mechanism	Potentiodynamic polarization	[22]
Fe-26Al	0.5 M H_2SO_4,	Dependence to surface crystallography	Potentiodynamic Polarizaton, EIS	[130]
Fe-24wtAl	0.5 M H_2SO_4 (deareated)	Mechanism behind anodic polarization	Potentiodynamic polarization, Polarization resistance (R_p) tecnique	[19]
Fe-28Al	1M H_2SO_4, 1M NaOH, 0.05 M Na_2SO_4 + 500 ppm NaCl	Dependence to pH, passive film stability, effect of alloying element	Potentiodynamic polarization	[71]

Table 3.3 (continued) : Studies on the electrochemical corrosion behaviour of iron aluminides in aqueous environments.

Alloy (at.%)	Electrolyte	Approach	Method	Ref
Fe-73Al	0.01-0.1-0.6M NaCl	Effect of intermetallic particles on localized corrosion	Microelectrochemical testing	[115]
Fe-28Al	Cl^-: 50 ppm/thiosulfate 10 ppm	Repassivation behavior, effect of alloying elements	Cyclic potentiodynamic polarization, EIS	[118]
Fe26.6Al	Hank's solution	Dependence to crystal structure	Anodic polarization, EIS	[103]
Fe-8Al Fe-15Al Fe-22Al	1M NaOH 0.005 M H2S04/0.5 M Na2S04	Dependence to pH, passive film formation mechanism	Potentiodynamic cyclovoltammogramms	[21]
Fe-76wtAl	Artificial seawater	Corrosion dependence to pH	Ptentiodynamic polarization, linear polarization resistance, EIS	[117]

3.2.1 Electrochemical corrosion behavior of bulk iron aluminides

According to systematic researches, passive film formation, which is one of the fundamentals of corrosion resistance of iron aluminides, is prepossessed by the addition of a remarkable aluminum [123]. In reference to the Pourbaix diagram (Figure 3.1), the thermodynamic stability of aluminum provided by a protective and insoluble oxide/hydroxide film can be deduced as a function of pH and potential at room temperature and in Cl^- free near neutral solutions [132].

Temperature, secondary phases or precipitates in the bulk material or oxide layer, solid solutions of aluminum and additions, diversify said passivity [133]. It would be prudent to begin to examine the electrochemical corrosion behavior of iron aluminides from the effects of their constituent elements, Fe and Al, on the polarization behavior.

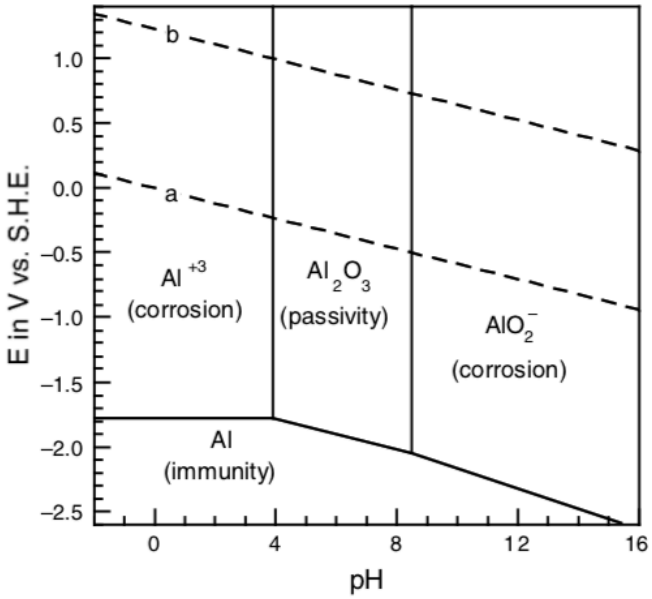

a: $2H^+ + 2e^- \Leftrightarrow H_2$

b: $\frac{1}{2}O_2 + 2H^+ + 2e^- \Leftrightarrow H_2O$

Figure 3.1 : Pourbaix diagram belongs to Al at 25°C [132].

According to the comparison of the polarization curves of Fe_3Al based iron aluminide, pure Al (99.99%) and Armco Fe in Figure 3.2 obtained from the study carried out in 0.25 M H_2SO_4 [107], although all materials differ in terms of their transition from active state to passive state, all materials have passivated. While pure aluminum passivated just above its open circuit potential (OCP), iron was actively dissolved and then suddenly passivated and iron aluminide went through an ordinary transition. The coordination of iron with lower current density in the passive region and aluminum with passivity in a wider potential range; it appears to have a supporting effect on the alloy. In the low potential region close to the corrosion potential of the iron aluminide, the reduced active dissolution rate due to the Al_2O_3 film formed by passivation of Al was supported by the presence of iron oxide at high potentials, and as a result, the current density in the passive region of the iron aluminide was lower than that of pure iron. However, the larger difference between corrosion potential (E_{corr}) and passive potential (E_{pass}) of iron aluminide than that of stainless steel, higher anodic critical current density (i_{crit}=20mA/cm^2) than its limiting current density ($i_{L=}$0.1A/cm^2) for oxygen reduction, are disadvantages for self-passivation of iron aluminides in

ventilated environments. In the meantime, it is seen that the transpassive behavior of iron aluminides (the transpassive potential is superior to equilibrium potential for oxygen formation 0.96 V_{SCE} at a measured pH of 0.6 and 1 atm assuming oxygen partial pressure) is parallel to that of iron.

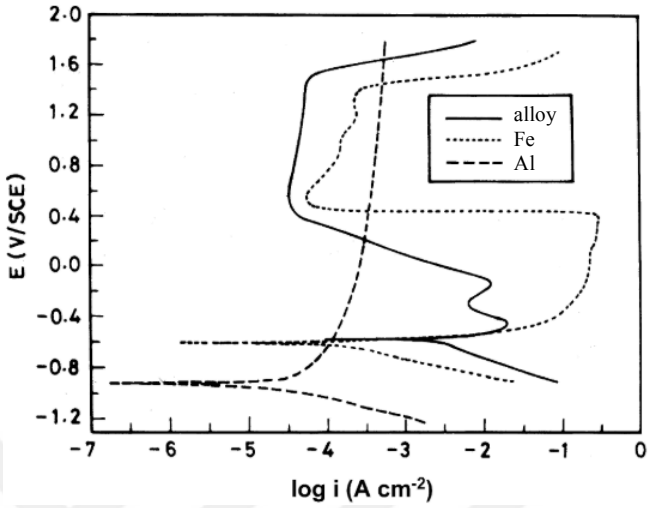

Figure 3.2 : Polarization curves of Fe_3Al and constituents of it in 0.25 M H_2SO_4 [107].

Similarly, in the study carried out by Chiang et al. [16] the passivation behavior of Fe-Al alloys containing Al in the range of 3.4-41.7% was investigated in 0.1 N H_2SO_4 solution. According to the potentiodynamic polarization curves in the Figure 3.3, when the Al content exceeds 18%, the alloy reaches a lower passive current density (i_p), indicating a relatively stable passive film. Furthermore, it is suggested that for the alloy containing 19.5% Al, the decrease in the passive potential (E_{pass}) and the significant increase in difference between breakdown potential (E_b) – passive potential (E_{pass}), compared to the alloy containing 18.7% Al, evidence that more than 19% Al enhances passivation noteworthily.

According to a potentiostatic polarization based study of Frangini et al. [22] who have worked a lot about this; While B2-FeAl (24.4%Al) and Fe that were settled in the passive region potential in 0.5 M H_2SO_4, were displaying similar behavior in terms of the change in current density, with time ($\log(i)/\log(t)$ is ≈ -1) at the region where the transition has begun, B2-FeAl reached steady-state case faster than pure iron did. Therefore, they attributed the former to oxide growth mechanisms that are high ion conduction [134] and place exchange [135], and the latter to that passive layer formation is supported by Al addition to Fe.

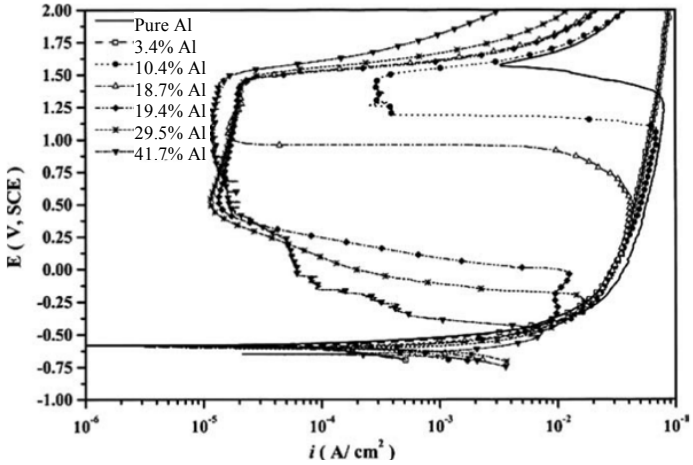

Figure 3.3 : Polarization curves of Fe-Al alloys with different amount of Al content (3.4-41.7%) and pure Fe in 1N H_2SO_4 [16].

An experiment [104] was established with rapid scratched electrode method to eliminate the oxide layer that is always present on the surface, in order examining the re-passivation kinetics. The typical current transient curves obtained from the study are given in Figure 3.4, and the results can be explained by correlating with Figure 3.2 since the selected materials and conditions are repetitions of the first study given above.

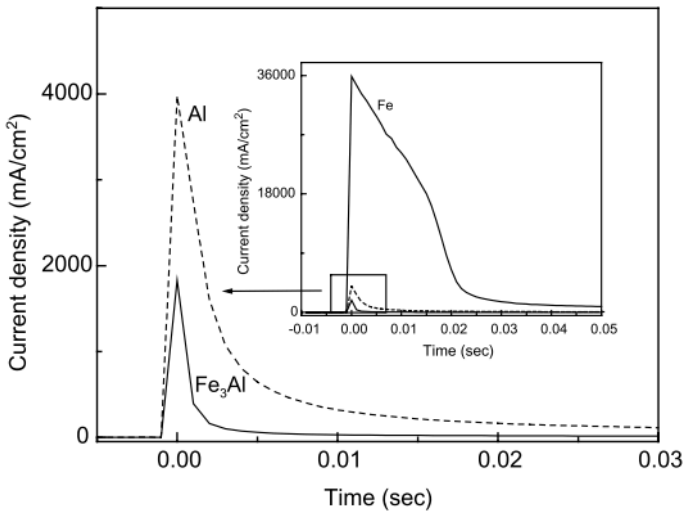

Figure 3.4 : Repassivation kinetics of Fe_3Al, Fe and Al from 0.25 M H_2SO_4 [104].

Whereupon the passive film is demolished by surface scratching, the suddenly rising current due to anodic dissolution, begins to fall with repassivation. The repassivation current density of iron is quite large, followed by that of aluminum and Fe_3Al, respectively. The discrepancy between the lower passive current density of Fe than Al and its slower repassivity than the others, put Fe_3Al with low passive current density and high repassivation rate, ahead of Fe and Al.

After having an idea about the kinetics of Fe and Al on polarization, in the grand scheme of things of the electrochemical corrosion behavior of iron aluminides: In 1974, aqueous corrosion of iron aluminates was mentioned for the first time [126]. The corrosion behavior of Fe-Al alloys containing 6-16% Al was investigated by the method of mass loss (not electrochemical in this respect) in seawater electrolyte. It was claimed that it should contain at least 10wt.% Al for corrosion resistance and the most durable alloy was subjected to erosion corrosion test. Immediately afterward, in 1976, for the first time, an electrochemical study [124] was carried out in a sulfuric acid environment with 2wt.% Al-containing cast iron, and in 1977 the same researcher repeated the experiments [116] using cast iron containing 25wt.% Al and obtained Figure 3.5.

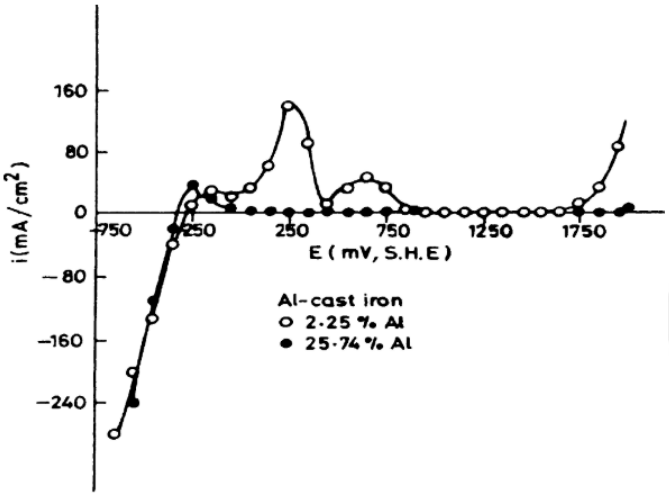

Figure 3.5 : Potentiokinetic polarization curves of cast iron containin 2.25wt.%Al and 25.74wt.%Al [116].

According to the potentiokinetic polarization curve, due to the dissolution of iron, there are two anodic peaks which are not for the alloy with a high percentage of aluminum, since the protective aluminum oxide layer presents in Al-rich alloy prevents iron dissolution.

The correlation of iron aluminides with pH was investigated in a study conducted by Schaepers and Strehblow [21], by cyclic voltammogram responses of alloys containing 8-15-22% Al, in H_2SO_4/Na_2SO_4 solution with pH of 3.8 and in a borate buffer solution with pH of 9.3. Although the polarization behavior of the alloys is similar in alkaline solution, this situation is different in acidic solution. While the low current density in alkaline solution prevents deduce the Al assistance on passivation behavior, the increasing current density in acidic solution decreased at -0.1 V_{SHE} after a few scan

rates later for the alloy containing higher amount of Al, since the oxide layer was preserved. In the study, it was concluded that the increasing amount of Al in acidic environments supports passivation.

In the manner of passivation of iron aluminides and breaking of the passivity, a study was conducted by De Cristofaro et al. [131], with FeAl intermetallic containing 24wt.% Al in borate buffer solutions, containing sulfates, chlorides, and a mixture of the two. According to the voltammetry results, a typical oxidation/reduction peak, which coincides with the study of the Frangini [106], in which is attributed to the anodic behavior of FeAl controlled by iron dissolution in the active corrosion zone and oxidation of iron in the passivity zone, was observed. The result that the oxide layer formed on the surface of the intermetallic in the borate solution with added sulfate is nobler was associated with the passive layer accomplished by Fe (1) and Fe (2) in the presence of sulfate while accomplishing by Fe (3) in the absence of sulfate. It has been observed that alloying with Al supports passivation in this environment. However, when more than $6x10^{-4}$M NaCl was added to the buffer borate solution, FeAl (the iron already suffered from the localized corrosion) that had not been suffered from localized corrosion until then starts to suffer from pitting. The pitting corrosion potential of FeAl is affected by Cl^- concentration as a decrease with a linear slope of 0.40V/decade by increasing concentration. This highlights the importance of the electrolyte and comprised ions, on the corrosion behavior.

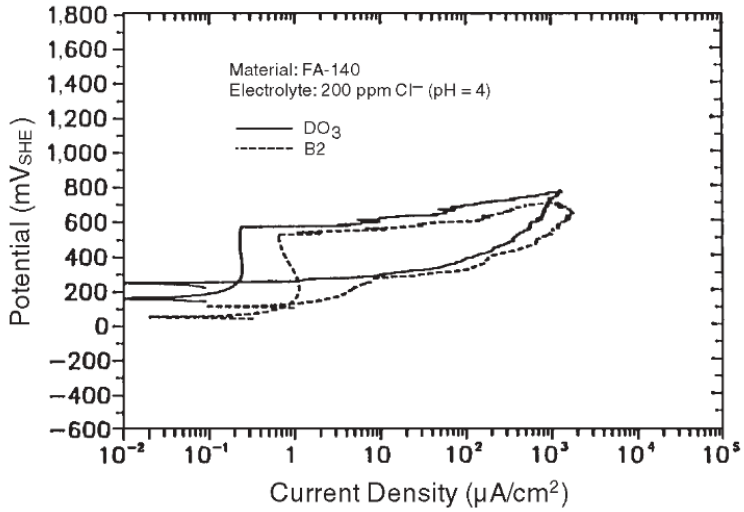

Figure 3.6 : Cylic anodic polarization behaviors of DO_3 and B2 structures of iron aluminde in aerated 200ppm Cl^- solution with pH=4 [25].

Once again in a solution containing Cl^-, which is for simulating severe acid rain, a study was accomplished by Kim and Buchanan [25] to determine the corrosion behavior of Fe_3Al in the form of both B2 and $D0_3$ structures. The localized corrosion of $D0_3$ superior to that of B2, inferred from the lower passive current density and higher breakdown potential, of $D0_3$ as in the Figure 3.6.

Another study on the effect of different structures on the corrosion behavior was done by García-Alonso [103] in Hank's solution. According to the claim, all the structures of alloy exhibited similar uniform corrosion properties, but disordered structures were subjected to localized corrosion more than ordered ones. Moreover, Fe_3Al in four different structures, which exhibit close uniform corrosion behavior with 316L stainless steel, also performed local corrosion resistance superior to 316L stainless steel, but once suffered from pitting, their repassivation behavior was observed to be poorer. In Figure 3.7, it is possible to see the crystallographic nature of the attack occurring in 0.5M NaCl in ordered form of Fe_3Al and the grains inside localized corrosion [81].

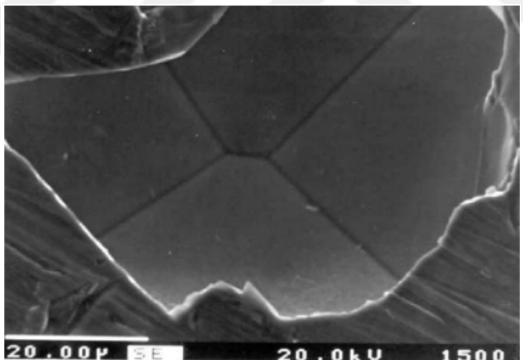

Figure 3.7 : SEM image of pit formed on ordered Fe_3Al in 0.5M NaCl [81].

Later on the studies about structure related corrosion properties, Brito et al. [130] conducted a study on the relationship between the surface crystal structure of the Fe_3Al ($D0_3$) alloy and its corrosion behavior. Single crystals of Fe-26Al with crystallographic planes of (100), (110) and (111) were subjected to 0.5M H_2SO_4. If planes with higher planar density exhibit better corrosion behavior due to their higher chemical stability, this order would be (111) > (100) > (110). It was revealed that crystal orientation affects electrochemical corrosion rate; however, according to i_{crit} values obtained from polarization curves, corrosion rate followed the order of (100) < (110) ≈ (111) which deny above assumption.

As follows, the studies on the regressive effects of Al on cathodic potentials below the open circuit potentials of iron aluminides are given, until now its contribution to the passivation behavior above this potential has been described.

In a study [19] in which linear polarization resistance was used to determine the corrosion current density corresponding to the open circuit potential, this regressive effect of aluminum was investigated in 0.5M H_2SO_4 solution with B2-FeAl. Frangini indicated that the addition of aluminum causes an increase at corrosion rate, which is deduced from that the hydrogen evolution reaction, initially drawn with a slope of 120 mV / decade as same for iron and B2-FeAl, decreased over time for the latter (Figure 3.8).

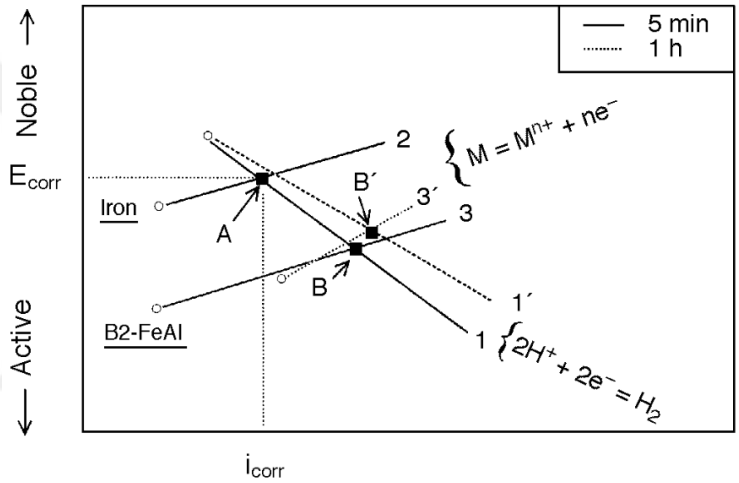

Figure 3.8 : Sketched Evans diagram with electrode reactions on pure Fe and B2 FeAl [19].

Then, in the study performed by Shankar Rao et al. [107] in 0.25M H_2SO_4 solution, it was revealed that the hydrogen exchange current density of Fe_3Al, hence the corrosion rate, was greater than that of iron. It is worth mentioning here that the diffusivity of liberated nascent hydrogen in the lattice of iron aluminide is very low and generally decreases with increasing Al content in intermetallics[108].

Electrochemical impedance spectroscopy, a technique used for the last 3 decades to study passive film behavior, was first applied in a study by Frangini and Lascovich [111]. In this study, where the passive film properties formed on FeAl were examined in terms of impedance at potentials corresponding to the full passivity region and the thickness of the passive film, the experiment was set up in 0.5M H_2SO_4 solution. At a low-frequency corresponding to 70 Hz, the presence of two time-constants deduced from the breaking point of both the phase shift and the impedance (Figure 3.9), are

predicated to the charge transfer on scale-solution interface and ion conduction within the passive film. Above 1.0 VSCE, the reduction in passive film thickness together with the reduction in capacitance is an indication of the initial non-porous structure and subsequently losing compactness. The ion conduction in the film on the alloy surface predominantly in regions of low electric field strength, which is propounded via *i*R is taken as a function of the potential change, shows that passive film exhibits Ohm's type behavior.

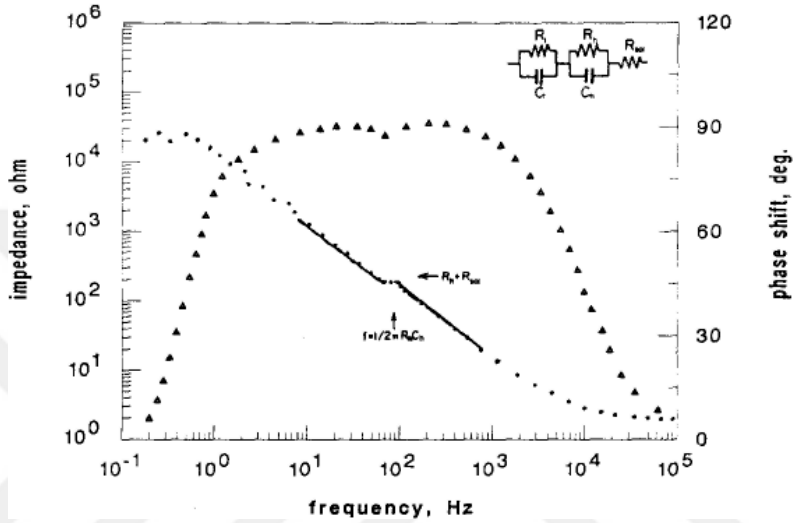

Figure 3.9 : Bode (**Δ**) and phase shift (·) diagrams of FeAl pasivated at 1.0 V and equivalent circuit [111].

The protection provided by the alumina layer formed on the surfaces of iron aluminides in high temperature applications led to the idea of using this inert layer at low temperatures. For this reason, in the study conducted by López and Escudero [120], the aqueous corrosion resistance of iron aluminides that both is highly alloyed and one is strengthened by oxide dispersion (ODS), by the form of heat-treated (at 1100 degrees for 2 hours) and untreated, were examined in a solution containing Cl^- (pH= 7.4). In the study, by using AC impedance, the resistance of charge transfer (R_t) and apparent capacitance (C_{ap}) values were obtained for samples that were oxidized by heat treatment and untreated. However, contrary to the expected improvement, low protectiveness was found, attributed to the presence of oxides other than alumina in the layer. Again, in a later study conducted by Escudero and López [125], the corrosion behavior of highly alloyed Fe-40Al in Hank's solution after pre-oxidizing was investigated. Although the resistance in the bode diagram was higher for all frequency values for the sample with an oxide layer on it, a complete corrosion protection could not be mentioned due to the discontinuity of the oxide layer.

3.2.2 Effect of alloying elements on corrosion behavior of bulk iron aluminides

Alloying with an element other than iron and aluminum has been used to improve mechanical properties as strength drop at high temperatures, poor ductility at low temperatures, and oxidation behavior, of iron aluminides. This later gave rise to the approach to investigate the effect of alloying elements on aqueous corrosion behavior [81]. Within the scope of this approach, in line with the contributions of the Cr add-on; in the study conducted by Kim and Buchanan [25] to examine the pitting and crevice corrosion behavior of Fe-28Al, in H2SO4 solution containing 200ppm Cl^-; it was revealed that the corrosion behavior changes positively, in the point of breakdown potential shifting to noble directions with direct proportion to the add-on. In his study, Balasubramaniam [136] applied the mixed-potential theory for the first time to iron aluminates in order to clarify the contribution of Cr addition, by positioning the experimental polarization results for Fe-25Al and Fe-28Al-5Cr on the Evans diagram theoretically. But this theory has not gained much thrust in published works related with corrosion behavior of iron aluminides after this. In addition to bulk material alloying with Cr, studies have also been carried out on the corrosion behavior of iron aluminides if Cr is included in the process from solution. In a chloride borate solution, Frangini et al. [24] compared the pitting corrosion resistance of Fe-Cr steel (12-24% Cr) with that of FeAl, on which a passive film formed by consecutive cycles of oxidation/reduction reactions in an alkaline chromate solution. The analogous pitting potential of stainless steel and iron aluminide, despite higher Cr in the passive film formed on the former than formed on the latter; was attributed to the simultaneous existence of Cr and Al.

Mo positively affects the corrosion resistance and adhesion of the alumina layer formed on the surface, respectively, of stainless steel and iron aluminides. In this respect, one of the studies, by Choe et al. [114], it was investigated how positively effect Mo and Cr additions improve the corrosion of Fe_3Al in 0.25M H_2SO_4. It is revealed that alloying with Mo accompanied by Cr improves the corrosion behavior, in regards to cause an increase in corrosion potential and decrease in active, passive and critical current densities. Since the addition of Mo makes it difficult to adsorb Cl^- ions on the surface, as expected, it was observed according to the cyclic polarization test that pitting and repassivation potentials were increased by Mo addition more than that were increased by Cr addition, in 0.1M HCl solution. Related images can be seen

in Figure 3.10. In addition to Mo and Cr, the corrosion resistance of iron aluminides alloyed with B was also subject to this study. Boron, which could not provide an improvement in corrosion behavior according to the polarization curve, increased intergranular and granular corrosion by settling at the boundaries according to the EPR (electrochemical potentiokinetic reactivation) test.

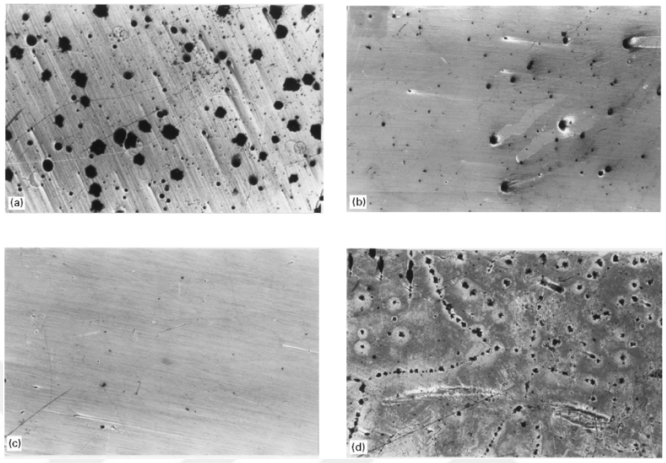

Figure 3.10 : Optical micrographs of iron aluminides after CPP test in 0.5M HCl (a)Fe-28Al, (b) Fe-28Al-6Cr, (c) Fe-28Al-6Cr-1Mo, (d) Fe-28Al-6Cr-0.02B [114].

The passive film behavior of Fe-Al-Cr alloys with different amounts of Mo addition has been investigated in thiosulfate–chloride solution (simulation of sulfur bearing environment) by AC impedance method at the states of breakdown, passivation and repassivation, by Choi and Kim [118]. It was deduced that alloys alloyed with Mo exhibit higher R thus, higher resistance to corrosion. Furthermore, they revealed that best pitting potential is gathered in coexistence of Mo and Cr in agreement with Choe et al. [114].

With the recognition of the forward hydrogen embrittlement properties of Fe_3Al-Fe_3AlC dual-phase compared to that of single-phase, studies were carried out with the expectation that the C addition will affect the electrochemical corrosion behavior in the same way [23,107,129]. According to Figure 3.11 gathered from the study in which the effect of different amount of C additions to corrosion behavior of Fe_3Al (16 wt.% Al) in 0.25 M H_2SO_4 solution was examined, corrosion rate increases proportionally with C content. The regression on corrosion behavior was attributed to the selective dissolution (Figure 3.12) of the second phase carbides (Fe_3AlC), which precipitated in the Fe_3Al matrix and had an increasing volume fraction in proportion to the increasing amount of C [107].

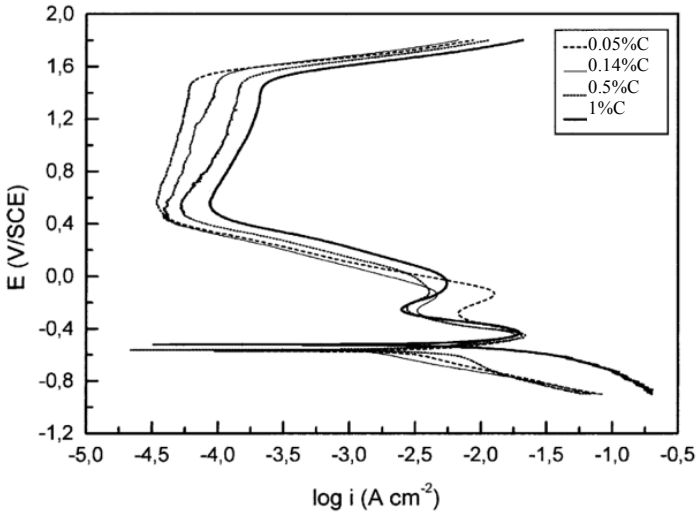

Figure 3.11 : Polarization behavior of iron aluminides containing different amount of C in 0.5N H_2SO_4 [107].

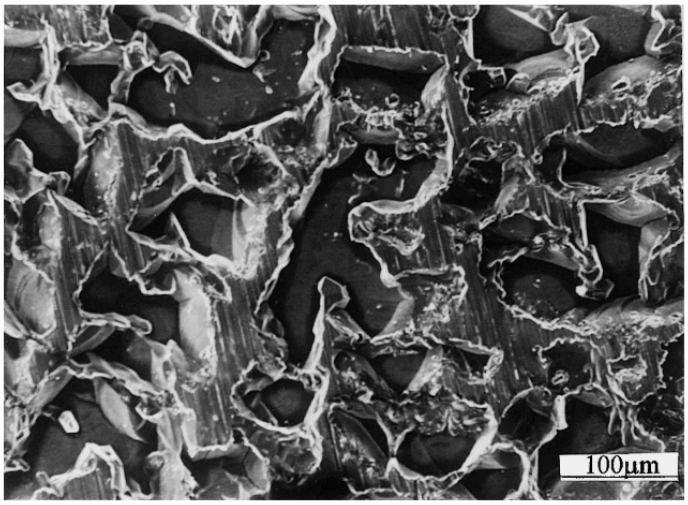

Figure 3.12 : SEM micrograph of iron aluminide (containing 1% C) immersed in 0.5N H_2SO_4 [107].

According to a study that is a continuation of former study, the reduction of Al content from Fe-Al-C alloys did not cause a change in corrosion rate in the active region, although it negatively affected the corrosion behavior in terms of causing an increase in passive current density and in critical current density, just as in Fe-Al binary alloys [23]. There is a striking point in these studies that the carbide phases are selectively dissolved in alloys with high Al content, while the situation is changed as a uniform dissolution for alloys with low Al; is not arises from increased corrosion resistance of the carbide phase, but the reduced corrosion resistance of the matrix phase as a result of the decrease of Al only from the matrix phase [23,107].

3.2.3 Chemistry and mechanism of the passive film formed on iron aluminide

After, mentioning the corrosion kinetics of iron aluminides under the headings above, when the sequence comes to the structure and chemistry of the passive film formed on the surface, similar inferences have been made in studies conducted with different Al contents in different environments [21,22,24]. Namely; Al (III) oxide / hydroxide formation on the surface during passivation (Al enrichment); increased Al content in passive film evenly by amount of Al in alloy; iron oxide formation accompanying the that of aluminum oxide on the surface; formation of other oxides accompanying the formation of alumina with the addition of alloying elements [81]. The XPS spectra obtained from one of the studies carried out to clarify the structure of the oxide film formed on the surface of iron aluminides exposed to electrochemical corrosion in line with the XPS results of the layer on the surface of Fe_3Al oxidized in the air, are given below in Figure 3.13 The peak, in the binding energy of Al^{+3} ion for oxidized iron aluminide corresponds to Al_2O_3 (74.2 eV), this energy peak corresponds to Al_2O_3 (74.49 eV) and AlOOH (75.29 eV) for the one exposed to the electrochemical environment. The peaks corresponding to Fe^{+3} ions (711±2 eV) are the same in both cases. The uniformity of Fe peaks versus the diversity of Al peaks shows us the form of these metals that can be found in the film [104].

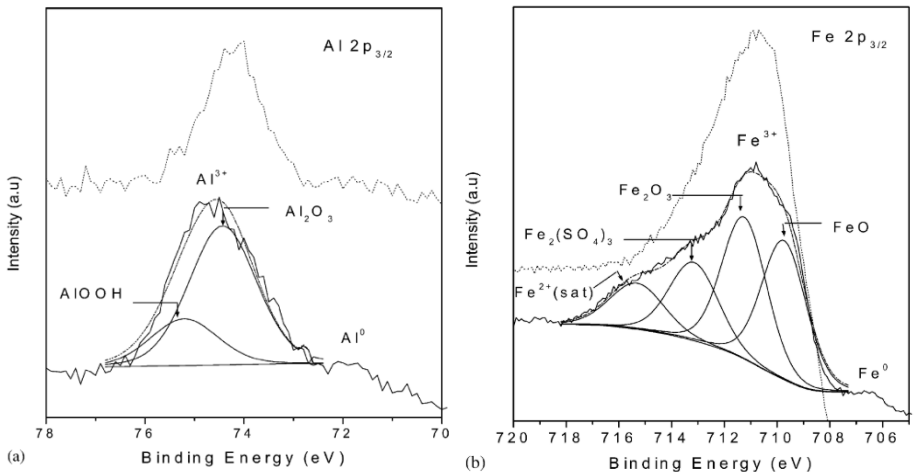

Figure 3.13 : XPS spectra for (a) Al2p3/2 and (b) Fe2p3/2 for oxidized (dashed line) samples at 800ºC and passivated (solid line) samples in 0.25M H_2SO_4 [104].

According to Frangini [24], for FeAl, while there are both Fe and Al oxides and hydroxides on the near-surface, as descended towards the alloy these oxides are replaced by only Al-rich oxide phases for the passivated surface in which a lower Al/Fe ratio than in the oxidized film exists. In a study with α-Fe(Al), the film started to form

as Al_2O_3 and AlOOH on the surface and as passivation continued, these were replaced by Fe/Al oxides and hydroxides, thus Al(III) enrichment occurred in the middle of the film [21].

It is essential to unravel the chemical/electrochemical reactions that occur at the beginning and in-process of passivation after an iron aluminide is introduced into the environment, to comprehend the mechanism of the protective layer that forms, which is essential to sense the corrosion behavior.

In an acidic solution, when the iron aluminide is polarized anodically, the reactions that take place depending on the amount of Al (FeAl-Fe_3Al) at the very beginning of the process are as follows (anode reactions and cathode reaction respectively).

$$FeAl + 6H^+ = Fe^{3+} + Al^{3+} + 3H_2 \quad (3.1)$$

$$Fe_3Al + 6H^+ = + 3Fe^{3+} + Al^{3+} + 3H_2 + 3e^- \quad (3.2)$$

$$Fe_3Al + 6H^+ = + 3Fe^{2+} + Al^{3+} + 3H_2 + 6e^- \quad (3.3)$$

$$2H_2O + 2e^- = H_2 + 2OH^- \quad (3.4)$$

Immediately afterward, Al^{3+} begin to accumulate on the surface as Al_2O_3 (as below reaction). $Fe^{3+/2+}$ with more positive free energy [21] and higher mobility [22] than Al^{3+} (thermodynamic and kinetic factors respectively), goes into solution.

$$2Al^{3+} + 2H_2O = Al_2O_3 + 6H^+ \quad (3.5)$$

The logical entailment, in which the Al_2O_3 film prevents further dissolution of $Fe^{3+/2+}$, related with the kinetic and thermodynamic factors given above, is amissed by the fact that the porous structure of Al oxide formed in an acidic environment [107]. However, with reaching the potential for pre-passivation, iron oxides take place to form on the surface (equation 3.6, 3.7).

$$2Fe^{3+} + 3H_2O = Fe_2O_3 + 6H^+ \quad (3.6)$$

$$Fe^{3+} + 3H_2O = FeO + 2H^+ \quad (3.7)$$

The pores in the oxide layer on the surface are compensated with FeO/Fe_2O_3 and a more protective film is constituted. With the onset of the presence of this protective mixed oxide layer on the surface, the lowest current density in the passive zone is reached.

AlOOH occurring at more positive potentials attributed to the below reaction.

$$Al_2O_3 + 3H_2O = 2Al(OH)_3 \quad (3.8)$$

Since these mixed oxide/hydroxides decomposition occurs at potentials more positive than the oxygen evolution, the reaction given below occurs in the transpassive zone.

$$2H_2O = O_2 + 4H^+ + 4e^- \quad (3.9)$$

The passivation mechanism of iron aluminides is shown in Figure3.14 in which mixed oxides expressed as a monolayer [81].

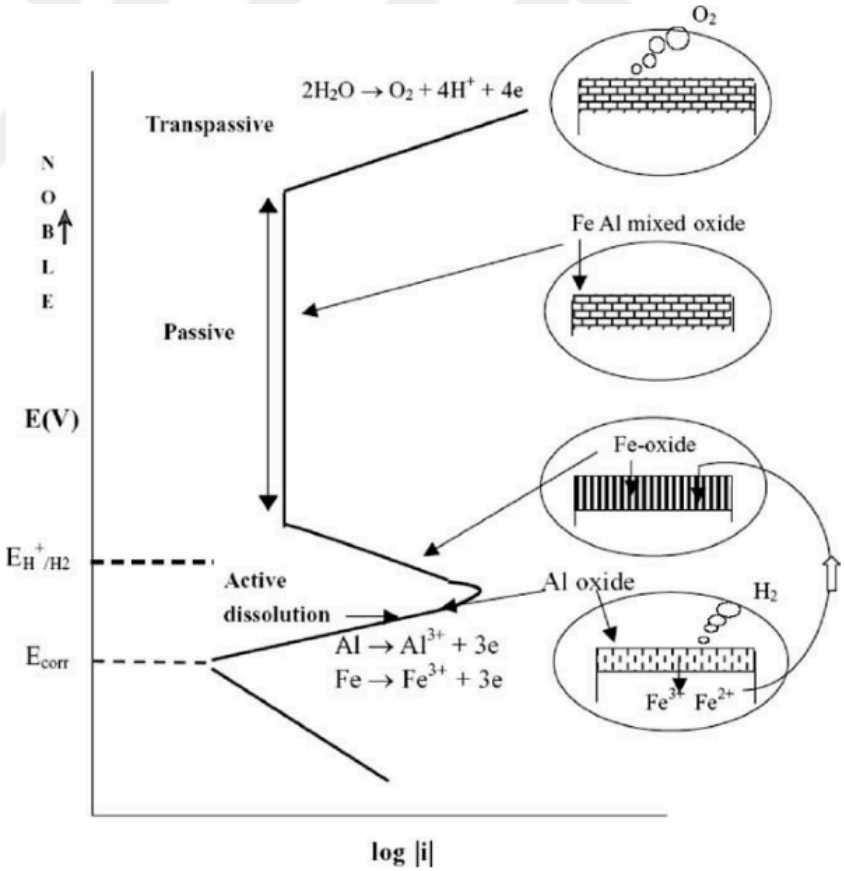

Figure 3.14 : Represantative schema for passivation mechanism of iron aluminides in acidic media [81].

3.2.4 Comparative study between corrosion behavior of bulk iron aluminide and stainless steel

The application areas of iron aluminides that intersect with those of stainless steel have led to the idea that these alloys can also be used in place of stainless steel. This possibility has encouraged studies on the use of iron aluminides as an alternative material.

In the first study conducted in this context, Kim and Bunchanan [25] compared the electrochemical behavior, in terms of pitting and crevice, of 304L stainless steel and Fe_3Al containing 28%Al. According to the study conducted in simulated acid rain, Fe_3Al exhibited worse corrosion behavior. Moreover, in the study conducted by the same researchers, the active corrosion rate of Fe_3Al in acidic and sulfur compound solutions is relatively high, while in alkaline (1M/L NaOH) solutions they exhibit quite similar behavior as both show passivation behavior at open circuit potential. In Figure 3.15, electrochemical polarization curves of 430SS (Fe-18wt%Cr) and Fe-16wt%Al in 0.25 M H_2SO_4 are given. As can be deduced from here, steel and iron aluminide do not show similar properties in the active zone [81]. Although the value corresponding to the critical current density value is slightly higher for iron aluminide, this is negligible in view of the fact that the amount of Cr contained in the steel. This resemblance is attributed to the fact that the rate of corrosion said steel in the active corrosion region depends on the preferred dissolution of iron, as the same indicated for iron aluminides by Frangini [19]. The onset of the differentiation in the behavior of the two, corresponds to shortly before the initiation of passivation. It is clear that steel makes transition to passive zone sooner which is ascribed to porous passive film formed on iron aluminides. The chemical composition of the film formed on the surface also has an effect on this, which in turn corresponds to the oxides of Cr and oxides of Fe and Al for steel and iron aluminides respectively [33]. When it comes to the region where passivation takes place completely, it is clear that stainless steel exhibits this behavior in a narrower region than iron aluminide despite its lower passive current density. The passivation zone withstands high potentials for iron aluminides, allowing interference with the oxygen evolution reaction. However, this transition will be in more active potentials for 430SS, which is associated with the dissolution of Cr oxide.

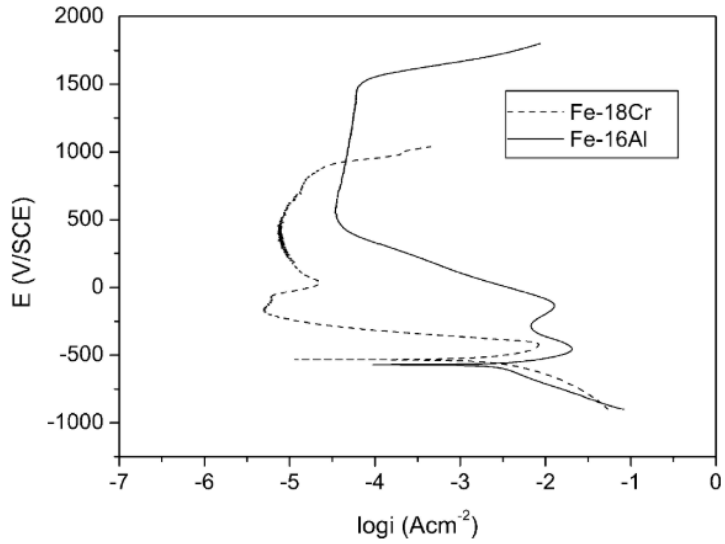

Figure 3.15 : Polarization behavior of Fe-16Al and Fe-18Cr alloys in 0.25M H_2SO_4 [81].

In order to explain the supporting effects of Cr and Al in terms of each other, a study was conducted by Wolff et al. In stainless steel containing 40wt%Cr, 5wt%Cr was replaced with Al and although the corrosion behavior of these two showed similar properties in sulfuric acid, it was observed that Al-free steel in the presence of Cl^- provided better local corrosion resistance [137]. This study is similar in approach to the effects of alloying of iron alumina on corrosion behavior.

3.3 Electrochemical Corrosion of Aluminized Steel

In order to protect steel from environmental degradation, galvanizing is one of the common methods used. It is known that the zinc layer exposed to the environment on the steel provides cathodic protection to the steel by sacrificing itself in the presence of cavity created by possible damage. Due to the decrease in zinc resources and environmental factors, aluminizing has initiate to be considered as an alternative to galvanizing. Considering that zinc is in a continuous dissolution state on the contrary to aluminum that passivates and forms an inert structure, it should be kept in mind that unlike zinc, which acts as a sacrificial anode, aluminum provides such protection only in the circumstances of the protective film is broken. The corrosion behavior of aluminized steel parts has been examined mostly in two terms, the first of which is the corrosion behavior of the top layer in the host environment and the second is whether this layer will protect the steel against corrosion in case of damages that expose sublayer or substrate in service conditions or during production [6,26–29,32]. In both

respects, since the electrochemical attack on the aluminized surface in contact with the environment is the initial governing factor, understanding the electrochemical behavior of bulk iron aluminides, which is accounted in the previous header, is a proper reference for interpreting that of aluminized steel. In Table 3.4, the studies on the electrochemical corrosion behavior of aluminized steel which is with different methods, the approach to the investigation and electrolyte where it takes place are presented with the references.

Table 3.4 : Previous stduies on electrochemical behavior of aluminized steel.

Alumination Method	Electrolyte	Approach	Method	Ref.
Hot dipping	1M NaCl	Effect of coating composition	Potentiodynamic and potentiostatic polarization	[27]
Hot dipping	1M NaCl	Cathodic protection	Localized potentiodynamic polarization	[26]
Hot dipping	Atmospheric environment	Barrier/Cathodic protection	Potendiodynamic polarization/weight loss	[28]
Pack aluminizing	Artificial sea water	Barrier/Cathodic protection	Potendiodynamic polarization-waight loss	[6]

Before proceeding to the electrochemical behavior of aluminized steels, it is useful to explain the hot stamping which is assumed depending on its purpose as a production method of aluminized steel or an application for produced version of it.

3.3.1 Hot stamping

Hot stamping steels are used as complex high strength structural components mainly for automotive applications. The process (Figure 3.16) is basically the heating of the steel to 900-950^{o}C in the furnace followed by pressing and shaping, at 600-800^{o}C and quenching to 200^{o}C by die cooling at the same time. Since the use of bare steel in this procedure, which takes place in an atmospheric environment, will cause oxidation and decarburization, and therefore undesirable effects on mechanical properties, either lubricant oil is used or coated steels are preferred which also positively affect the corrosion resistance.

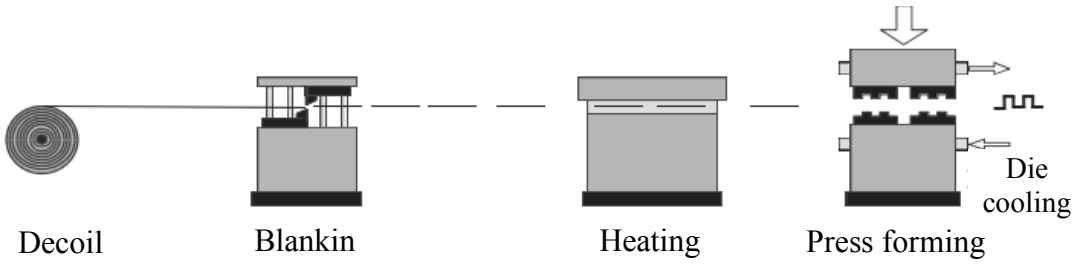

Figure 3.16 : Schematic representatin of hot stamping process [138].

Aluminized coatings are one of the favored coating kinds to ensure oxidation and corrosion resistance and painting without phosphating. There are two types of aluminized coatings used for hot stamping parts, the first is Al-Si alloy (Type1) close to eutectic composition (7-11wt.% Si), the second contains pure aluminum (Type2). These coatings are generally produced by hot dipping method. The second of these is used in applications that require a mirror-like appearance, but the first coatings are generally preferred in terms of providing phase control with the τ_5-Fe_2SiAl_7 phase acting as inhibition layer between substrate and coating. Schematic illustration of aluminized steel (Type1) before hot stamping process is given in Figure 3.17a. The presence of this phase slows down the formation of the hard and brittle Fe_2Al_5 phase during the hot dipping process. During hot stamping process, iron content of coating increases because of its interaction with substrate. Process time and temperature increase the coating thickness increases as well. Final structure is mainly Al_2O_3 at the top and five layers which is dependent to process time temperature and the pre-process coating thickness. Those layers, from top to bottom are Fe_2Al_5, τ_1-Fe_2SiAl_2, $FeAl_2$, τ_1 Fe_2SiAl_2 and diffusion layer (Fe_3Al) (Figure 3.17b). The τ_1-Fe_2SiAl_2 phase has island-type morphology, although it gains more uniform distribution and layered morphology with increasing process time, this increase affect process efficiency negatively. There is also void formation in the coating, arising from different diffusion rates of iron and aluminum in the different layers. Thus, the avoidance of the formation of brittle phases and controlling their thickness is critical in this process for controlling the cracking. Besides brittle phases, different thermal expansion coefficients of phases also give rise to these cracks [138].

Kim and Choe proposed a method [139] as to use heat treated Type1 prior to hot stamping process as called aluminide coating. By this method they expected to eliminate Fe_2Al_5 phase and obtain ductile phases to enable plastic deformation thus formation without crack propagation, during process. Additionally, it has also been

observed that these phases provide a good corrosion barrier in the absence of cracks [140]. Proposed morphology illustrated in the Figure 3.17c [138].

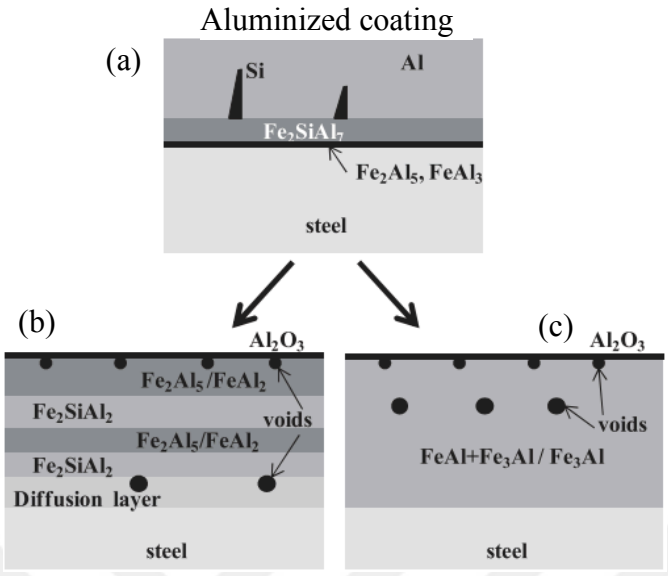

Figure 3.17 : Representative coating morphology of (a) aluminized coating prior to hot stamping, (b) aluminize coating post to hot stamping and (c) aluminized followed by heat treatment post to hot stamping [138].

3.3.2 Electrochemical corrosion behavior of aluminized steel

Since the main purpose of aluminizing steels is focused on atmospheric utilization, studies on the electrochemical behavior of aluminized steels have mostly been carried out in Cl^- containing environments [6,26–29,32].

In the study of Fleischanderl and Faderl, they determined that aluminized steel behave as a barrier to corrosion in the solution of NaCl and $ZnSO_4$; however, in the presence of a fracture when the steel exposed to solution, did not provide a cathodic protection [141]. Maki [28] examined corrosion resistance of Type1 and Type2 aluminized steels with exposing atmospheric conditions in Yawata Works, Kitatyuhu altitude of 500m for 50 years. In the Type1, since corrosion resistance of acicular Si in the Fe_2Al_8Si is higher than Al, Al corroded selectively instead of this phase (Figure 3.18a). Once the corrosion propagate it progress through aluminized layer (Figure 3.18b) and arrives substrate through alloyed layer (Figure 3.18c). Corrosion takes place along the zone between layer and steel and gets deep since steel which has a more active corrosion potential than alloyed layer.

On the other hand, for Type2, alloy layer (Fe_2Al_5 and $FeAl_2$) act as sacrifice for steel and corrode preferentially at the side where it is contacts with steel ($FeAl_2$). Thus,

corrosion depth in Type1 was less than in Type2. SEM micrographs of Type1 and Type2 before and after corrosion test in the atmospheric environment for 50 years, are given Figure3.19.

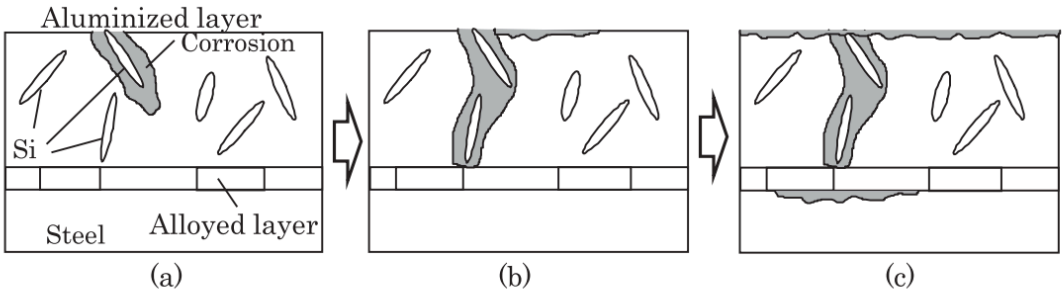

Figure 3.18 : Illustration of corrosion mechanism for Type1 (bath containing 10wt.%Si) aluminized steel (a) corrosion af Al adjacent to Si, (b) corrosion along aluminized layer to alloyed layer, (c) corrosion of steel throug cracks in the alloyed layer [28].

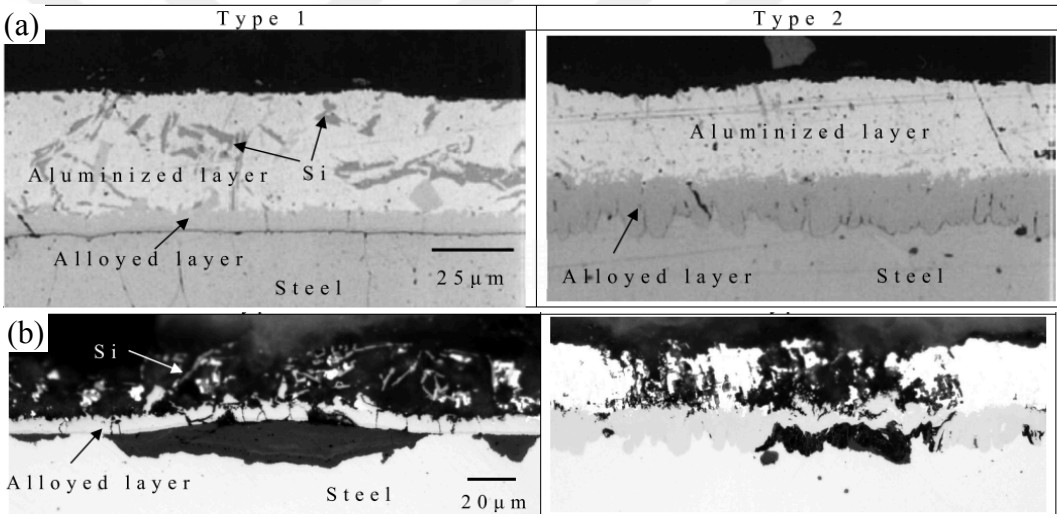

Figure 3.19 : SEM micrographs of Type1 and Type2 as (a) aluminized and (b) after atmospheric corrosion test [28].

Based on these results, in the same study, Maki examine corrosion behaviors of four different Fe-Al alloy namely, FeAl, $FeAl_2$, Fe_2Al_5 and $FeAl_3$ in simulated rain environment (200ppm Cl^- and 200ppm SO_4^2) and as a result of polarisation curves as seen in the Figure3.20a, corrosion potentials were found as the order of $FeAl_3$> Fe_2Al_5> $FeAl_2$> FeAl. Corrosion potential of aluminized steel was close to that of $FeAl_3$ and that of steel was between $FeAl_3$ and Fe_2Al_5 (Figure 3.20b).

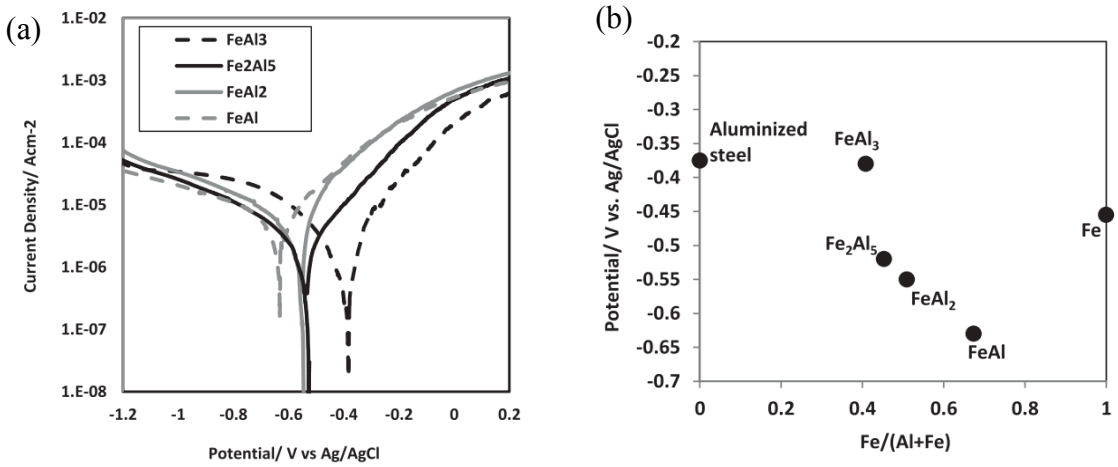

Figure 3.20 : Corrosion behaviors in in simulated rain environment in the manner of (a) polarizaton behavior of intermetallic layers and (b) corrosion potentials of intermallic layers, aluminized steel and and substrate [28].

Another study on the electrochemical interaction of cladding alloy and diffusion sublayers with the substrate was conducted by De Graeva et al. [26]. In the study, the local corrosion behavior of hot-dip aluminized IF steel, in 1M NaCl by electrochemical microcell, was investigated. On the surfaces of the samples treated in two types of aluminum baths (with and without Si), formed layers classified as the free Al layer at the outer layer, and as the diffusion layer which is divided into the upper diffusion layer ($FeAl_3$) and the lower diffusion layer (Fe_2Al_5). It is observed that as Si amount increases in the bath smother layers are obtained by preventing the formation of fingerlike morphology and the thickness of the diffusion layer is decreased. Considering the polarization curves (Figure 3.21) extracted for the phases of Si-free aluminized steel, the conclusive galvanic series is obtained in the order of $E_{corr,}Al < E_{corr}steel < E_{corr}FeAl_3 < E_{corr}\ Fe_2Al_5$. According to the order, it is concluded that the outer free Al layer provides cathodic protection to all layers including steel substrate. Among the diffusion layers of $FeAl_3$ and Fe_2Al_5 with more noble potential compared to steel, the former with its less noble potential compared to the latter due to the lower Fe content, provides cathodic protection to the latter, while the steel acts sacrificially to the latter. It is indicated that the upper layers provide cathodic protection to lower layers in case of a defect that is not reached to the steel substrate. However, in the presence of a defect that reachs to the steel, insufficient estimation could be provided.

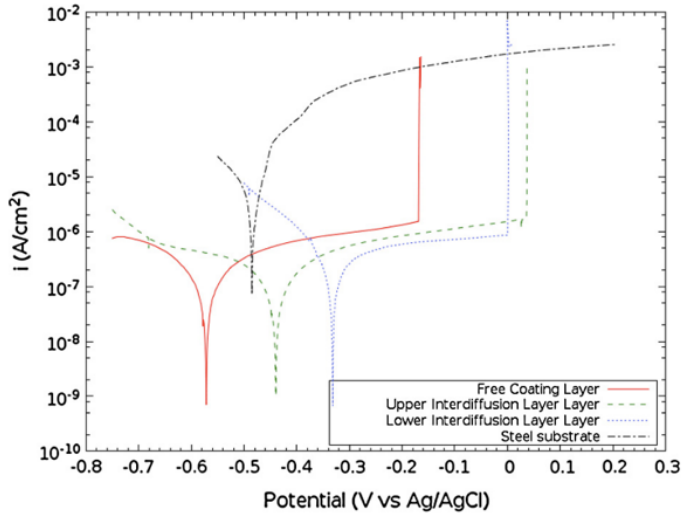

Figure 3.21 : Polarization curve obtained by the electrochemical micro-cell positioned to the Si-free aluminized steel layers of free Al, upper diffusion ($FeAl_3$), lower diffusion (Fe_2Al_5) and steel in 0.1M NaCl [26].

Besides, the passivation behavior of Fe-Al phases, which sustains up to the breakdown potential, due to included Al content, may cause a failure to protect steel by preventing sacrificial behavior. The lower breakdown potential of the free-Al layer compared to Fe-Al phases is attributed to galvanic coupling arisen from Fe_3Al precipitates in the layer. The less noble breakdown potential of the free-Al layer of Si-containing aluminized steel, than that of Si-free aluminized steel, is attributed to the higher galvanic coupling driving force caused by Al-Fe-Si precipitates in the latter compared to that caused by $FeAl_3$ in the former. Although aluminized steels may be preferred to galvanized steels in terms of not dissolving due to their passivation properties as long as they are not deformed, they are insufficient to provide cathodic protection provided by galvanized steels in the presence of a defect.

Electrochemical corrosion behavior of pack aluminized low carbon steel are examined in artificial sea water in recognition of mass loss and potentiodynamic polarization results, in the study of Li et al. [6]. The phases of $FeAl_3$ and Fe_2Al_5 were formed on the samples processed at 650°C and 750°C, which are designated as Condition1 and Condition2, respectively. The concluded Fe_2Al_5 phase is higher for the latter which exhibits a thicker aluminize layer. It has been observed that the corrosion current density of the steel is higher than that of both aluminized surfaces at the same potential, while the one with higher Fe_2Al_5 content exhibits the lowest value among themselves. According to the obtained polarization curves given in Figure 3.22, a breakdown

potential which is designated by P is observed for the sample containing a higher Fe_2Al_5 phase, that is indicating the breakdown of the passive film.

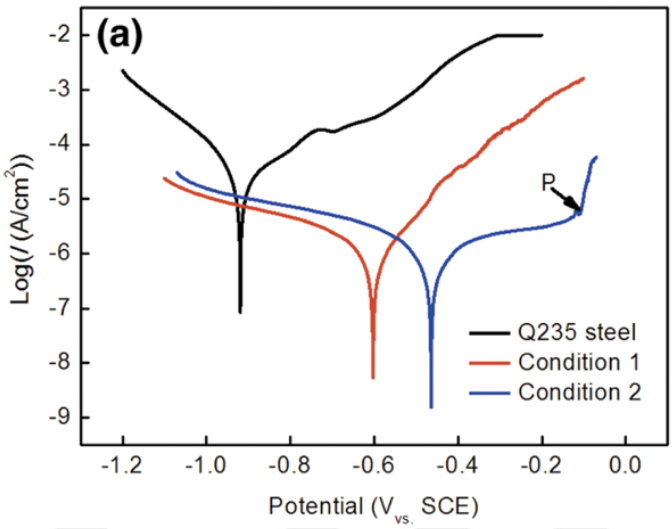

Figure 3.22 : Polarization curves of aluminized steel (at 650ºC and 750ºC) and Q235 steel in artificial sea water [6].

According to the results of mass loss measurements, corrosion products formed on aluminized surfaces accumulate on the surface and decrease the corrosion rate by covering pit, unlike bare steel, after a certain period of time.

Considering the fact that, the electrochemical behavior of aluminized steels depends on various factors such as the environment in which it is located, the composition of the aluminized layer formed, thus the passivation behavior so-called atmosphere and the order of the layers formed, to straightforward interpret the contribution of aluminizing to steel straightforward comprehensive studies are required.

In the grand scheme of things, on the other hand, to obtain true phases in the exact order is essential to obtain impeccable mechanical properties, formability, high-temperature corrosion, and electrochemical corrosion behavior, thus, performance is possible with controlled diffusion. Considering the facts as followed that; It is essential to obtain alloy stripped from external elements other than Fe and Al, for better corrosion performance; the formation of cracks thus of brittle phases should be prevented for better formability; multi-stage processes were needed to obtain these conditions up to now; producing iron aluminides with CA-EMIT process and to examine their electrochemical corrosion allows us to satisfy all in the single process.

4. EXPERIMENTAL PROCEDURE

In this study, it is aimed to investigate the electrochemical behavior of Fe-Al intermetallics with different phase layer sequences produced by CA-EMIT PVD method in different environments and the effect of this phase sequence on corrosion behavior and to obtain the exact phase sequence in the host environment. Accordingly, different phases and phase sequences were obtained by changing the process temperature and time in CA-EMIT PVD method. Process parameters were selected considering the phases obtained in another study conducted by the team [142]. In order to control the formation of phases with application temperature and time parameters and to exclude other factors, IF steel, whose composition is very close to pure iron, was chosen as the substrate. XRD analysis for the determination of the formed phases and SEM characterization for their morphologies were applied. In order to examine the corrosion behavior of the analyzed phases, the corrosion behavior of iron-aluminum intermetallics in sulfuric acid and chlorine-containing electrolytes was investigated, considering their host environment of use such as; sulfur-containing environments, seawater, and atmospheric conditions involving acid rain which are accredited with, respectively, fossil energy plants, pipes/tubes used to desalinize the seawater and with substitution usage of conventional stainless steel. In this context, potentiodynamic polarization curves of the samples whose open circuit potentials were measured were extracted. With the results obtained from the polarization curves, the galvanic series of the phases in their related environment were constructed. SEM images of the samples subjected to corrosion test were examined and material losses were determined by an optical profilometer. In order to examine the effect of the sequence of the formed phase layers on the corrosion behavior, that is, to examine whether the relevant phase on the surface from the sequential phases only act as a barrier or would provide cathodic protection simultaneously, cracks were created in the samples and some corrosion tests and characterizations were repeated. This is to examine the electrochemical behavior of the system as a result of the interaction of the phases with each other, in the presence of cracks occurring through a possible impact during the production process or utilization.

4.1 Production of Samples

4.1.1 Preparation of substrate

The IF steel which was kindly supplied by Erdemir, with a nominal composition of 0.0068% C, 0.0029% Si, 0.018% Mn, 0.0008% Cr, base-Fe was used as the substrate in this study. Substrates with in the dimensions of 2.5 x 5 x 0.3 cm, was ground with SiC paper in the mesh range of 600-1200. After giving mirror-like finishing by polishing with 3μm diamond paste, samples were cleaned in acetone and 99.99% ethanol placed in ultrasonic bath for 10 minutes for each at room temperature. After rinsing, the dried samples were placed in the vacuum chamber by hanging on the steel holder.

4.1.2 CA-EMIT

In this study, CA-EMIT method developed by Öncel and Ürgen [11] was used for diffusion treatment. Novatec-SIE brand, NVT-12 model, CA-PVD unit, which is a standard PVD unit, was used for the process. While IF steel was used as a substrate to be treated, 100 mm diameter high purity Al was used as the cathode (Al source). During process, cathode-substrate distance of 15cm was kept constant. The system was vacuumed up to $5x10^{-5}$ Torr before diffusion treatment, and in order to ensure the continuity of the arc in the coating and diffusion stages, the pressure was increased to approximately $6x10^{-4}$ Torr by introducing argon gas, and kept at this value throughout the process. A constant current of 90 A (Ampere) was applied to the cathode during all experiments. 50Hz (Hertz) frequency AC power supply is used as a bias. In order to remove oxides and impurities on the surface, metal ion etching was applied to the surface of the substrate, respectively, at -600V and -800V bias voltage for 30 seconds, then -1000V bias voltage for 60 seconds in argon environment. The temperature of the substrate material could be precisely adjusted by the amplitude of the applied AC voltage. During heating and coatings, the temperature of the sample surface was measured and recorded with the DIAS Pyrospot IR 10 optical infrared pyrometer. Samples were treated on one side. The samples and treatment parameters are given in Table 4.1. The treatment parameters were determined by considering the phases formed in the previous study [142] by the team.

Table 4.1 : Treated samples and treatment parameters in CA-EMIT process.

Sample No	Substrate	Cathode Material	Cathode Evaporation Current (A)	AC Bias (Vrms)	Process Time (min)	Substrate temperature (°C)
Fe_2Al_5+Fe_4Al_{13}	IF-Steel	Al	90	17	90	1100
Fe_2Al_5	IF-Steel	Al	90	17	90	1100(+50)
Fe_3Al+FeAl	IF-Steel	Al	90	23	30	1200

4.2 Characterization of Treated Samples

Before characterization, samples were ultrasonically cleaned in acetone and 99.99% ethanol. Microstructural and chemical characterization of surface and cross section of treated samples were examined by means of, respectively, scanning electron microscopy (SEM) (Jeol JSM-5410) and energy dispersive spectrometry (EDS) (Noran 2100 EDS) attached to SEM. Phase analyses of surface were performed by Philips PW3710 X-ray diffraction (XRD) equipped with a CuKa-X-ray source. For the evaluation of the XRD patterns, JCPDS cards of iron aluminides with the following numbers are used: Fe_3Al-00-050-0955, FeAl-00-033-0020, Fe_2Al_5-01-073-8846, Fe_4Al_{13}($FeAl_3$)-01-073-3008. To reveal microstructures of phases from surface through substrate, cross-section of samples, additionally, investigated via SEM images after etched. Etching was done respectively with HCl-HNO_3-CH_3COOH-H_2O with a volume ratio of 22:20:50:8 for, then with 3% nital for 30 seconds.

4.3 Electrochemical Experiments

Electrochemical experiments have been carried out to examine the corrosion behavior of the formed phases in the aqueous environment. Along with the improvements in mechanical properties, the need to examine the aqueous environment corrosion behavior of iron aluminides, whose ambient temperature usage areas have increased, has arisen. Considering the mechanical and superior corrosion properties at high temperatures, along with these developments, iron aluminides become prevalent in such areas; concertedly or substitutional by stainless steel as which, structural materials in atmospheric conditions and biomaterials in contact with body fluid for instance medical equipment/implant; in the food industry instead of Cr-Ni based harmful alloys; in carrier parts in sea water treatment plants. Considering the above-

mentioned environments, corrosion experiments were carried out in two different electrolytes as, 0.5M H_2SO_4 and 200ppmCl^- (pH4 adjusted with H_2SO_4) electrolyte, the former of which was attributed to iron aluminides' usual usage area of sulfur bearing atmosphere and the latter to simulated acid rain environment. The three-electrode cell type was used in electrochemical experiments. The cell used for the polarization studies was a glass vessel similar to ASTM designation G5-14 [143] with 1000ml capacity. Electrochemical tests were accomplished with an IVIUM CompactStat.h potentiostat connected to a computer system. The sample which was cleaned by acetone and ethanol in ultrasonic bath (for 15 minutes for each) followed by masking with the intention of leaving 1cm^2 exposing area, used as the working electrode. Ag/AgCl(+199mV / SHE, 25^{o}C) was used as the reference electrode and graphite as the counter electrode. During the experiments, ambient and solution temperature were 25±5^{o}C. Before each measurement, the electrolyte was de-aerated by flushing with argon (99.999%) for 30 minutes. Flushing argon gas continued throughout the experiment. All measurements were carried out in Faraday cage in order not to be affected by electromagnetic. In order to avoid infiltration of electrolyte at the metal/holder interface that often causes random errors, the electrodes were covered with a Teflon film. Nontreated IF steel and Al were used for comparison. Electrochemical techniques were used as follows: OCP measurement, and potentiodynamic polarization for obtaining polarization curves. Corrosion current and corrosion potentials were found by Tafel extrapolation method. These steps are explained in detail below.

4.3.1 Open circuit potential measurement

Prior to performing polarization measurements, for each material and electrolyte combination, the corrosion sample was allowed to stabilize in the electrolyte and the open circuit potential (OCP) was monitored for 1800 sec.

4.3.2 Potentiodynamic polarization experiment

Polarization behavior of iron aluminides was studied using potentiodynamic polarization technique via polarization curve determination with a scan rate of 0.8 mV/s. The measurement was started at a negative value, about 150 Volts more than the OCP, and continued to the point where the current density corresponds to the value of 600mA. After polarization curves were monitored, corrosion current density (i_{corr})

and corrosion potential (E_{corr}) were determined by Tafel plot extrapolation. Other electrochemical parameters namely, primary passivation potential (E_{pp}), critical current density (i_{crit}), passivation current density (i_{pass}, minimum current density in passivation region), transpassive breakthrough potential (E_b) were extracted from potentiodynamic polarization curves.

4.4 Characterization of Samples After Electrochemical Corrosion Experiments

Samples were viewed under a scanning electron microscopy (SEM) and EDS analyses are conducted to examine the nature of attack and behavior of phases morphologically. After then, step heights of the samples were extracted in 3D with Wyko Veeco NT1100 optical profilometer and corrosion rates were determined in terms of material loss.

4.5 Creation of Galvanic Pairs

The possibility of cracks that may occur on the surface as a result of a possible impact or during production processes, revealing the phases below the surface phase in a way that they interact with the environment has been considered. After a galvanic series was formed by means of the corrosion potentials of the phases in their host medium, a series of experiments were carried out in order to observe corrosion behavior in the event that the exposed phases form galvanic couples with the phases on the surface. In this way, it was examined whether the phase on the surface only acts as a corrosion barrier or also provides cathodic protection. In this context, first, cracks were formed on the surfaces of the samples, the areas where cracks were formed were marked and then these areas were subjected to electrochemical testing. SEM images of the marked regions before and after the electrochemical experiments were obtained and compared with each other, then reliability of the galvanic series that has been determined before these experiments was examined. Electrochemical experiments were carried out only in mild acid-chloride (Cl^-) solution [25] to simulate an aggressive acid rain-type atmospheric corrosion situation, which is also adequate for simulating a mild seawater atmosphere [103].

4.5.1 Forming cracks on treated surfaces

Following the revealing galvanic series, the phases were treated in such a way that the relevant phase is exposed to the environment while the phase (IF-steel) associated with

the galvanic series created before remains in the substrate and is exposed by the crack. In this scope, treatment parameters to obtain the desired phase sequence and the sufficient applied load, are determined from the study conducted by Celikel et al. [142] for each sample to reach the layer underneath the surface is determined considering their harness value

Cracks are formed on the surfaces of samples via indenting hardness tip with a applied load of 2000gf in Leica VH-MOT. The applied load value is sufficient to obtain the crack reaching underneath the phase layer of the said phases . The scratching method where load increases throughout scratching and reaches a peak value at the end, was applied to create cracks on the surface of Fe-rich phase with high ductility value [142] where no crack impression can be created on the surface by hardness indentation.

4.5.2 Electrochemical experiments on cracked surfaces

The areas where the cracks formed on the surface of the samples were marked and the remaining parts of the sample were masked so that they were within the $1cm^2$ exposing area. In the electrochemical experiment set up as described in the previous section and same experimental sequence was followed: After OCP measurement, curves of potentiodynamically polarized samples were extracted. In this instance, experiment was conducted only in 200ppmCl^- electrolyte.

4.5.3 Characterization of the cracked samples after electrochemical experiments

SEM characterization and EDS analyses of marked cracked areas were performed both before and after electrochemical experiments. By comparing the micrographs and analyses results belongs to before and after the electrochemical experiments, electrochemical behavior of the phases was discussed.

5. RESULTS AND DISCUSSION

5.1 SEM Characterization and Phase Analysis of Treated Samples

The XRD patterns of samples treated at different temperatures and with different treatment times are illustrated comparatively in Figure 5.1. According to the XRD analysis taken from the surface of the sample treated at 1200°C for 30 minutes, Fe_3Al and FeAl phases coexist on the surface. The result of XRD analysis taken from the upper part of the sample treated at 1100°C for 90 minutes inferred the Fe_2Al_5 phase; whereas the peaks characterized by Fe_2Al_5 and Fe_3Al_{14} are observed in those taken from the lower part of it. Different analysis results obtained from two different regions on the same sample may arise from temperature difference between the upper part and the lower part (50 °C), during the treatment procedure. Thus, these phases are considered as the 1100/90 and 1100(+50)/90.

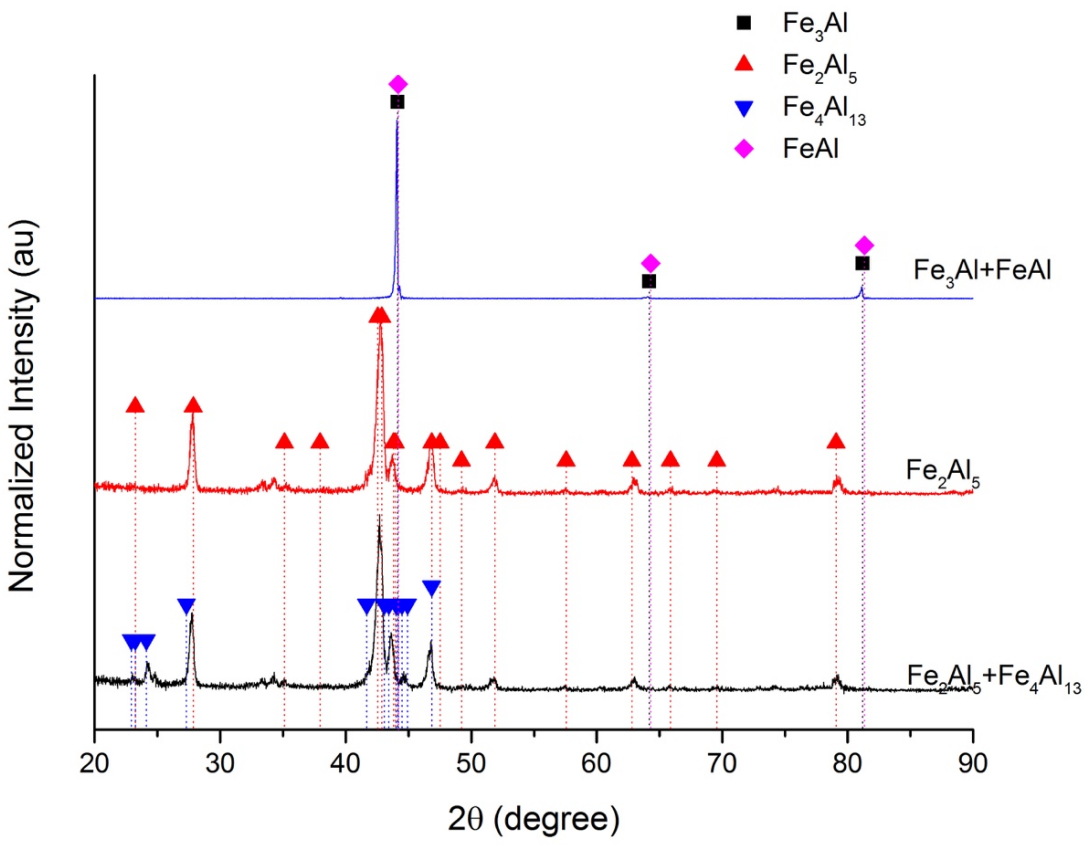

Figure 5.1 : XRD patterns of treated samples.

Secondary electron and backscattered electron images (SEi, BSEi) of cross-section of samples before and after etching, which were subjected to distinguish the phases, are examined below.

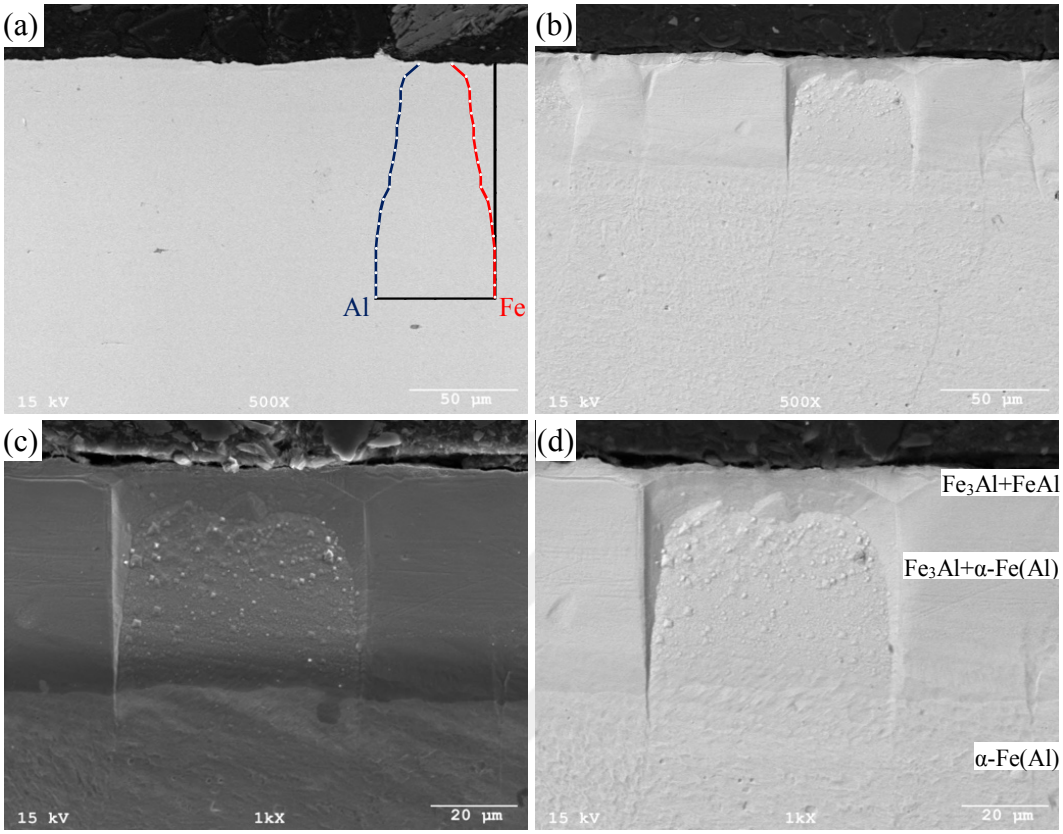

Figure 5.2 : Cross-section view of sample treated at 1200°C for 30 minutes: (a) before etching BSEi and linescan EDS analysis, (b) BSEi, higher magnification (c) SEi and (d) BSEi after etching.

In Figure 5.2, SEM images and EDS results of sample treated in 1200°C for 30 minutes are shown. When the surface layer is examined, on the contrary to XRD results that represent Fe_3Al+FeAl peaks; according to the graph of the distance-dependent change of the Al concentration obtained from the EDS analysis taken as line-scan, given with the electron image in the Figure 5.2a, Al concentration on the surface corresponds to Fe_3Al phase region. This was attributed to the FeAl phases that remained in the structure while transforming into the Fe_3Al phase (second ordered transformation) during cooling after the preferential formation of the FeAl phase, which arises from its more negative formation enthalpy than the other phases [142]. Thus, at the surface of the sample where the sum diffusion zone is 85µm thick, the region along 10 cm corresponds to the Fe_3Al+FeAl binary phase region. Under this phase, there are FeAl-α-Fe(Al) and α-Fe(Al) phases, respectively, according to their composition. In the close look given in Figure 5.2c and Figure 5.2d, phases are distinguished clearly.

At the Fe_3Al phase region, grains with different etching shapes are observed. This situation coincide with the observations of Brito et al. [130] that differently oriented Fe_3Al single crystals tend to dissolve with different morphologies in 0.5M H_2SO_4 solution. In the study, it is indicated that crystals with (100), (110), (111) orientations exhibit cavities in the shape of a square, diamond, tetrahedral, respectively, as presented in Figure 5.3.

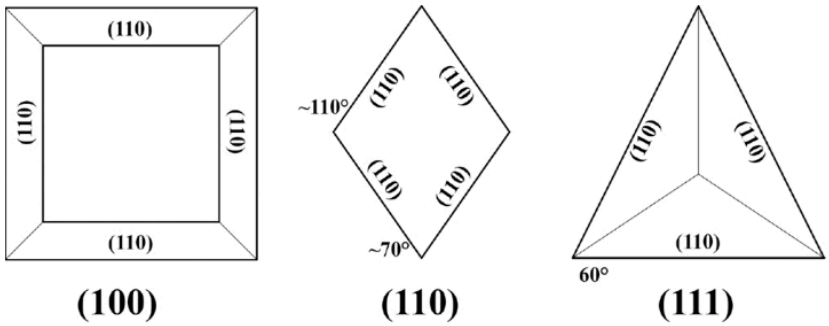

Figure 5.3 : Schematic representation of surface cavities of Fe_3Al formed in 0.5M H_2SO_4 [130].

In the study conducted by Çelikel [142], similar Fe-rich phases were formed at the same temperature. The formation of Fe-rich phases was attributed to the fact that the 1200 ^oC is above the region where the Fe_2Al_5, $FeAl_2$, Fe_3Al_{14} phases are stable and therefore, a diffusion takes place without the formation of Al-rich phases in the structure. However, the fact that the phases obtained are not exactly the same, and different, absence of the $FeAl_2$ phase in this study may arise from the relatively slow cooling rate due to the higher thickness of the sample used. For this sample, overall diffusion zone is obtained in a thickness of ~ 85µm

According to the EDS analysis taken from the surface of the sample, there was a thin FeAl layer on the outer surface. The existence of this layer is attributed to remnant FeAl that is left on the surface without transformation. This FeAl layer was removed from the surface by polishing before electrochemical testing during surface preparation, the relevant phase considered as the Fe_3Al+FeAl.

In the Figure 5.4, cross-section SEM images of the lower part of the sample produced at 1100 ^oC for 90 minutes are given, with the overlaid aluminum concentration as a function of distance (Figure 5.4a). The phase sequence obtained is given with the higher magnification BSEi in the Figure 5.4d is extracted as a Fe_2Al_5+Fe_4Al_{13} at the top with a thickness of ~6µm followed by Fe_2Al_5+$FeAl_2$ layer with same thickness and

$FeAl_2$+FeAl layer with a thickness of ~13µm. The underneath porosity before reaching the region of the stoichiometric composition of the Fe_3Al+FeAl phase is revealed as the Kirkendall porosity arisen from the difference between the diffusion rate of Fe and Al in the preformed FeAl phase [142]. According to the composition obtained from EDS analysis, Fe_3Al+α-Fe(Al) and α-Fe(Al) phases are followed the Fe_3Al+FeAl phase layer, respectively. At the layers underneath the porosity, phases follow the grain orientation of IF-steel substrate. The overall diffusion zone reaches a thickness of 90µm.

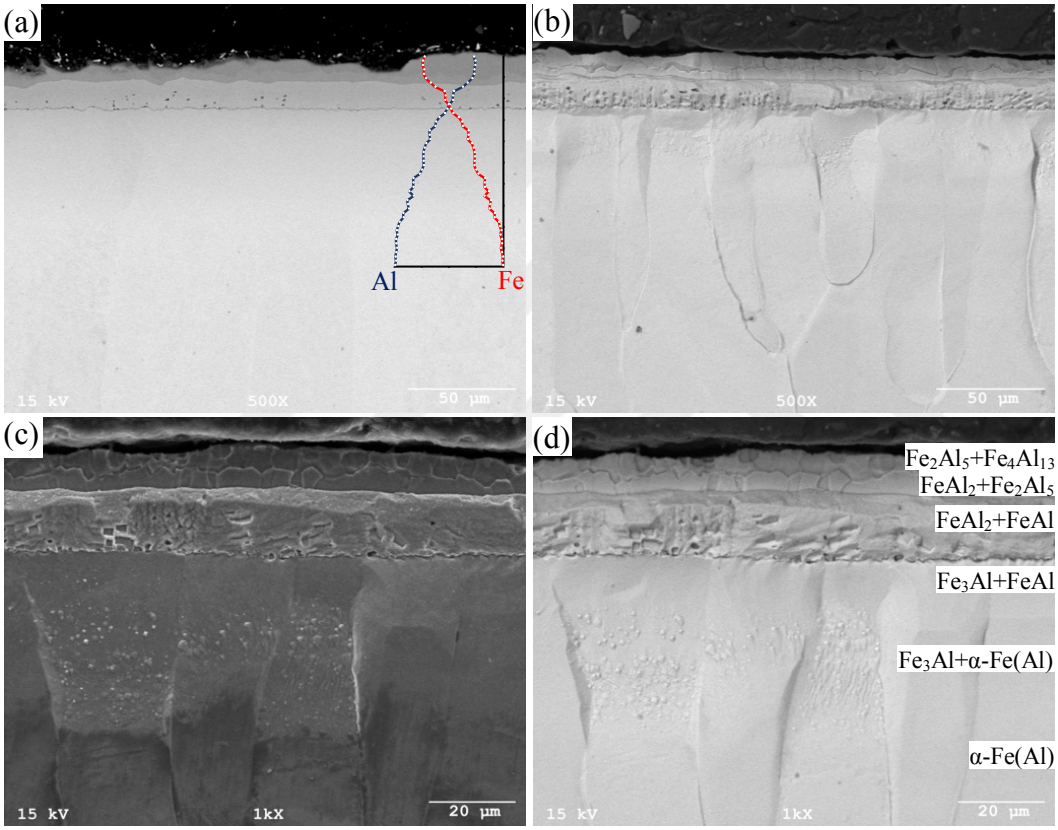

Figure 5.4 : Cross-section view of the sample treated at 1100°C for 90 minutes: the (a) BSEi before etching and linescan EDS analysis, (b) BSEi, (c) higher magnification SEi and (d) BSEi after etching.

The cross-sectional microstructures and composition profiles of the upper side, namely the sample treated at 1100(+50) for 90 minutes presented in Figure 5.5a. As seen clearly in the Figure 5.5b, the thick layer formed corresponds to the Fe_2Al_5 phase. The layers below is followed as Fe_2Al_5+$FeAl_2$ and $FeAl_2$ thin phases respectively and with a drastic decrease in the Al content, Fe_3Al+FeAl, Fe_3Al+α-Fe(Al), α-Fe(Al) phases are aligned, respectively.

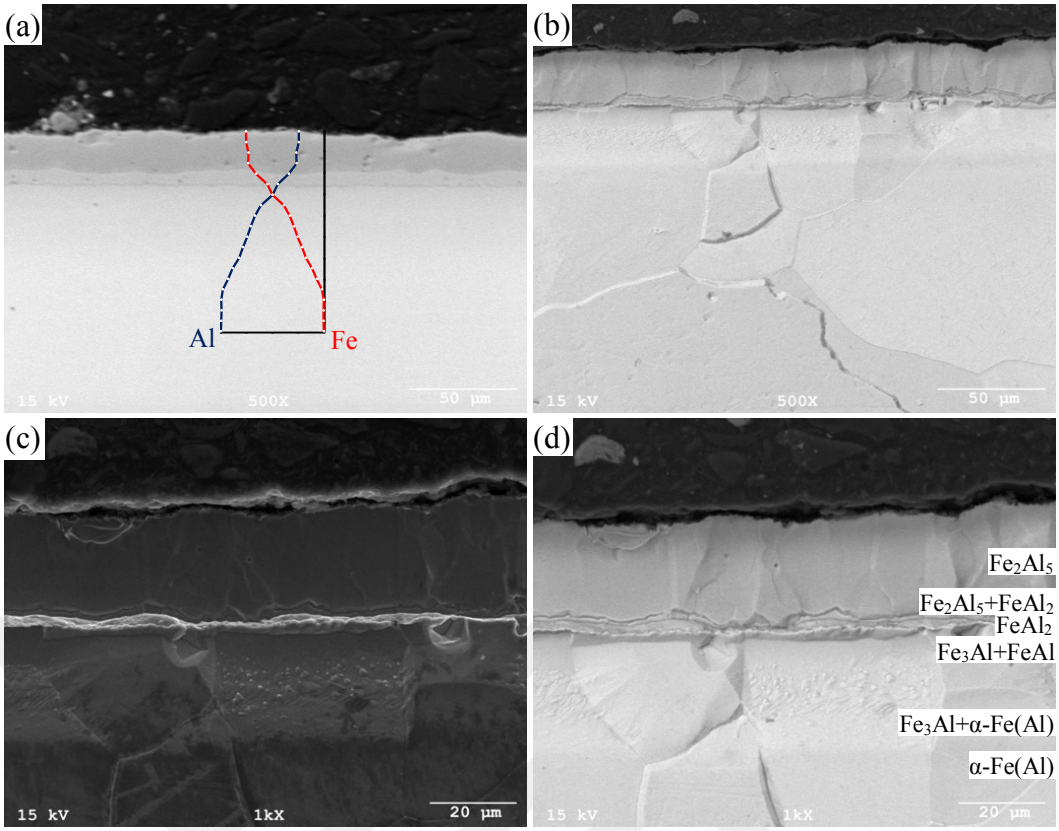

Figure 5.5 : Cross-section view of the sample treated at 1100(+50)ºC for 90 minutes: (a) the BSEi before etching and linescan EDS analysis, (b) BSEi, higher magnification (c) SEi and (d) BSEi after etching.

From now, the samples will be designated with the phases formed on their surfaces. Namely, Fe_3Al-FeAl for the sample treated at 1200ºC for 30 minutes, Fe_2Al_5 and Fe_2Al_5-Fe_4Al_{13} respectively for the upper and lower regions of the sample treated at 1100(+50)ºC/1100ºC for 90 minutes.

5.2 Electrochemical Behavior in 0.5 M H_2SO_4

In this section, the electrochemical behavior of samples in 0.5M H_2SO_4 electrolyte are examined.

5.2.1 Open circuit potential

The variation of OCP over time for pure Al, IF-steel, and Fe-Al phases in de-aerated 0.5M H_2SO_4 are presented in the Figure 5.6. While the IF-steel and Fe_3Al-FeAl phase exhibit positive trends, pure-Al, Fe_2Al_5 and Fe_2Al_5-Fe_4Al_{13} phases exhibit negative trends in potential shift, until they reach steady states. The OCP values of the Fe-Al phases shifted towards more negative values with increasing aluminum concentration.

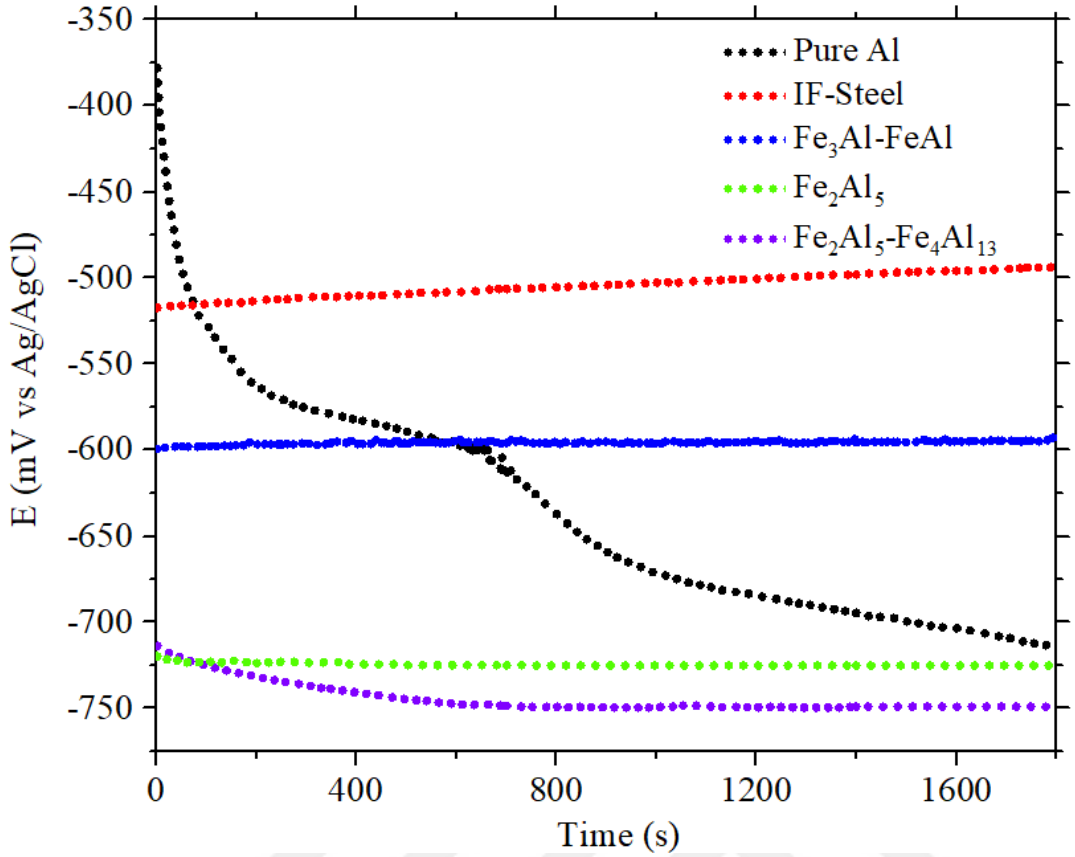

Figure 5.6 : OCP measurement in 0.5M H_2SO_4.

5.2.2 Potentiodynamic polarization behavior

The potentiodynamic polarization curves obtained for the IF steel, pure-Al and Fe-Al phases, in de-aerated 0.5M H_2SO_4 are presented in Figure 5.7. According to the presented figure, all phases exhibit Tafelian behavior in the cathodic and anodic active region. While the IF-steel and Fe-Al phases exhibit active-passive-transpassive features, spontaneous passivation is observed for pure-Al. This behavior of aluminum in acidic environment can be explained as the anodic dissolution that occurs as a result of the delayed surface-solution interaction in the presence of a protective oxide film on its surface [22]. The active dissolution zones of the Fe-Al phases are in a more negative position than that of the IF-steel, with the occupied positions between pure-Al and IF-steel, as expected.

Kinetic electrochemical parameters derived from the polarization curves are exhibited in Table 5.1 as followed: Electrochemical corrosion potential (E_{corr}) and electrochemical corrosion current density (i_{corr}) values extracted from Figure 5.7 by Tafel Extrapolation; potential of primary passivation (E_{pp}) which is the potential value corresponding to the point where the current starts to decrease after reaching its peak

value, and critical current density (i_{crit}) which is the highest current recorded at the point corresponding to the primary passivation potential; potential of complete passivation (E_{cp}), passive current density (i_p) which corresponds to the minimum current density value reached in complete passivation zone; and the breakdown potential (E_b) where the current exhibit an apparent increase after passivation. Besides, the potential range of the passive zone is included in the Table 5.1 in the form of E_{pp}-E_b.

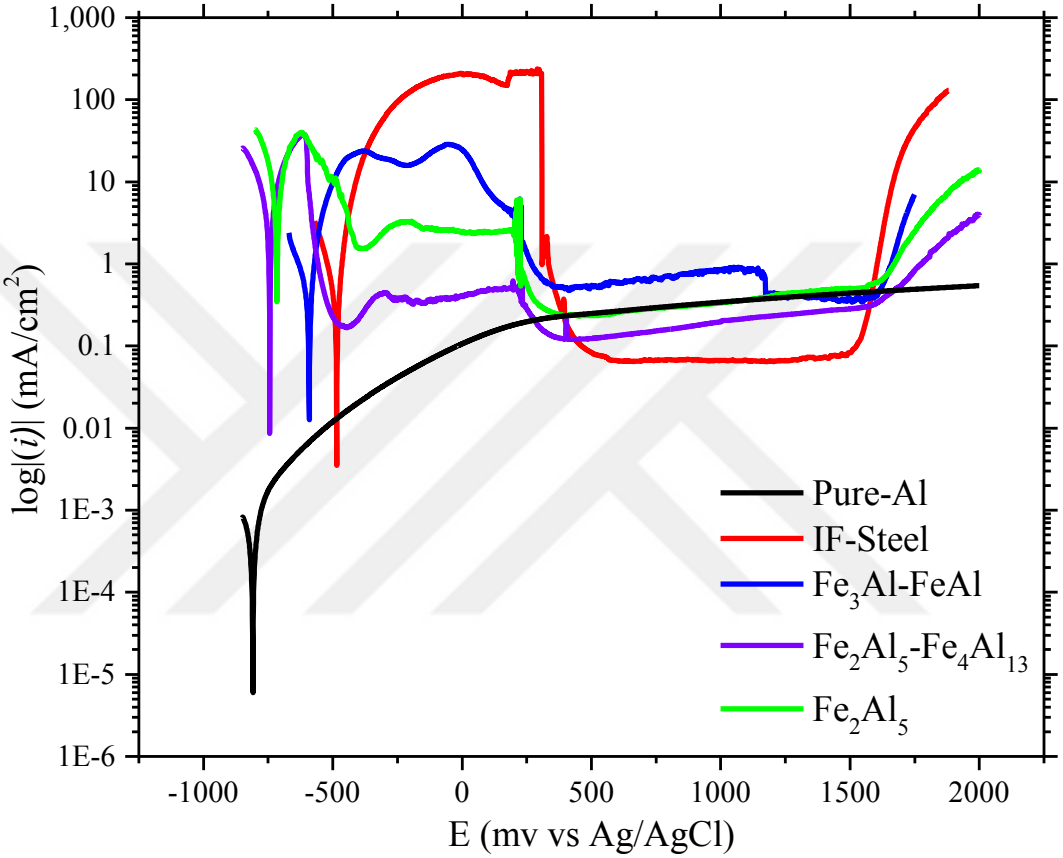

Figure 5.7 : Overlaid potentiodynamic polarization curves of pure-Al, IF-steel and Fe-Al phases in 0.5M H_2SO_4.

When the active (anodic dissolution) region of polarization curves are examined: The corrosion potential value of -484mV found for IF-steel, whose shape of polarization curve coincides with that of obtained in previous studies for pure iron in the same environment, is also quite compatible with the values obtained in these studies [105]. The E_{corr} value of -809mV obtained for pure-Al in this study, is in well agreement with the values given in the study of Peng et al. [17].

On the other hand, for the Fe-Al phases, E_{corr} values of -606, -730, -747mV obtained for Fe_3Al-FeAl, Fe_2Al_5 and Fe_2Al_5-Fe_4Al_{13}, respectively. Corrosion potentials of the layers, tend to decrease to negative direction with increasing Al content as consistent

with previous studies [17–19]. The active corrosion rate (i_{corr}) of Fe-Al phases, which increases in line with Al concentration, are one order magnitude higher than that of IF-steel. However, unexpectedly the corrosion rate of the Fe_2Al_5 phase is higher than that of Fe_2Al_5-Fe_4Al_{13} , this observation will be further disccussed in the section 5.2.3.

Table 5.1 : Electrochemical parameters for the pure-Al, IF-steel, and Fe-Al phases, derived from polarization curves in de-aerated 0.5M H_2SO_4.

Sample	E_{corr} ($mV_{Ag/AgCl}$)	i_{corr} ($mA.cm^{-2}$)	E_{pp} ($mV_{Ag/AgCl}$)	i_{crit} ($mA.cm^{-2}$)	E_{cp} ($mV_{Ag/AgCl}$)	i_p ($mA.cm^{-2}$)	E_b ($mV_{Ag/AgCl}$)	E_{pp}-E_b
Al	-809	0.0003	-	-	-	-	-	-
IF-Steel	-484	0.43	240	215	565	0.07	1504	1304
Fe_3Al-FeAl	-606	1.6	-53	23.7	352	0.53	1592	1645
Fe_2Al_5	-730	14.2	-621	39.6	403	0.23	1566	2187
Fe_2Al_5-Fe_4Al_{13}	-747	6.7	-614	37.8	394	0.12	1594	2208

Since the E_{corr} values obtained for Fe-Al phases are below the hydrogen evolution reaction (given in equation 5.1) potential of -240mVAg/AgCl, which was calculated by assuming the pH of 0.5M H_2SO_4 as 0.3 and partial pressure of H_2 1atm. Thus, the exchange current density of hydrogen ($i_o{}^{H^+}/_{H_2}$), which exhibits hydrogen evolution rate on these phases, are critical. As well known the $i_o{}^{H^+}/_{H_2}$ values for Fe in 0.5 N sulfuric acid is 5 order of magnitude higher than Al. According to the study of Shankar Rao [23] the $i_o{}^{H^+}/_{H_2}$ value for 16wt% Al containing iron-aluminum alloys are placed in right side of the $i_o{}^{H^+}/_{H_2}$ values of iron and aluminum.

$$H^+_{(aq)} = H_2 + 2e^- \quad (5.1)$$

$$Fe_{(s)} = Fe^{2+}_{(aq)} + 2e^- \quad (5.2)$$

$$Al_{(s)} = Al^{3+}_{(aq)} + 3e^- \quad (5.3)$$

The reason for the observation of higher rates of Fe-Al alloys can be explained as follows:

As stated in the study of Brito et al. [130], the active dissolution of iron aluminides, initially controlled by the dissolution of Fe^{2+} [19,130]. Thus, the corrosion rates of

aluminum containing iron alloys are higher than aluminum beacuse of the shift of the corrosion potential (E_{corr}) of Fe-Al alloys towards negative direction with the presence of Al.

For interpretation the initial stage active dissolution mechanism of Fe-Al phases on the basis of mix potential theory, the proposed Evans diagram is illustrated in the Figure 5.8 by considering as follows: The $i_o{}^{H^+}/_{H_2}$ values of constituent elements and Fe-Al phases; calculated electrode potential values for the dissolution of Al^{3+} and Fe^2 from pure metals and conventional E_{corr} values of Fe-Al phases obtained from experimental results.

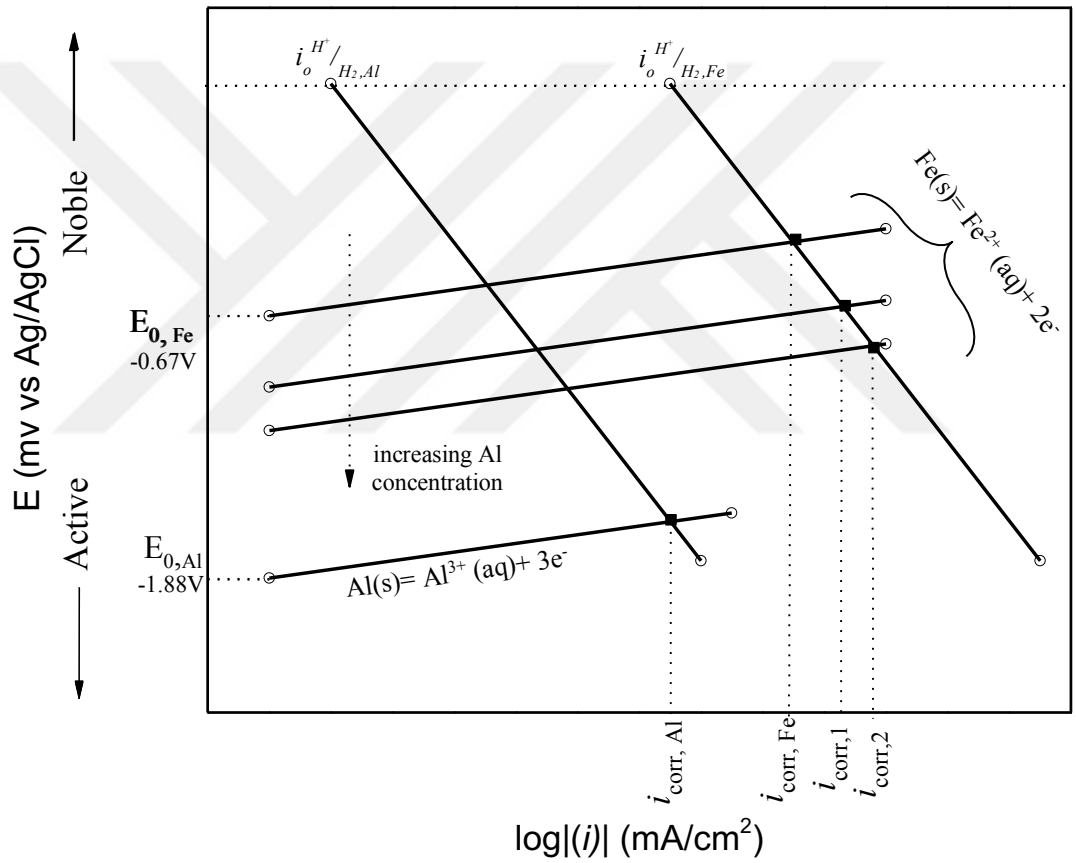

Figure 5.8 : Illustrated Evans diagram for polarization of Fe-Al phases in 0.5M H_2SO_4.

Since the addition of aluminum to iron moved the anodic curve in Figure 5.8 to more active potentials, the intersection of the cathodic and anodic curves for the Fe-Al phases occurred at lower E_{corr} values and and yield higher corrosion rates (from $i_{corr,\ Fe}$ to $i_{corr,\ 1}$ and $i_{corr,\ 2}$). With the further increase in Al content, at the point where pure-Al

content is reached, the anodic curve intersects the cathodic curve ($i_{o\ H^+/H_2}$ for Al) at a lower corrosion rate ($i_{corr,\ Al}$).

For the active-passive transition, passive, transpassivation regions, the overlaid polarization curves in Figure 5.7 are brought out separately to reveal the critical values clearly in Figure 5.9.

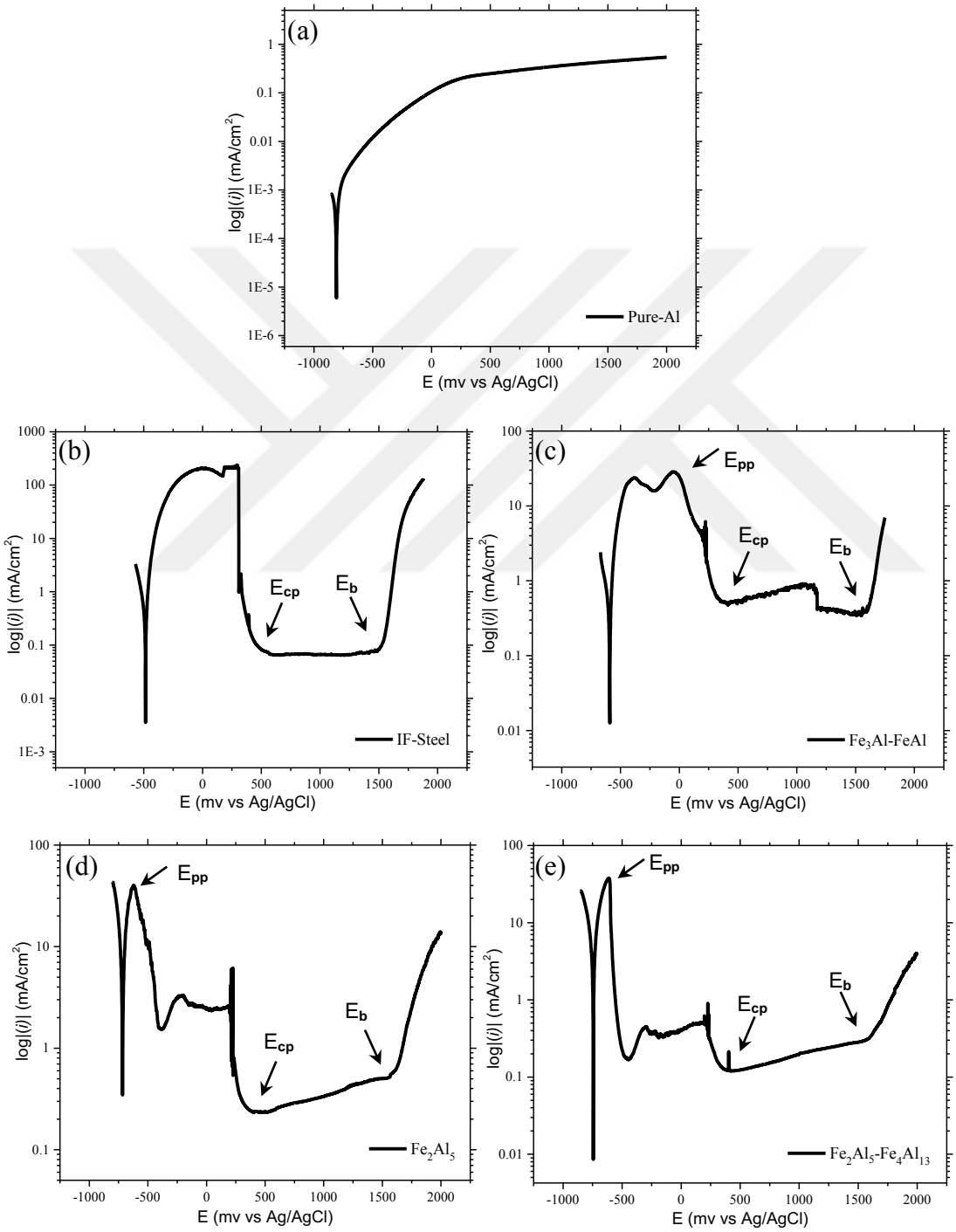

Figure 5.9 : Polarization curves of (a)Pure Al, (b)IF-steel, (c)Fe_3Al-FeAl, (d)Fe_2Al_5, (e)Fe_2Al_5-F_4Al_{13}.

When pre-passivation region of polarization curves examined: As can be seen in the active-passive transition region of the curve obtained for IF-Steel, the flat point, where the current remains constant for a while after reaching its peak point and makes slight oscillations, prevents to define a critical current density (i_{crit}) value literally. For this reason, the maximum value of the current in the middle of the plateau is accepted as the critical current density (i_{crit}) for IF-Steel, while the potential corresponding to this value is accepted as the primary passivation potential (E_{pp}). This fluctuation in the active-passive transition zone has been attributed to the alternating destruction and regeneration of the Fe_2O_3 film, which was mechanically formed and thickened with increasing potential, and completely separated from the surface shortly before transition to passive zone, in previous studies [105]. The dark-colored layer formed on the surface during the experiment and flake off after a short time supports this claim.

Fe-Al phases exhibit lower i_{crit} compared to IF-steel, while Al-rich phases exhibit higher i_{crit} than Fe_3Al-FeAl, which indicates that the Al-rich phases dissolve actively more than the Fe-rich phase. However, Al-rich phases exhibit, compared to Fe-rich phase, a sharper decrease at current once i_{crit} is reached, which indicates a higher tendency to passivation, while the latter exhibits a wider active region.

It is a common assent that at potentials adjacent to the E_{corr} of FeAl phases, anodic dissolution rate is dominated by Fe^{2+} dissolution at the metal-solution interface, instead of the Al^{3+} dissolution at the metal-oxide interface (It is known that Al dissolution is dominated by the Al ion trasfer throug metal to metal-oxide interface in a strong acid environment). Further dissolution of Fe^{2+} from the remainder deformed surface caused by departing Fe^{2+}, is blocked by the initiation of a protective layer arising from the oxidation of Al^{3+} on the surface[19].

Considering the mechanism; the increase in the amount of dissolved Al in proportion to the increasing Al content followed by simultaneous reaction of dissolved Al^{+3} to form protective film may have caused higher i_{crit} values and sharper current decrease, respectively, at Al-rich phases.

When the active-passive transition behavior of the Fe_3Al-FeAl phase is examined, other than i_{crit} a current maximum value corresponding to the initiation of transition to the passive region (at $240mV_{Ag/AgCl}$), is observed. The peak referred as the secondary anodic peak by Shankar Rao [129], is followed by a broad active-passive transition

until complete passivation is reached. This transition to complete passivation characterized by a broad zone, which were attributed to sequential oxidation of aluminum and iron, in the previous studies, is wider for Al rich phases.

It is observed that compared to the IF-steel, the Fe-Al phases passivate primarily, at more negative potential values (E_{pp}) which shifts negative direction with the increasing amount of Al. However, the reverse shift is observed between Fe_2Al_5 and $Fe2Al_5$-Fe_4Al_{13} phases with a negligible difference. For the complete passivation potentials (E_{cp}), it is seen that Fe-Al phases exhibit almost the same value among themselves, at a slightly more negative than for IF-steel.

These results supports, the ones given in the study of Shankar Rao [129]. In the study, where a potentiostatically conducted electrochemical test at the potentials corresponding values to between two anodic peaks and to the region of complete passivation to examine the passive film structure, the higher Al/Fe ratio in the film content of the former indicate that complete passivation is obtained by oxidation of Fe. In the passive film formed through the complete passivation region, Rao observed only oxides of Fe yet both oxides and hydroxides of Al. It is worth noting that, mixed oxides and hydroxides were detected along the passive film in both of studies conducted by Schaepers-Strehblow [21] and Frangini et al. [106], in spite of lower amount of iron hydroxide observed along the one obtained in the former.

With regards to behavior in passive region, contrary to the results obtained for from the study conducted by Frangini et al. [106], for Al and IF-steel it is obtained that the i_{pass} value of the former is more positive than that of the latter. However, these values are quite coincide with the values obtained by Shankar Rao et al. [107]. In the polarization curves of the Fe-Al phases, the shape of the passive region where the complete passivation takes place is similar to that of IF-Steel. This similarity corroborates the studies, which came to a common belief that complete passivation is achieved by complete inhibition resulting from the formation of iron oxides and/or hydroxides, although they proposed different mechanisms for passivation. In other words, complete passivation of the Fe-Al phases is governed by the passivation of iron. When the i_{pass} values obtained for the Fe-Al phases are examined, with the increasing amount of Al content, the i_{pass} values decrease to remain between the values obtained for pure-Al and IF-steel. The expectation of obtaining lower i_{pass} values for Fe-Al

phases than that for IF-steel, as observed in [107] bulk iron aluminides, is failed to be satisfied in this study. This can be attributed to the following reasons:

- The porous nature of the aluminum oxide film (it is a known fact that aluminum oxide has a porous structure in H_2SO_4 [107]) compared to iron oxide; The presence of cracks on the surface for the Fe_2Al_5 phase with high hardness, and the presence of secondary phases, in which one of them exhibit electrochemically sacrificial behavior, for Fe_3Al-FeAl and Fe_2Al_5-Fe_4Al_{13}; The existence of multiple layers of Fe-Al phases instead of bulk alloy.
- The fact that primary passivation is obtained at a current density value close to the one corresponding the complete passivation (i_p), for the Fe_2Al_5-Fe_4Al_{13} phase, may stems from the lower contribution of Fe passivation due to the lowest Fe content. Thus, the protective film may dominated by Al-rich oxides.

For the explanation of passive layer formation in the passivation region three models are proposed in the literature. In the sandwich-like 3 layer structure model proposed by Schaepers et al, center layer is enriched by an Al oxide film while mixture of oxides of Fe and Al exist at outer and inner sides. In two layered model proposed by Frangini et al., upper layer involves aluminium-iron oxy-hydroxide while the inner layer involves Al-rich oxide. In the single layer model proposed by Shankar Rao, mixture of Al and Fe oxides are involved along the layer.

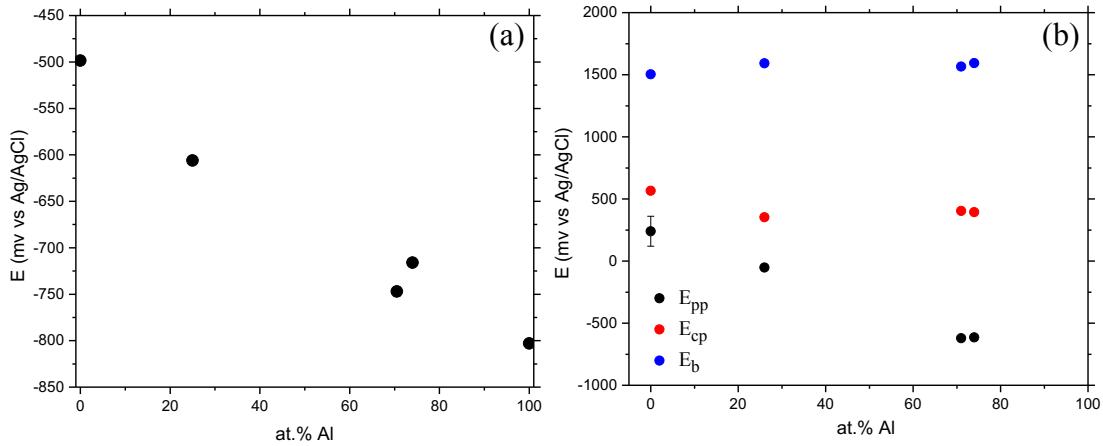

Figure 5.10 : (a)Active corrosion potentials (E_{corr}), (b)passive and complete passivation zone widths (E_{pp}-E_b, E_{cp}-E_b) of IF-steel, pure-Al and Fe-Al phases as a function of Al content.

The difference between primer passivation potential and breakdown potential (E_{pp}-E_b) for Fe-Al phases is greater than that for steel, which indicates that Fe-Al phases exhibit

passivation property in a wider potential range. The increase observed in Epp-Eb with the increased amount of Al contained for the Fe-Al phase, becomes negligible between the Fe_2Al_5 and Fe_2Al_5-Fe_4Al_{13}phases. This situation is in good agreement with the results of Chiang [16] in which the E_{pp}-E_b increases slightly after 25% Al content is reached. Active corrosion potentials (E_{corr}), passive and complete passivation zone widths (E_{pp}-E_b, E_{cp}-E_b) of IF-steel, Al and Fe-Al phases as a function of Al content are displayed in Figure 5.10a and Figure 5.10b, respectively.

The region corresponding to the transpassivation region of the curves of the Fe-Al phases coincides well with that of IF-Steel, This similarity indicates that the protective film in this region has the same electrochemical properties as IF-steel, emphasizing the contribution of iron oxide/hydroxides in the conversion, as claimed by Frangini et al. and Shankar Rao et al. [106,107].

5.2.3 Surface morphology and dissolution depth of samples

Electrochemical results of pure-Al, IF-Steel, and Fe-Al phases in terms of nature of attack characterizaed by SEM are given below as seconder electron images (SEi) and backscattered electron images (BSEi).

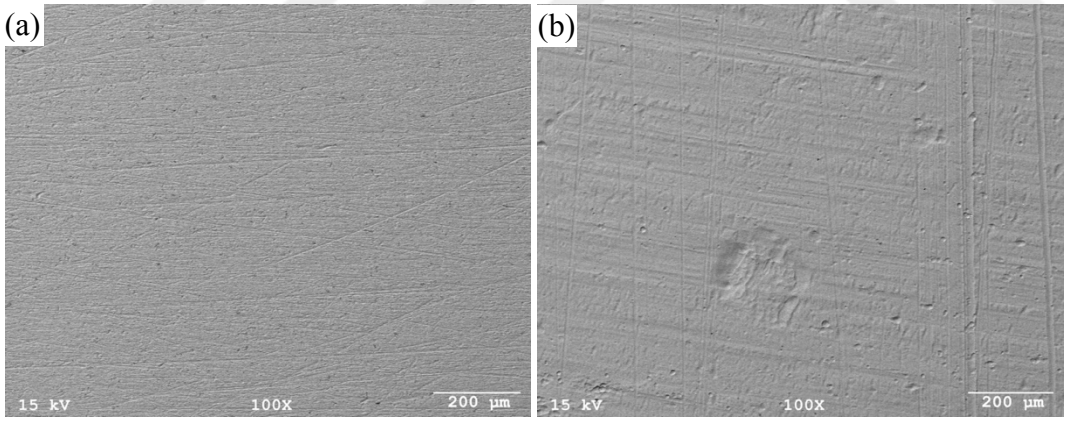

Figure 5.11 : SEM micrograph of of pure-Al (a) before and (b) after subjected to 0.5M H_2SO_4.

As expected, the even surface of pure-Al given in Figure 5.11a is preserved, as seen in Figure 5.11b, which indicates a protective film. These results in good agreement with the low i_{corr} obtained in the polarization curve of pure-Al which passivates spontaneously.

Local dissolution regions are observed on the surface of IF-steel (Figure 5.12b). According to the results of the EDS analysis, it is stems from the selective dissolution

of Fe which act as less noble, around the impurity. Dissolved sites and surrounding corrosion products are visible in images taken at higher magnifications (Figure 5.12c-d).

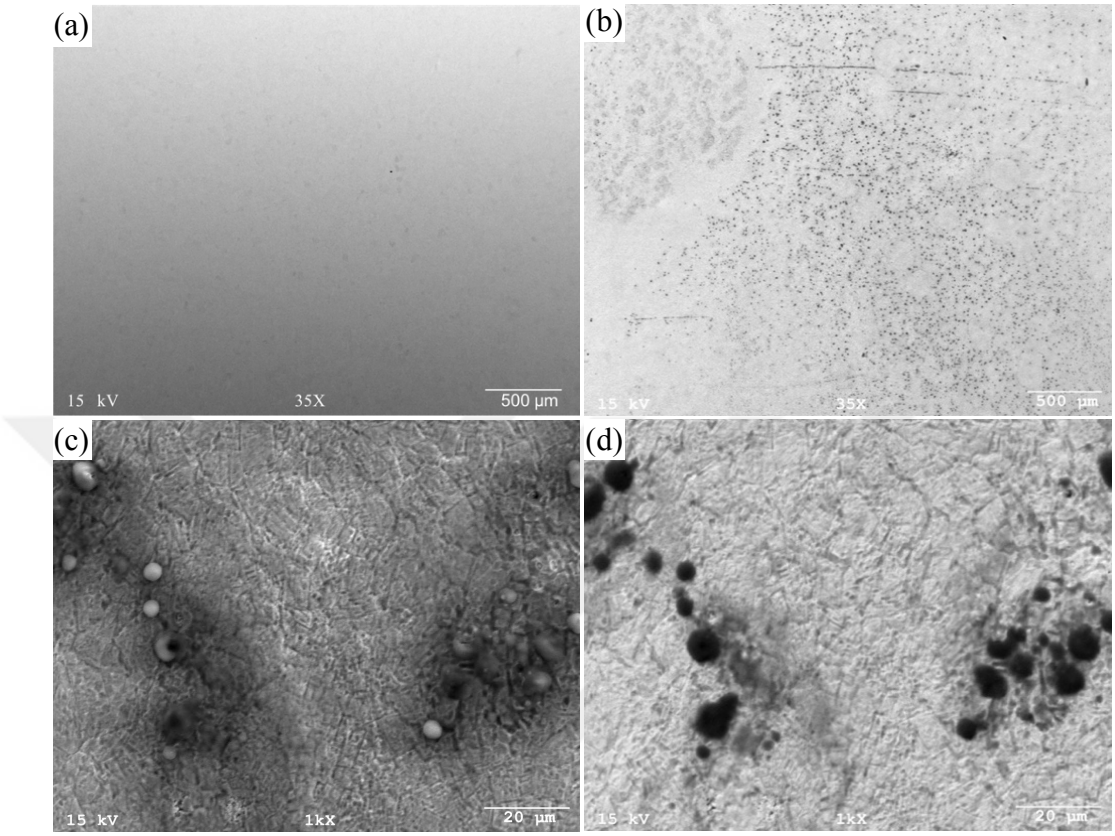

Figure 5.12 : SEM micrograph of IF-steel: (a) BSEi of treated surface (b) BSEi, higher magnification (c) SEi, (d) BSEi of electrochemically subjected surface in 0.5M H_2SO_4.

In the Figure 5.13, surface of Fe_3Al-FeAl as treated (Figure 5.13a) and as electrochemically exposed (Figure 5.13b-c-d) are presented. According to the Figure 5.13b, grains become distinguished are observed. When higher magnification images (Figure 5.13c-d) are examined, certain grains are detected as dissolved with a higher rate in a way to splited naturally from the surface. Different orientated grains are appeared remaining under the splited grains. This morphology may attributed to the different corrosion rate of grains which differ from each other in surface oriantation as revealed in the study conducted by Brito et al. [130]. Brito revealed corrosion rate dependance to the crystallographic orientation, in the tend of (100)<(110)≈(111) for Fe_3Al phase. However, considering the fact that relevant phase is the Fe_3Al-FeAl dual phase, grains that discriminated from each other in terms of dissolution rate may arise

from higher affinity of one of the phases (FeAl in the circumstance) as claimed by Chiang et al. [16].

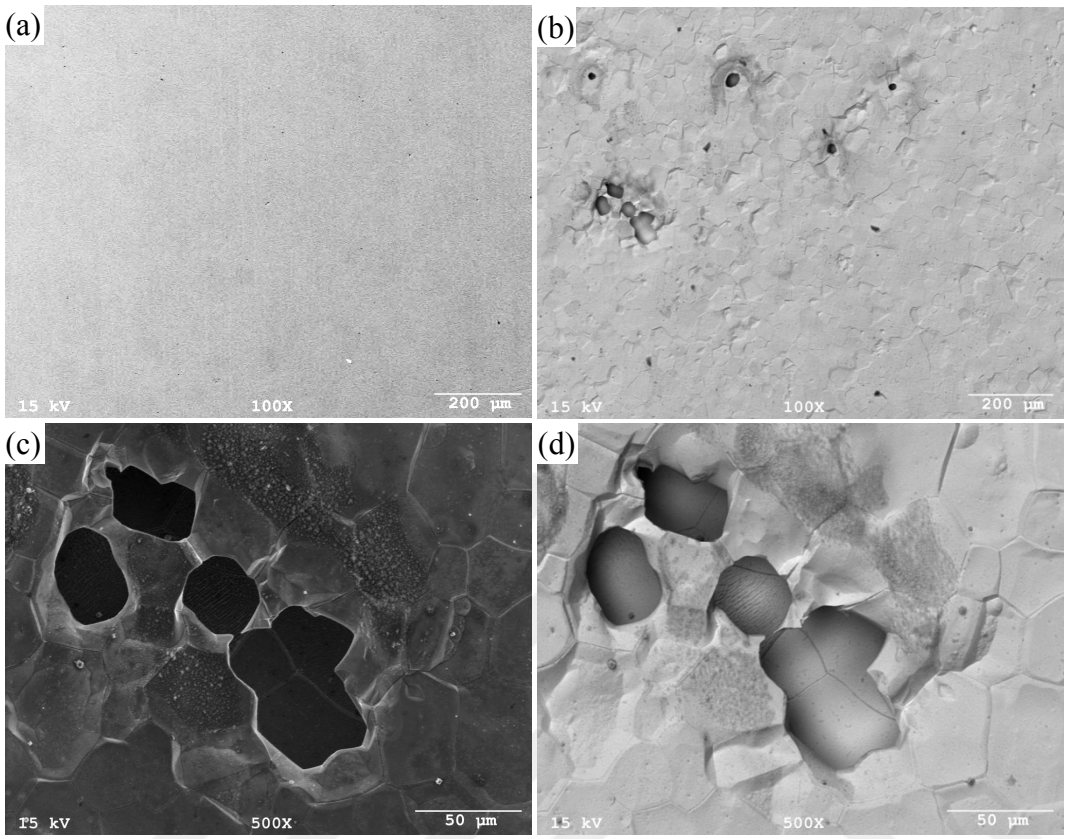

Figure 5.13 : SEM micrograph of Fe_3Al-FeAl: (a) BSEi of treated surface (b) BSEi, higher magnification (c) SEi, (d) BSEi of electrochemically subjected surface in 0.5M H_2SO_4.

Surface morphology of Fe_2Al_5 phase as treated and subjected to electrochemical testing are given respectively in Figure 5.14a and Figure 5.14b. where the crack formation is observed with the dissolved surface. When the crack existed regions are examined in higher magnification (Figure 5.14c-d), it is observed that certain grains are dissolved preferentially around transgranularly extended cracks. According to the study conducted by Çelikel [142], the hardness of the Fe_2Al_5 phase (1280 HV) is higher compared to Fe-rich and other Al-rich phases. Considering the susceptibility of iron aluminides to stress cracking corrosion (SCC) and hydrogen embrittlement [144,145], cracking of the film is not unexpected, however further wotk is needed for understanding the mechanism behind this failure. This cracking may be the reason for high active corrosion rate and higher passive currents of this layer (Table 5.1 and Figure 5.7).

In the Figure 5.15, surface morphologies related to Fe_2Al_5-Fe_4Al_{13} phase is presented. The presence of two different phases at the treated surface is evident with the contrast difference according to BSEi (Figure 5.15a), in which the lighter color indicates the heavier phase, in this case, Fe_2Al_5. Selective dissolution of certain regions is apparent in Figure 5.15b. Considering, the contribution of Al content on passivation behavior according to polarization data, less dissolved regions represent, probably, Al-rich regions with a higher tendency to passivation. Dissolved morphology and corrosion by-products are clear in higher magnification images (Figure 5.15c-d).

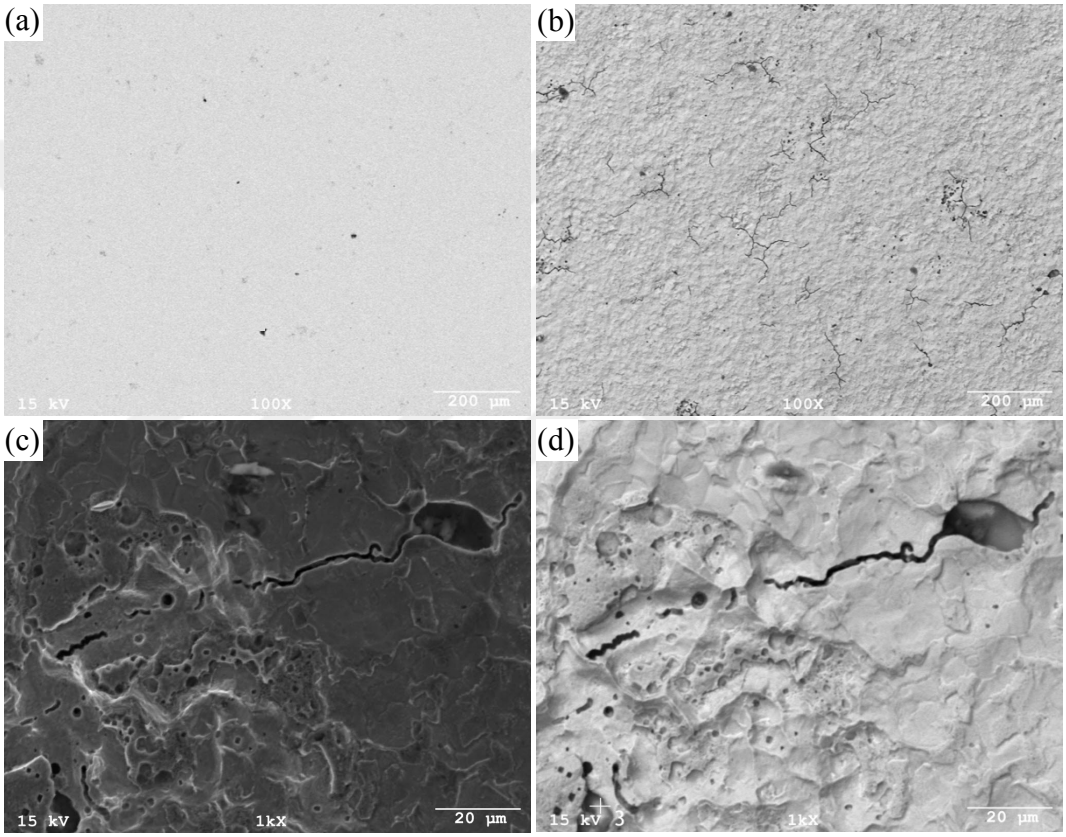

Figure 5.14 : SEM micrograph of Fe_2Al_5: (a) BSEi of treated surface (b) BSEi, higher magnification (c) SEi, (d) BSEi of electrochemically subjected surface in 0.5M H_2SO_4.

In Figure 5.16, 3D depth profile obtained by optical profilometer measurement reveals for all Fe-Al phases that the progression of corrosion was limited to the exposed layer since the depth where the lower layers exist is not reached.

The absence of a change in the depth profile of Al in Figure 5.16a, confirms the slight dissolution rate arisen from spontaneous passivation behavior. On the contrary, with the lowest tendency to passivation arisen from the highest critical current density (i_{crit}) among all, IF-steel exhibits 45µm dissolution depth (Figure 5.16b). The depth profile

(Figure 5.16c) presenting that Fe_3A-FeAl is dissolved to a small extent is consistent with its, compared to Al-rich Fe-Al phases, low active dissolution rate (i_{corr}) and high passivation tendency indicated by the i_{crit}. Considering its highest i_{crit}, and active dissolution rate (i_{corr}) among all Fe-Al phases, it is reasonable that Fe_2Al_5 exhibits the most dissolved profile (Figure 5.16d) among the Fe-Al phases. Besides, dissolution is enhanced probably from the cracks observed on the surface according to the SEM images of Fe_2Al_5. The Fe_2Al_5-Fe_4Al_{13} phase with lower i_{crit} and i_{corr} values compared to Fe_2Al_5, exhibits less amount of dissolution consistent with these behaviors (Figure 5.16e).

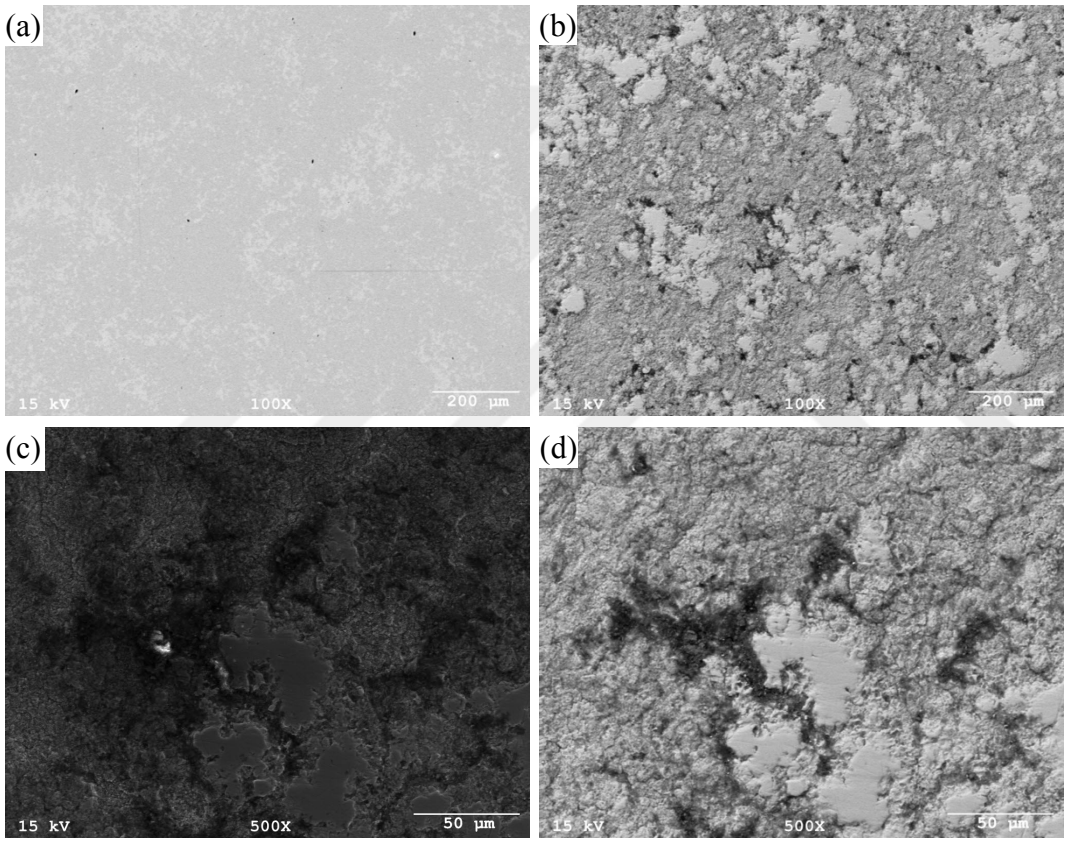

Figure 5.15 : SEM micrograph of Fe_2Al_5-Fe_4Al_{13}: (a) BSEi of treated surface (b) BSEi, higher magnification (c) SEi, (d) BSEi of electrochemically subjected surface in 0.5M H_2SO_4.

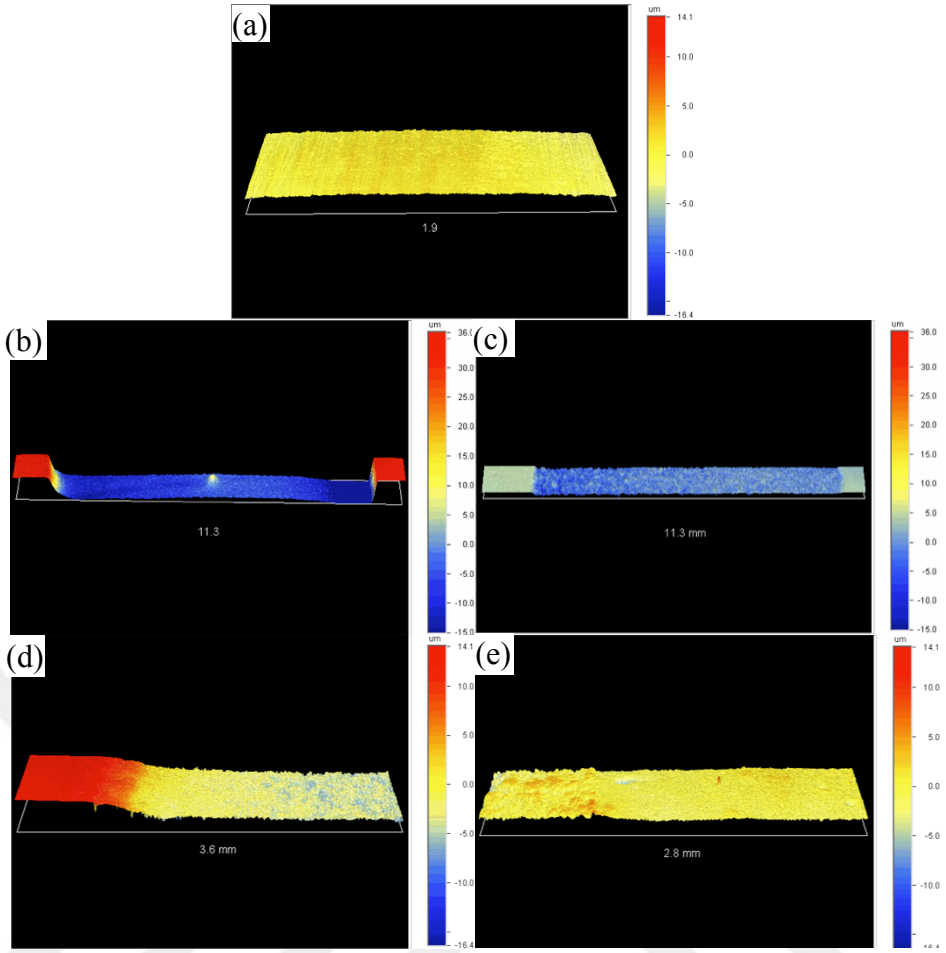

Figure 5.16 : 3D depth profile of (a) pure-Al, (b) IF-steel, (c) Fe_3A-FeAl, (d) Fe_2Al_5, (e) Fe_2Al_5-Fe_4Al_{13} obtained by optical profilometer after subjecting to artificial acid rain.

5.3 Electrochemical Behavior in Simulated Acid Rain

The electrochemical behaviors of pure-Al, IF-steel, and Fe-Al phases are also examined in artificial acid rain (200ppm Cl^- solution with the pH of 0.4 adjusted by H_2SO_4 [25])

5.3.1 Open circuit potentials

The variation of OCP over time for, IF-steel, and Fe-Al phases in artificial acid rain media (200ppm Cl^- pH4 adjusted with H_2SO_4) are presented in the Figure 5.17. While the Fe_2Al_5 and Fe_2Al_5-Fe_4Al_{13} phases exhibit positive trends, IF-steel and Fe_3Al-FeAl phase exhibit positive trends followed by initial negative trends in potential shift, until they reach steady states. The OCP values of the Fe-Al phases shifted towards more negative values with increasing aluminum concentration.

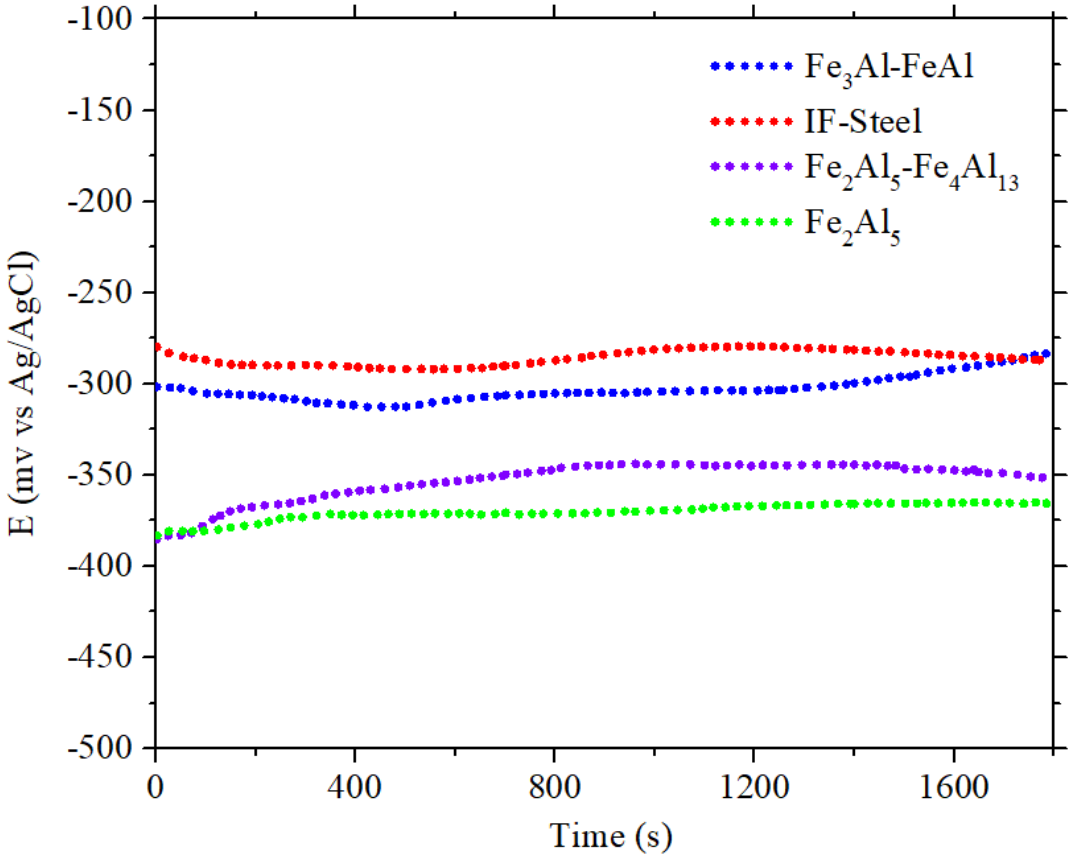

Figure 5.17 : OCP of pure Al, IF-steel and Fe-Al phases in artificial acid rain.

5.3.2 Potentiodynamic polarization behaviors

The overlaid potentiodynamic polarization curves obtained for the pure-Al, IF steel, and Fe-Al phases, in artificial acid rain are presented in Figure 5.18.

The linear polarization curve of the current density is presented in Figure 5.19 for profiling the breakdown potential of the samples. In Table 5.2 corrosion potential (E_{corr}), and breakdown potential (E_b) values of pure-Al, IF-steel, and Fe-Al phases are listed. The i_{corr} and E_{corr} values are extracted by Tafel Extrapolation from Figure 5.18. The Ep value which implies the potential of either the initiation of localized corrosion or the vanishing of the passive film by rapid dissolution is extracted from Figure 5.19 as the potential corresponding to the initiation of sharp current increase.

According to extracted values, the active dissolution rate (i_{corr}) of Al and Al-rich phases is lower than that of IF-steel and Fe-rich phase in one order of magnitude.

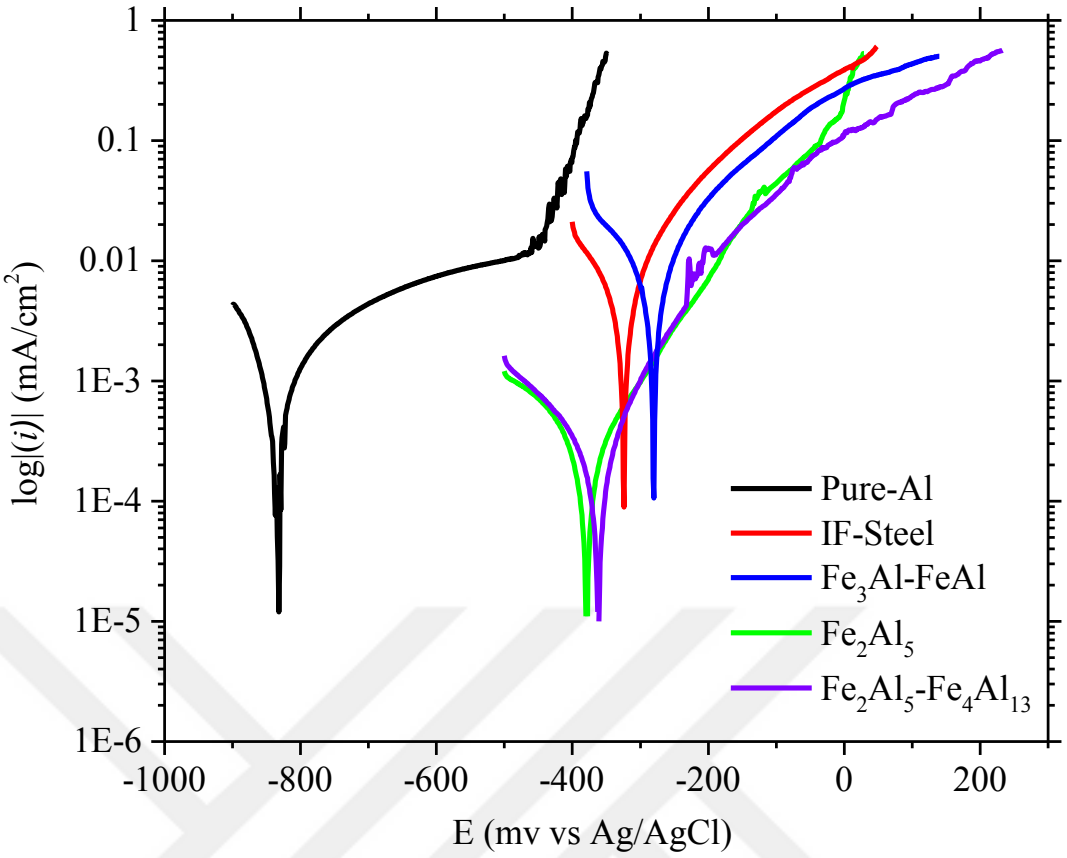

Figure 5.18 : Polarization curve of pure-Al, IF-Steel and Fe-Al phases in artificial acid rain.

When the corrosion potentials of samples are examined, Al exhibits the most active potential. It is known that Al exhibits less noble potential then steel with the presence of chloride ions [28]. Among Fe-Al phases, Al rich phases exhibit more active potential than IF-steel, positioning between pure Al and IF-steel. Fe_3A-FeAl phase has the most noble value compared to the all. Considering the obtained E_{corr} of samples, a galvanic series ranking in the order of Fe_3Al-FeAl>IF-Steel>Fe_2Al_5-Fe_4Al_{13}>Fe_2Al_5 is revealed. The E_{corr} values of samples as a function of Al content and relevantly formed galvanic series is given in the Figure 5.20. Concerning the cathodic protection in the existence of a defect, the revealed galvanic series in the artificial rain environment suggests that Al-rich layers with their negative potentials may sacrifice to protect the steel substrate. Among these Al-rich layers, Fe_2Al_5 act sacrificially compared to Fe_2Al_5-Fe_4Al_{13}. On the other hand, Fe_3Al-FeAl with the most noble potential is protected by steel and other Fe-Al phases. In this respect, with their relatively low active corrosion rates compared to the Fe-rich phase and IF-steel, and acting anodic compared to steel, phases rich in Al provide better protection to steel than the Fe-rich phase provide.

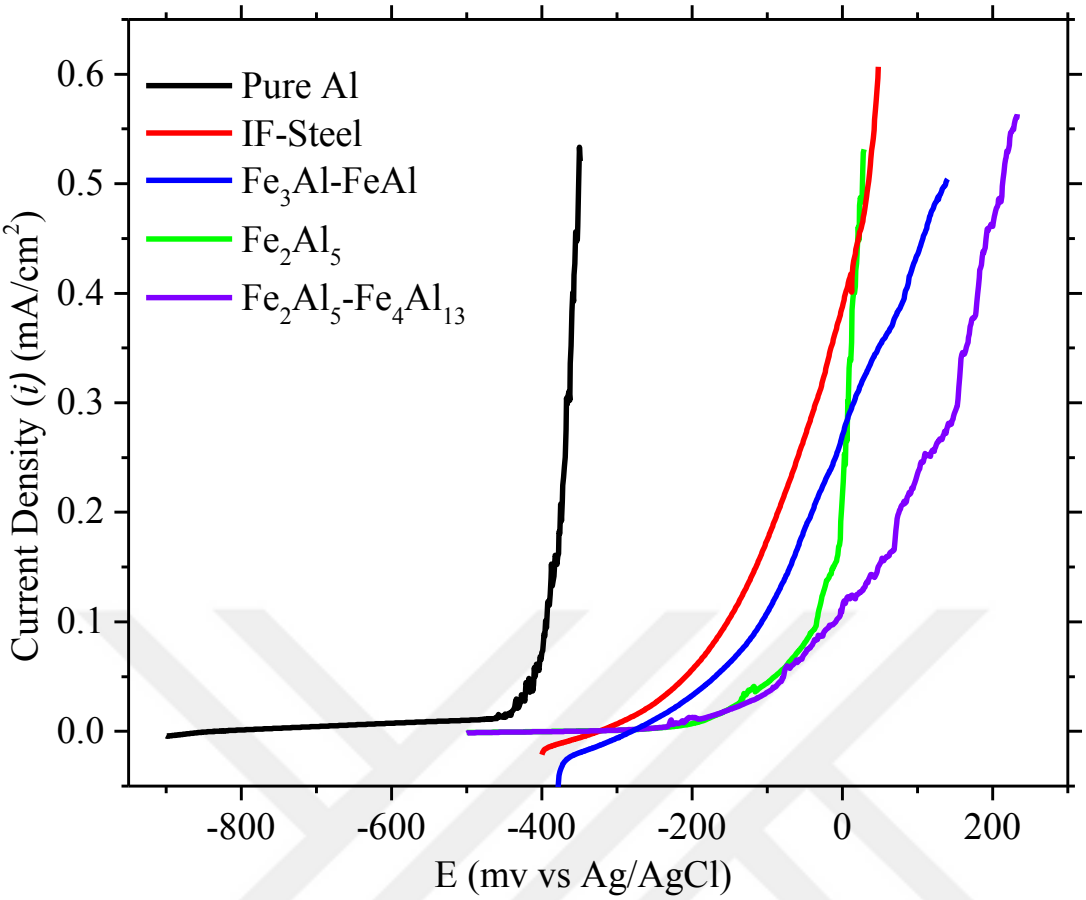

Figure 5.19 : Linear polarization curve of pure-Al, IF-steel and Fe-Al phases in artificial acid rain.

Table 5.2 : Electrochemical parameters for the pure-Al, IF-steel, and Fe-Al phases, derived from polarization curves in de-aerated artifical acid rain.

Sample	E_{corr} ($mV_{Ag/AgCl}$)	i_{corr} ($mA.cm^{-2}$)	E_b ($mV_{Ag/AgCl}$)
Al	-830	$3x10^{-4}$	-425
IF-Steel	-342	$4x10^{-3}$	-
Fe_3Al-FeAl	-283	$5.3\ x10^{-3}$	-
Fe_2Al_5	-360	$2.4\ x10^{-4}$	-117
Fe_2Al_5-Fe_4Al_{13}	-353	$2x10^{-4}$	-230

Regarding the breakdown behaviors, Al exhibits a characteristic sharp increase in current at -425mV which is the breakdown potential (E_b) of the protective oxide film. Contrary to Al, the steady state of current is absent for IF-steel and Fe-rich phase, instead, incrementally enhanced current indicates increased existing anodic activity. The absence of a protective film on the surface of Fe-rich layer elucidates its high current, in a similar manner to IF-steel. Aluminum is not exhibited an appreciable

contribution to the corrosion behavior of the Fe-rich phase. However, considering the existence of the second phase, which may cause a local galvanic coupling, in the structure, Al amount may not be the only factor in corrosion behavior. Both of the Al-rich phases exhibit the current plateau before the drastic increase in the current initiates. However, apparently, once the passivity breakdown occurs, the current increases more drastically for the Fe_2Al_5 phase than that for the Fe_2Al_5-Fe_4Al_{13}. Compared to Al, breakdown occurs at more noble potentials for Fe_2Al_5 (-117) and Fe_2Al_5-Fe_4Al_{13} (-230), while the former exhibits more noble E_b than the latter among themselves. Relatively more anodic Eb of Fe_2Al_5-Fe_4Al_{13} may attribute to the existence of the second phase which demonstrates varying susceptibility to localized corrosion. The contribution of aluminum to the Al-rich phases revealed as nobler E_b and low active corrosion rate (i_{corr}).

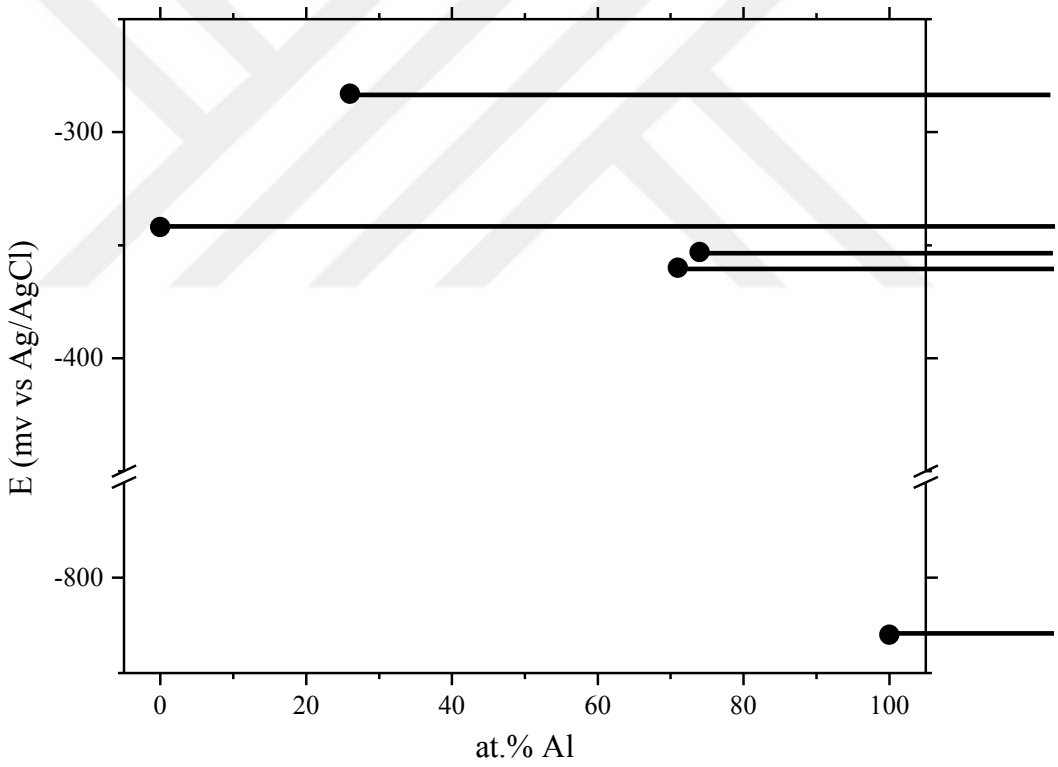

Figure 5.20 : The E_{corr} values of samples as a function of Al content and relevantly formed galvanic series.

Considering that certain Fe-Al phases exhibit passive properties at a range of potentials, the cathodic protection estimates made from the galvanic series created will not be sufficient for straightforward corrosion protection. Namely, spontaneous passivation may inhibit sacrificial dissolution of deformed active metal to noble sublayer.

For a more precise interpretation, allowing galvanic coupling of the relevant phases in the so-called environment is required.

5.3.3 Surface morphology of semples (SEM, EDS)

Electrochemical behavior of pure-Al, IF-steel, and Fe-Al phases in terms of the nature of the surface attack, is examined below.

In Figure 5.21, local corrosion regions formed after reaching the breakdown potential, which indicates the presence of passive film, are observed on the aluminum surface in artificial acid rain.

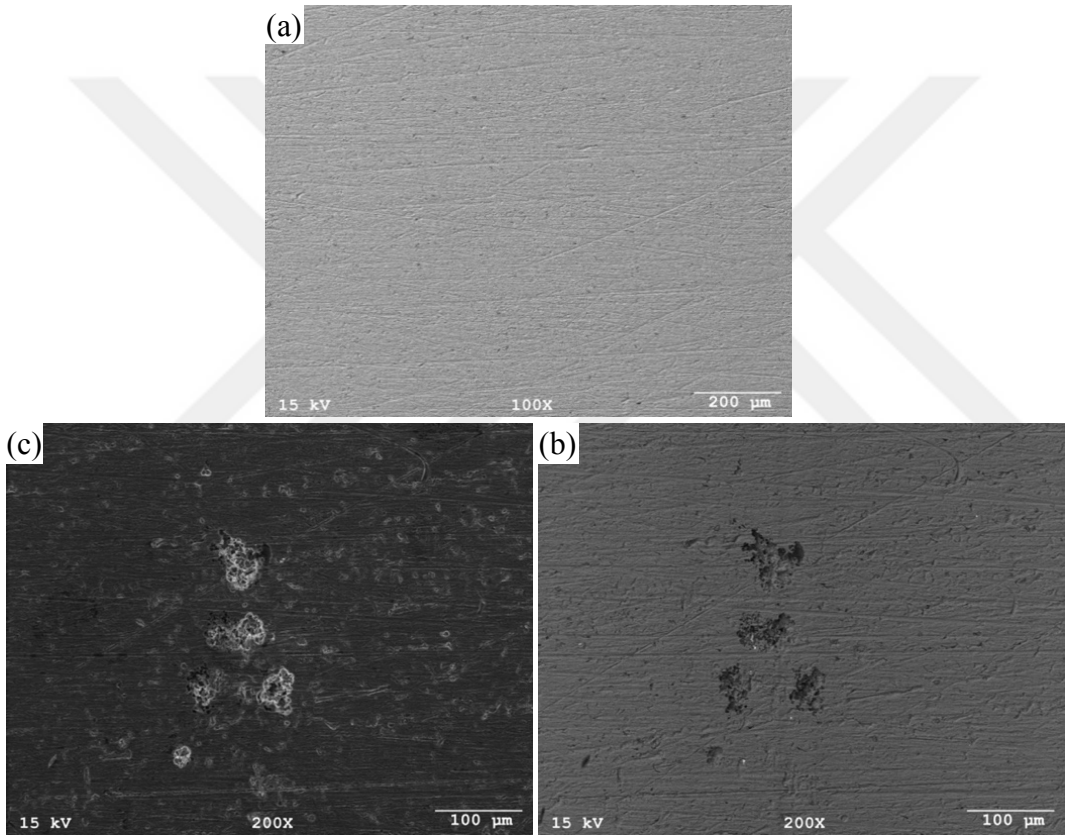

Figure 5.21 : SEM micrograph of Al: (a) BSEi before subjecting to artificial acid rain, (b)SEi, and (c)BSEi after subjected to artificial acid rain.

SEM micrograph of IF-steel given in Figure 5.22 confirms the extracted data from the polarization curve which indicates the enhanced existing initial dissolution rate of IF-steel by the increased potential. When the dissolved regions examined in higher magnifications, it is observed that dissolution takes place around the impurities which create local galvanic sites by acting more noble compared to Fe.

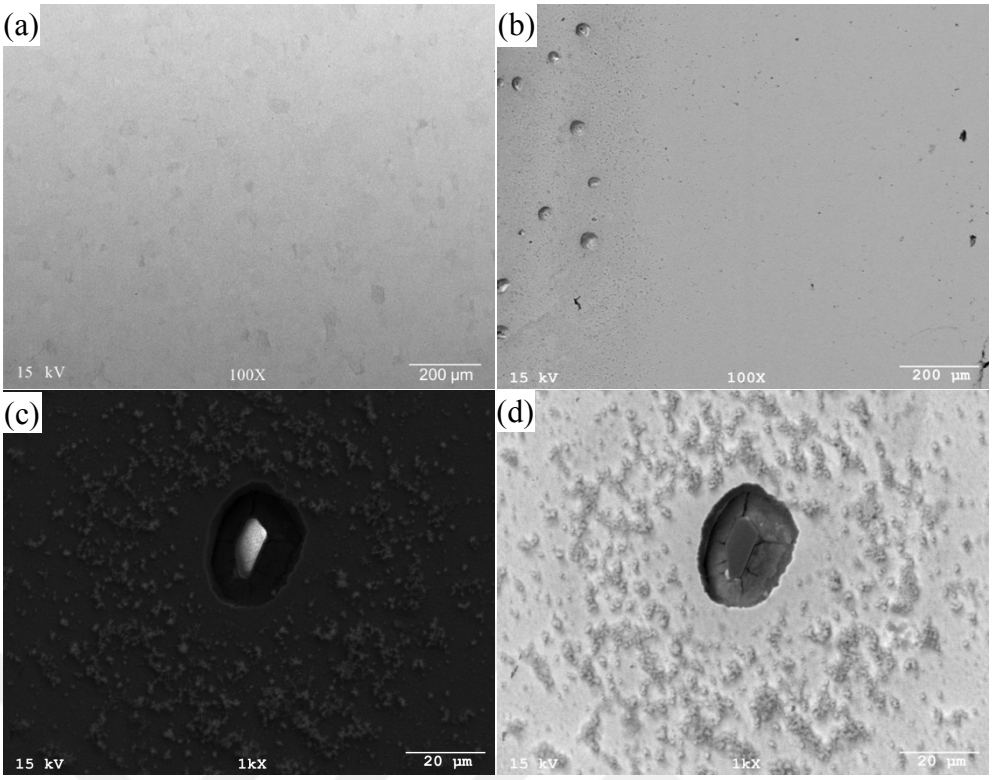

Figure 5.22 : SEM micrograph of IF-steel: (a) BSEi of treated surface (b) BSEi, higher magnification (c) SEi, (d) BSEi of electrochemically subjected surface in artificial acid rain.

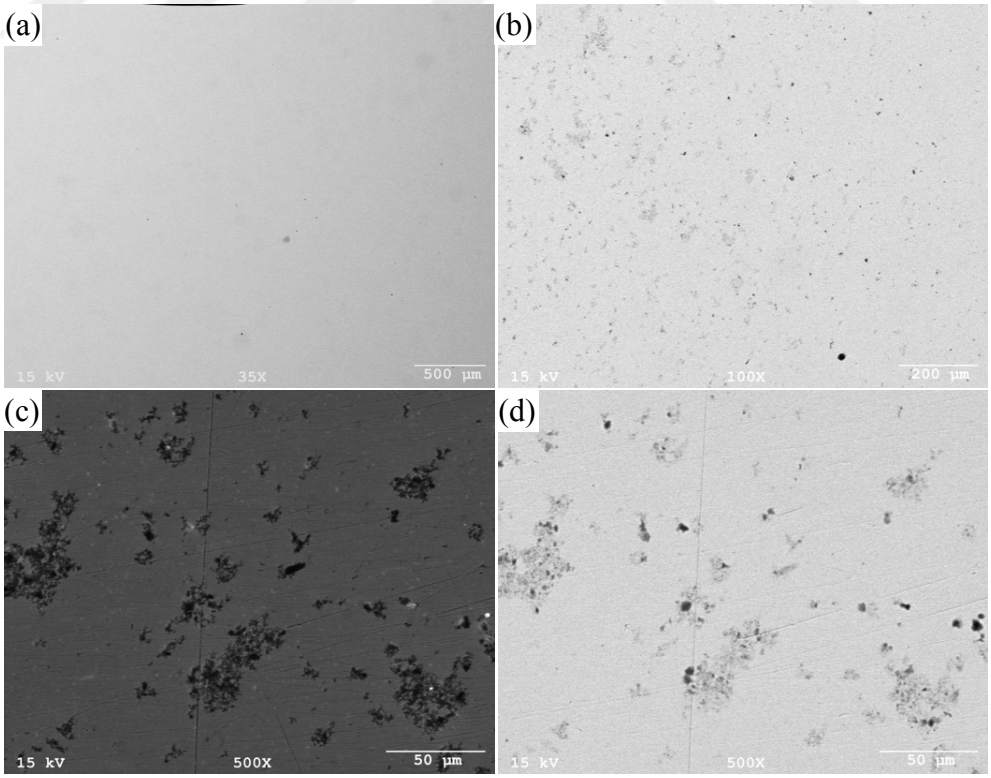

Figure 5.23 : SEM micrograph of Fe_3Al-FeAl: (a) BSEi of treated surface (b) BSEi, higher magnification (c) SEi, (d) BSEi of electrochemically subjected surface in artificial acid rain.

In the Figure 5.23, SEM images of Fe_3Al-FeAl phase subjected to artificial acid rain are presented. dissolution that takes place throughout the surface probably initiated once the sample immersed in the electrolyte, inferred from the absence of breakdown potential in the polarization curve of the phase.

In the SEM images of the Fe_2Al_5 given in Figure 5.24, pit formation on the surface is observed clearly. Linear polarizaton curve is in coincidence with the surface morphology. The breakdown potential and sharp increase at current corresponds the initiation of localized corrosion and enhanced pit formation, respectively. These results implies that Fe_2Al_5 phase provide barier corrosion protection to the underneath up to breakdown potential in artificial acid rain environment.

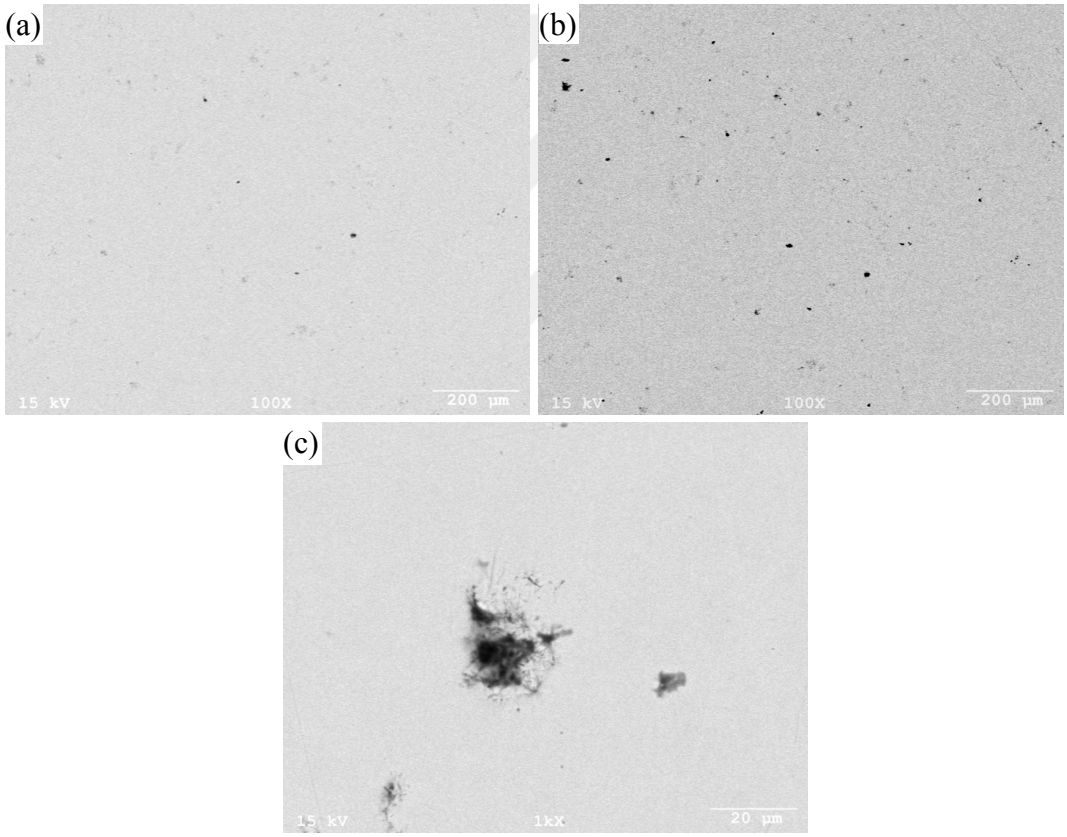

Figure 5.24 : SEM micrograph of Fe_2Al_5: (a) BSEi of treated surface, (b) BSEi, (c) higher magnification BSEi of electrochemically subjected surface in artificial acid rain.

Two phases of Fe_2Al_5-Fe_4Al_{13} that differ from each other by color contrast is clear in the Figure 5.25a. In the Figure 5.25b , a local flake off which seems to follow a certain phase, probably corresponding to the breakdown in the linear polarization curve is observed. The structure with cracks become apparent under the dissolved region. Once the breakdown initiated, one of the phases, the dissolved one, maybe sacrificing itself

locally as the other is acting nobler. Active breakdown potential of Fe_2Al_5-Fe_4Al_{13} than of Fe_2Al_5, despite the higher Al content of the former compared to the latter, may arise from as displayed sacrificial behavior of one phase for the other in the former. The drastic increase in the current density probably arises from the enhanced dissolution through the cracks. Fe_2Al_5-Fe_4Al_{13} provides barrier protection to the underneath up to its breakdown potential in the smilar trend with Fe_2Al_5 in the artificial acid rain environment.

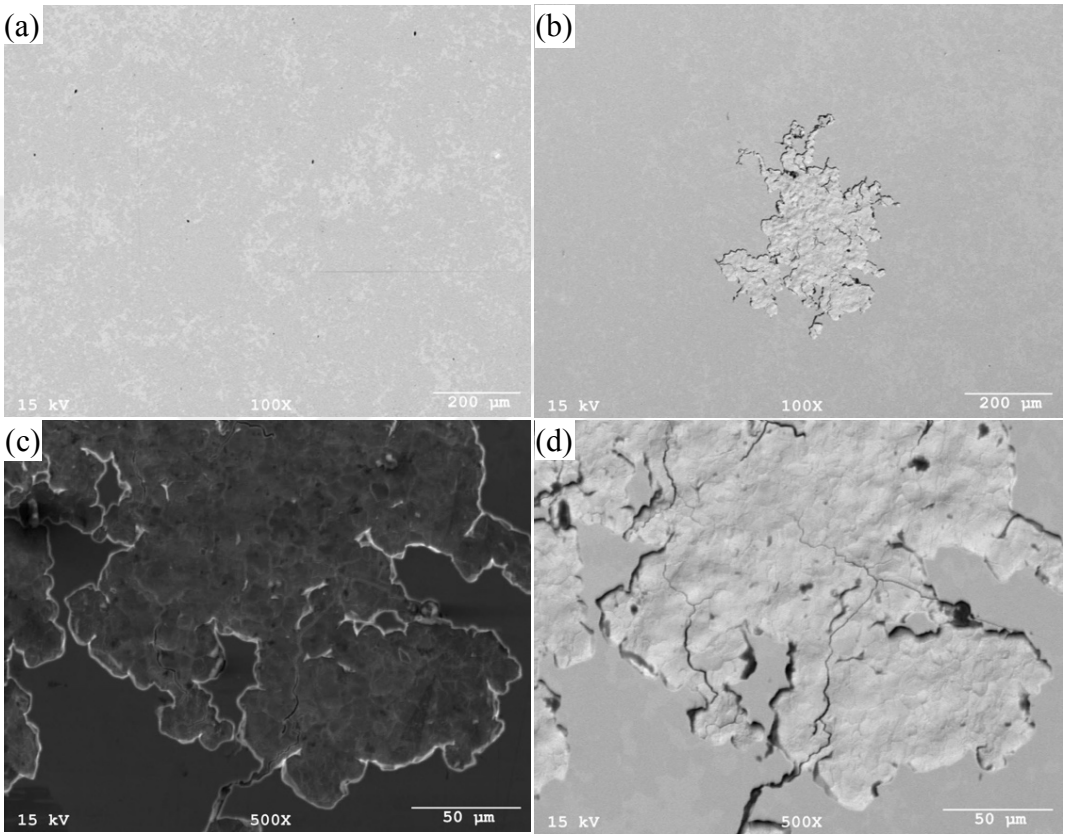

Figure 5.25 : SEM micrograph of Fe_2Al_5-Fe_4Al_{13}: (a) BSEi of treated surface (b) BSEi, higher magnification (c) SEi, (d) BSEi of electrochemically subjected surface in artificial acid rain.

According to the values obtained from polarization curves, and investigation of surface attack through SEM micrographs, Fe_2Al_5-Fe_4Al_{13} and Fe_2Al_5 provide barrier protection to the underneath in the so-called environment. Besides, due to their active corrosion potentials compared to other Fe-rich phase and IF-steel, they are assumed to provide cathodic protection. However, considering their passivation behavior to straightforward estimation on electrochemical behavior in term of the nature of protection, extensive studies are required.

5.3.4 Effects of surface cracks on electrochemical behavior of samples (creation of galvanic pairs) in artificial acid rain

In this section, the cathodic protection tendencies inferred according to the order in the galvanic series formed by the corrosion potential of the phases interpreted in terms of corrosion behavior, barrier protection they provide, and active dissolution rate are examined.

The treated samples are named with the phases interest exposed to the environment, which are the above-mentioned Fe_3Al-FeAl, Fe_2Al_5, Fe_2Al_5-Fe_4Al_{13} phases. Each phase is treated in a way that it contacts with IF-steel associated with the galvanic series in the sublayer The reason that the substrates in relation to the Fe-Al surface phase layer is obtained as α-Fe(Al) instead of IF-steel is a diffusion of some amount of aluminum always exists inside the IF-steel through the thick diffusion layer.

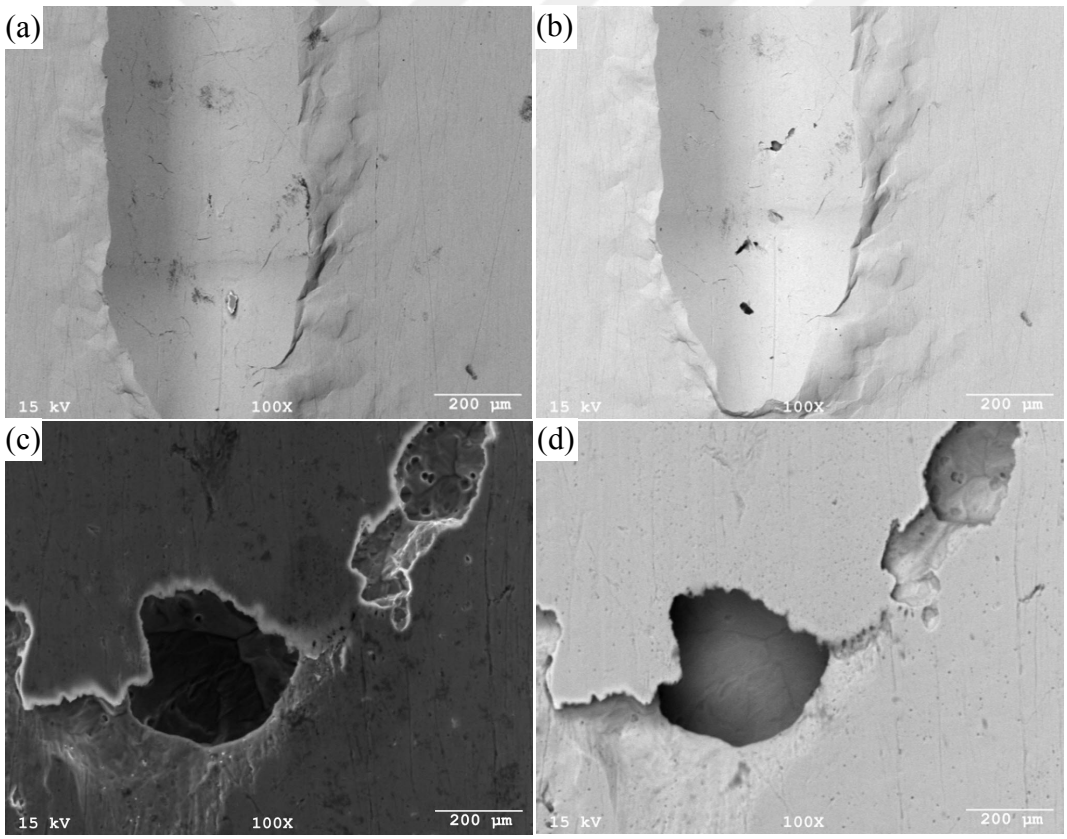

Figure 5.26 : Surface morphology of Fe_3Al-FeAl: (a) BSEi of scratched surface, (b) BSEi, higher magnification (c)SEİ, (d) BSEi of electrochemically exposured surface in artificial acid rain.

The electrochemical behavior of the samples in terms of cathodic protection are interpreted by the examination of SEM images obtained after being subjected to the

experiment by considering the revealing galvanic series in the potential order of Fe_3Al-FeAl > IF-steel> Fe_2Al_5-Fe_4Al_{13}> Fe_2Al_5.

The Figure 5.26a presents the cracks formed on the surface of the Fe_3Al-FeAl phase. After electrochemical exposure, local corrosion zones occurring within the cracks given in the Figure 5.26a are shown in the Figure 5.26b. When the pits formed are examined more closely in higher magnification images (Figure 5.26c-d), the grain structures of α-Fe(Al) and the pits that initiate to form in the grains are observed as a result of inward progress. The SEM results are in line with the electrochemical results as followed: The absence of breaking potential for Fe_3Al-FeAl and IF-steel which indicates dissolution with enhanced rate from the very beginning of exposure instead of passivation; The more noble position of Fe_3Al-FeAl than that of IF-steel in as-revealed galvanic series. According to SEM examination and as mentioned results it is averred that steel provide cathodic protection to Fe_3Al-FeAl by sacrificing itself.

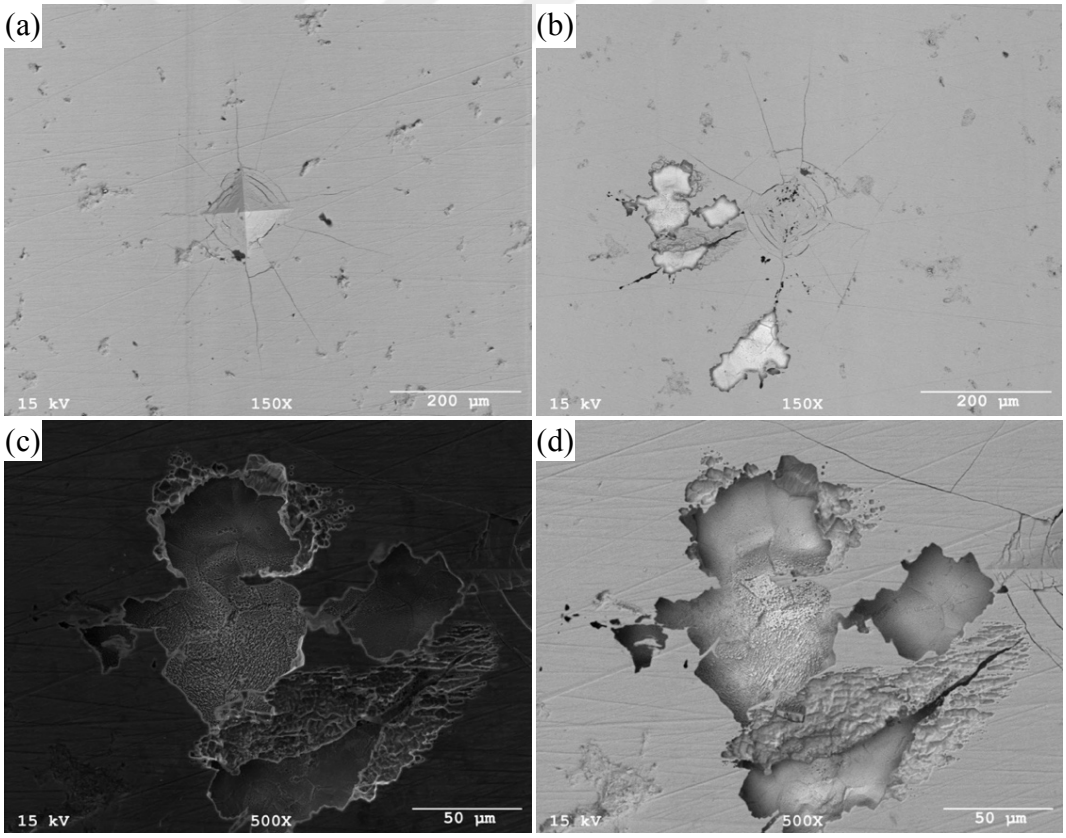

Figure 5.27 : Surface morphology of Fe_2Al_5: (a) BSEi of cracked surface, (b) BSEi, higher magnification (c)SEİ, (d) BSEi of electrochemically exposured surface in artificial acid rain.

In the Figure 5.27a, created cracks is presented. After exposed to the artificial acid rain, it is observed that the Fe_2Al_5 phase layer is flake off though the cracks in such a

way that exposure the steel substrate (Figure 5.27b). In higher magnification images (Figure 5.27c-d), grains of steel is distinguished clearly. considering electrochemical polarization results which reveals Fe_2Al_5 settles in a more active potential in the as-revealed galvanic series compared to IF-steel settles, it was claimed that the former provide cathodic protection to the latter by sacrificing itsel. On the other hand, considering the breakdown behavior which implies Fe_2Al_5 exhibits passivation behavior up to breakdown potential, this claim could be failed. However, The comparison results of SEM micrographs and electrochemical testing, it is concluded that Fe_2Al_5 provides cathodic protection to α-Fe(Al) substrate despite its passivation behavior.

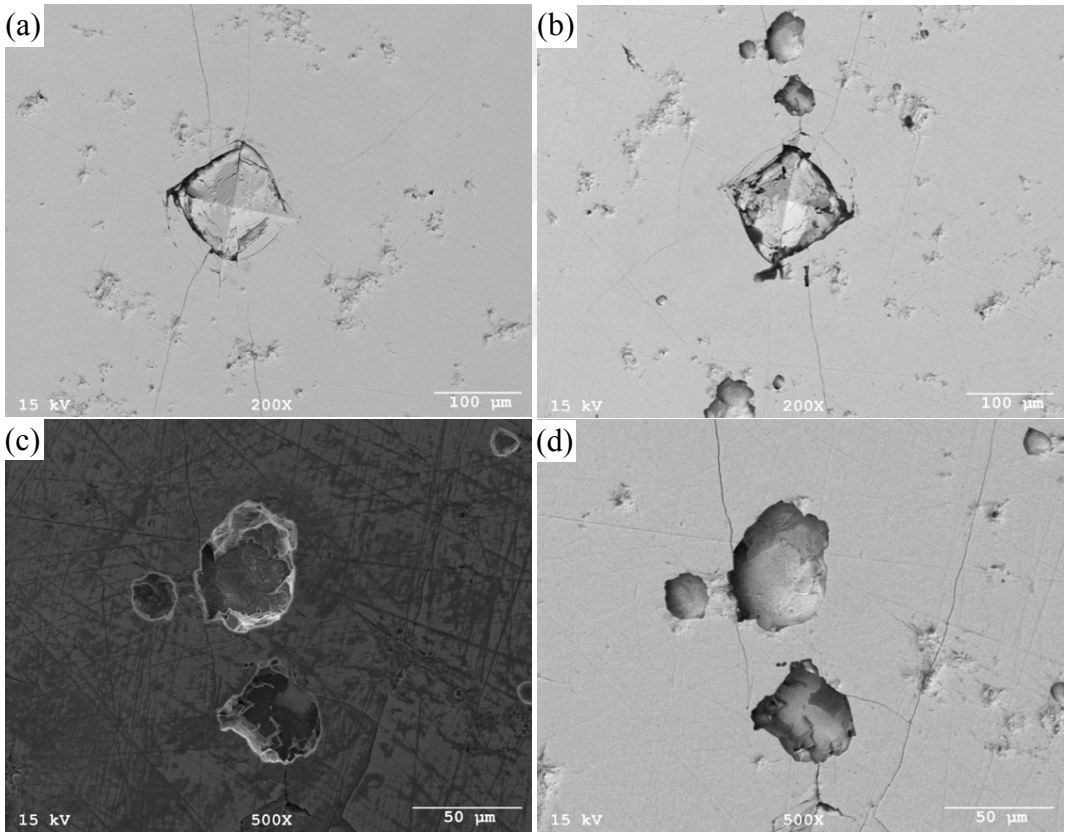

Figure 5.28 : Surface morphology of Fe_2Al_5-Fe_4Al_{13}: (a) BSEi of cracked surface, (b) BSEi, higher magnification (c)SEİ, (d) BSEi of electrochemically exposured surface in artificial acid rain.

In Figure 5.28a, cracks formed on the Fe_2Al_5-$Fe4Al_{13}$ phase layer is observed. In the Figure 5.28b which present the surface morphology after electrochemical testing, flake offs along cracks are appeared.The higher magnification images (Figure 5.28c-d) manifest the grains of iron the underneath. In spite of breakdown potential results which implies Fe_2Al_5-$Fe4Al_{13}$ phase exhibits passivation behavior in the same trend

with Fe_2Al_5, surface examination results in good agreement with the electrochemical results which implies, compared to the steel, Fe_2Al_5 presents exhibits more active potential, namely, the former is protected by the latter sacrificially.

6. CONCLUSION

In this thesis study, electrochemical corrosion experiments of IF-steel aluminized by CA-EMIT method were carried out in sulfuric acid environment (0.5M H_2SO_4) and in artificial acid rain containing 200ppm Cl^-.

Within the CA-EMIT procedure, the Al-rich phases with decreasing content of Al were formed on the surface of substrates at the temperature range of 1100 and 1150^oC (Fe_2Al_5-Fe_4Al_{13}, Fe_2Al_5, respectively). On the other hand, Fe-rich phases were formed on the surface of the substrate at the processing temperature of 1200 ^oC (Fe_3Al-FeAl).

In 0.5M H_2SO_4, the Fe-rich phase produced by the CA-EMIT method exhibited corrosion resistance similar to Fe-rich bulk iron aluminides, namely the presence of Al in the alloy improved the passivation behavior in sulfuric acid solutions. Al-rich intermetallics exhibited better passivation behavior owing to their higher Al content. However, some cracking took place during corrosion tests, which can be an indication of their sensitivity to-wards environmentally assisted cracking.

In the simulated acid rain environments, a galvanic series is produced by ranking the corrosion potentials (The nobility order: Fe_3Al-FeAl > IF-steel > Fe_2Al_5-Fe_4Al_{13} > Fe_2Al_5). The Al-rich intermetallic layers provided, to IF-steel substrate, both barrier corrosion protection by exhibiting passive behavior up to breakdown potential and cathodic protection by sacrificing themselves in the event of cracks. On the other hand, the Fe-rich intermetallic layer with the lack of passivation failed to act as a protective barrier, and in the presence of paths that allow electrolytic conduct between the substrate, it may create a problem of accelerating the corrosion of steel with galvanic action.

REFERENCES

[1] **McKamey, C. G., DeVan, J. H., Tortorelli, P. F., & Sikka, V. K.** (1991). A Review Of Recent Developments In Fe3Al- based alloys. *Journal of Materials Research*, *6*(8), 1779–1805.

[2] **Tewari, R., Sarkar, N. K., Harish, D., Vishwanadh, B., Dey, G. K., & Banerjee, S.** (2017). Intermetallics and Alloys for High Temperature Applications. In *Materials Under Extreme Conditions: Recent Trends and Future Prospects* (pp. 293–335). Elsevier Inc.

[3] **Morris, D. G., & Muñoz-Morris, M. A.** (2011). Recent developments toward the application of iron aluminides in fossil fuel technologies. *Advanced Engineering Materials*, *13*(1–2).

[4] **Luis, N. C.** (2017). Transition Metal Aluminide Coatings and Initial Steps on Additive Manufacturing. In A. Mahmood (Ed.), *Intermetallic Compounds - Formation and Applications* (pp. 167–191). IntechOpen.

[5] **Galetz, M. C.** (2015). Coatings for Superalloys. In M. Aliofkhazraei (Ed.), *Superalloys* (pp. 277–298). IntechOpen.

[6] **Li, N. N., Wang, M. Z., Li, Y. S., Chen, G., & Li, P.** (2016). Corrosion behavior of Fe-Al coatings fabricated by pack aluminizing method. *Acta Metallurgica Sinica (English Letters)*, *29*(9), 813–819.

[7] **Wang, Q., Leng, X. S., Yang, T. H., & Yan, J. C.** (2014). Effects of Fe - Al intermetallic compounds on interfacial bonding of clad materials. *Transactions of Nonferrous Metals Society of China (English Edition)*, *24*(1), 279–284.

[8] **Takata, N., Nishimoto, M., Kobayashi, S., & Takeyama, M.** (2015). Crystallography of Fe2Al5 phase at the interface between solid Fe and liquid Al. *Intermetallics*, *67*, 1–11.

[9] **John, J. T., Sundararaman, M., Dubey, V., & Srinivasa, R. S.** (2013). Structural characterisation of iron aluminide coatings prepared by chemical vapour deposition. *Materials Science and Technology (United Kingdom)*, *29*(3), 357–363.

[10] **Spiradek-hahn, K., & Gamo, R. M.** (2005). 10.4028/0-87849-366-2.251. *Del_Journal of Metastable and Nanocrystalline Materials: Winter e-Volume 2005*, *January*.

[11] **Ürgen, M. K., & Oncel, S.** (2015). *Method for controlled production of diffusion based coatings by vacuum cathodic arc systems* (Patent No. EP 2 829 635 B1). Europen Patent Office.

[12] **Babu, N., Balasubramaniam, R., & Ghosh, A.** (2001). High-temperature oxidation of Fe3Al-based iron aluminides in oxygen. *Corrosion Science*, *43*(12), 2239–2254.

[13] **Strafford, K. N., & Manifold, R.** (1972). The effects of aluminum alloying additions on the sulfidation behavior of iron. *Oxidation of Metals*, *5*(2), 85–112.

[14] **Tortorelli, P. F., & DeVan, J. H.** (1992). Behavior of iron aluminides in oxidizing and oxidizing/sulfidizing environments. In *Materials Science and Engineering A* (Vol. 153, Issues 1–2). ELSEVIER SEQUOIA S.A.

[15] **DeVan, J. H., & Tortorelli, P. F.** (1993). Oxidation/sulfidation of Iron-aluminium alloys. *Materials at High Temperatures*, *11*(1–4), 30–35.

[16] **Chiang, W. C., Luu, W. C., & Wu, J. K.** (2006). Effect of aluminum content on the passivation behavior of Fe-Al alloys in sulfuric acid solution. *Journal of Materials Science*, *41*(10), 3041–3044.

[17] **Peng, J., Moszner, F., Rechmann, J., Vogel, D., Palm, M., & Rohwerder, M.** (2019). Influence of Al content and pre-oxidation on the aqueous corrosion resistance of binary Fe-Al alloys in sulphuric acid. *Corrosion Science*, *149*(June 2018), 123–132.

[18] **Łosiewicz, B., Budniok, A., Freitag, M., & Kupka, M.** (2010). Structure and Electrochemical Corrosion Resistance of the Passivated Fe-40at.%Al Binary Alloy in Sulfuric Acid Solution. *Solid State Phenomena*, *163*, 68–71.

[19] **Frangini, S.** (1999). Corrosion rate and anodic dissolution behavior of a B2-iron aluminide alloy in sulfuric acid. *Corrosion*, *55*(1), 89–95.

[20] **Schaepers, D., & Strehblow, H.** (1995). Surface Analytical Investigations of Electrochemically Formed Passive Layers on Binary Fe/Al Alloys. *Journal of The Electrochemical Society*, *142*(7), 2210–2218.

[21] **Schaepers, D., & Strehblow, H.** (1997). An XPS and ISS investigation of passive layers on binary Fe-Al alloys. *Corrosion Science*, *39*(12), 2193–2213.

[22] **Frangini, S., De Cristofaro, N. B., Mignone, A., Lascovich, J., & Giorgi, R.** (1997). A combined electrochemical and XPS study on the passivity of B2 iron aluminides in sulphuric acid solution. *Corrosion Science*, *39*(8), 1431–1442.

[23] **Shankar Rao, V., Raja, V. S., Baligidad, R. G., & Raman, R.** (2003). Effect of aluminium on electrochemical corrosion behaviour of Fe-0.5C and Fe-1C alloys in 0.25M H2SO4. *Corrosion Engineering Science and Technology*, *38*(3), 235–238.

[24] **Frangini, S., Lascovich, J., & de Cristofaro, N.** (1995). Pitting susceptibility of chromium modified passive films of a B2-FeAl intermetallic alloy. *Materials Science Forum*, *185–188*, 1041–1048.

[25] **Kim, J. G., & Buchanan, R. A.** (1994). Pitting and crevice corrosion of iron aluminides in a mild acid-chloride solution. *Corrosion*, *50*(9), 658–668.

[26] **De Graeve, I., Schoukens, I., Lanzutti, A., Andreatta, F., Alvarez-Pampliega, A., De Strycker, J., Fedrizzi, L., & Terryn, H.** (2013). Mechanism of corrosion protection of hot-dip aluminium-silicon coatings on steel studied by electrochemical depth profiling. *Corrosion Science*, *76*, 325–336.

[27] **Schoukensa, I., De Graeve, I., De Strycker, J., & Terryn, H.** (2012). Effect of local surface microstructure and composition on the electrochemical behavior of hot dip aluminum-silicon coatings on steel. *Corrosion*, *68*(11), 982–993.

[28] **Maki, J.** (2019). Corrosion behavior of aluminized steel sheets in 50-year outdoor exposure test. *ISIJ International*, *59*(10), 1870–1877.

[29] **Dosdat, L., Petitjean, J., Vietoris, T., & Clauzeau, O.** (2011). Corrosion resistance of different metallic coatings on press-hardened steels for automotive. *Steel Research International*, *82*(6), 726–733.

[30] **Ahnia, F., & Demri, B.** (2013). Evaluation of aluminum coatings in simulated marine environment. *Surface and Coatings Technology*, *220*, 232–236.

[31] **Långberg, M., Örnek, C., Evertsson, J., Harlow, G. S., Linpé, W., Rullik, L., Carlà, F., Felici, R., Bettini, E., Kivisäkk, U., Lundgren, E., & Pan, J.** (2019). Redefining passivity breakdown of super duplex stainless steel by electrochemical operando synchrotron near surface X-ray analyses. *Npj Materials Degradation*, *3*(1), 1–11.

[32] **Panossian, Z., Mariaca, L., Morcillo, M., Flores, S., Rocha, J., Peña, J. J., Herrera, F., Corvo, F., Sanchez, M., Rincon, O. T., Pridybailo, G., & Simancas, J.** (2005). Steel cathodic protection afforded by zinc, aluminium and zinc/aluminium alloy coatings in the atmosphere. *Surface and Coatings Technology*, *190*(2–3), 244–248.

[33] **Stoloff, N. S., & Sikka, V. K.** (1996). Physical Metallurgy and processing of Intermetallic Compounds. In *Physical Metallurgy and processing of Intermetallic Compounds*. Springer US.

[34] **Cinca, N., Lima, C. R. C., & Guilemany, J. M.** (2013). An overview of intermetallics research and application: Status of thermal spray coatings. *Journal of Materials Research and Technology*, *2*(1), 75–86.

[35] **Deevi, S. C., & Sikka, V. K.** (1996). Nickel and iron aluminides: An overview on properties, processing, and applications. *Intermetallics*, *4*(5), 357–375.

[36] **Zamanzade, M., Barnoush, A., & Motz, H.** (2016). A review on the properties of iron aluminide intermetallics. *Crystals*, *6*(1).

[37] **Palm, M., Stein, F., & Dehm, G.** (2019). Iron Aluminides. *Annual Review of Materials Research*, *49*(1), 297–326.

[38] **Mckamey, C. G.** (1996). Iron Aluminides. In *Physical metallurgy and processing of intermetallic compounds* (pp. 351–391). Springer, Boston, MA.

[39] **von Goldbeck, O. K.** (1982). Iron—Aluminium Fe—Al. In *IRON-Binary Phase Diagrams* (pp. 5–9). Springer, Berlin, Heidelberg.

[40] **Kattner, U. R., & Burton, B. P.** (1993). Al-Fe (Aluminum-Iron). In H. Okamoto (Ed.), *Phase Diagrams of Binary Iron Alloys* (Issue July, pp. 12–28). ASM International.

[41] **Stein, F., & Palm, M.** (2007). Re-determination of transition temperatures in the Fe-Al system by differential thermal analysis. *Zeitschrift Fuer Metallkunde/Materials Research and Advanced Techniques*, *98*(7), 580–588.

[42] **Sundman, B., Ohnuma, I., Dupin, N., Kattner, U. R., & Fries, S. G.** (2009). An assessment of the entire Al-Fe system including D03 ordering. *Acta Materialia*, *57*(10), 2896–2908.

[43] **Li, X., Scherf, A., Heilmaier, M., & Stein, F.** (2016). The Al-Rich Part of the Fe-Al Phase Diagram. *Journal of Phase Equilibria and Diffusion*, *37*(2), 162–173.

[44] **Hadef, F.** (2016). Solid-state reactions during mechanical alloying of ternary Fe-Al-X (X=Ni, Mn, Cu, Ti, Cr, B, Si) systems: A review. *Journal of Magnetism and Magnetic Materials*, *419*, 105–118.

[45] **Ikeda, O., Ohnuma, I., Kainuma, R., & Ishida, K.** (2001). Phase equilibria and stability of ordered BCC phases in the Fe-rich portion of the Fe-Al system. *Intermetallics*, *9*(9), 755–761.

[46] **Mihalkovič, M., & Widom, M.** (2012). Structure and stability of Al 2Fe and Al 5Fe 2: First-principles total energy and phonon calculations. *Physical Review B - Condensed Matter and Materials Physics*, *85*(1), 1–5.

[47] **Oki, K., Hasaka, M., & Eguchi, T.** (1973). Process of Order-Disorder Transformation in Iron-Aluminum Alloys. *Japanese Journal of Applied Physics*, *12*(10), 1522–1530.

[48] **Stoloff, N. S.** (1998). Iron aluminides: Present status and future prospects. *Materials Science and Engineering A*, *258*(1–2), 1–14.

[49] **Plazaola, F., Apiñaniz, E., & Rodriguez, D. M.** (2012). Fe-Al Alloys ' Magnetism. In M. Leszek (Ed.), *Advanced Magnetic Materials* (pp. 133–170). IntechOpen.

[50] **Yildirim, M.** (2014). *Design and Development of Iron Aluminium Intermetallic compounds for structural applications at high temperatures* (Issue December). Middle East Technical University.

[51] **Kuentzler, R., Ordering, R. K., & Physique, J. De**. (1983). *Ordering effects in the Fe-Al system To cite this version : effects in the Fe-Al system*. *44*(10), 1167–1178.

[52] **Dash, S., Lukoyanov, A. V., Knyazev, Y. V., Kuz'Min, Y. I., Baglasov, E. D., Weise, B., Kumar, P., Vasundhara, M., & Patra, A. K.** (2019). Impression of magnetic clusters, critical behavior and magnetocaloric effect in Fe3Al alloys. *Physical Chemistry Chemical Physics*, *21*(20), 10823–10833.

[53] **Sina, H., Corneliusson, J., Turba, K., & Iyengar, S.** (2015). A study on the formation of iron aluminide (FeAl) from elemental powders. *Journal of Alloys and Compounds*, *636*(December 2017), 261–269.

[54] **Vogel, S. C., Stein, F., & Palm, M.** (2010). Investigation of the ε phase in the Fe-Al system by high-temperature neutron diffraction. *Applied Physics A: Materials Science and Processing*, *99*(3), 607–611.

[55] **Stein, F., Vogel, S. C., Eumann, M., & Palm, M.** (2010). Determination of the crystal structure of the ε phase in the Fe-Al system by high-temperature neutron diffraction. *Intermetallics*, *18*(1), 150–156.

[56] **Black, P. J.** (1955). The structure of FeAl 3 . I . *Acta Crystallographica*, *8*(1), 43–48.

[57] **Black, P. J.** (1955). The structure of FeAl3. II. *Acta Crystallographica*, *8*(3), 175–182.

[58] **Il'Inskii, A., Slyusarenko, S., Slukhovskii, O., Kaban, I., & Hoyer, W.** (2002). Structure of liquid Fe – Al alloys. *Materials Science and Engineering: A*, *325*(1–2), 98–102.

[59] **Palm, M., Stein, F., & Dehm, G.** (2019). Iron Aluminides. *Annual Review of Materials Research*, *49*(1), 297–326.

[60] **John, J, T., M, S., Dubey, V., & Srinivasa, R, S.** (2014). Structural characterisation of iron aluminide coatings prepared by chemical vapour deposition. *Materials Science and Technology*, *29*(3), 357–363.

[61] **Luis, C. N.** (2008). *Study of the Structure-Properties Relationship of Fe-AL, Nb-AL and Ni-Ti Intermetallic Coatings Obtained by Thermal Spray Technologies, PhD thesis, University de Barcelona*. Universitat de Barcelona.

[62] **Cebulski, J.** (2015). Application of feal intermetallic phase matrix based alloys in the turbine components of a turbocharger. *Metalurgija*, *54*(1), 154–156.

[63] **Nachman, J. F., & Buehler, W. J.** (1956). Fe-Al-Mo alloys for high-temperature use. *Metal Progr.*, *70*.

[64] **Zhang, H., Liu, X., Jiang, Y. Gao, L., Yu, L., Lin, N., He, Y., Liu, C. T., & T., C.** (2017). Direct separation of arsenic and antimony oxides by high-temperature filtration with porous FeAl intermetallic. *Journal of Hazardous Materials*, *338*, 364–371.

[65] **Schulz, R., & Savoie, S.** (2009). A new family of high performance nanostructured catalysts for the electrosynthesis of sodium chlorate. *Journal of Alloys and Compounds*, *483*(1), 510–513.

[66] **Landis, G. A.** (2007). Materials refining on the Moon. *Acta Astronautica*, *60*(10–11), 906–915.

[67] **Lepkowski, W. J., & Holladay, J. W.** (1957). *The present state of development of iron-aluminum-base alloys*.

[68] **Deevi, S. C., & Sikka, V. K.** (1997). Exo-melt™ process for melting and casting intermetallics. *Intermetallics*, *5*(1), 17–27.

[69] **Yasuda, H. Y., Nakano, K., Nakajima, T., Ueda, M., & Umakosh, Y.** (2003). Effect of ordering process on giant pseudoelasticity in Fe3Al single crystal. *Acta Materialia*, *51*(17), 5101–5112.

[70] **Osório, W. R., Peixoto, L. C., Goulart, P. R., & Garcia, A.** (2010). Electrochemical corrosion parameters of as-cast Al-Fe alloys in a NaCl solution. *Corrosion Science*, *52*(9), 2979–2993.

[71] **Sharma, G., Singh, P. R., Sharma, R. K., Gaonkar, K. B., & Ramanujan, R. V**. (2007). Aqueous corrosion behavior of iron aluminide intermetallics. *Journal of Materials Engineering and Performance*, *16*(6), 779–783.

[72] **Kowalski, K., Łosiewicz, B., Budniok, A., & Kupka, M.** (2011). Effect of alloying on corrosion resistance of B2 FeAl alloy in aqueous solution of sulfuric acid. *Materials Chemistry and Physics*, *126*(1–2), 314–318.

[73] **Masahashi, N., Kimura, G., Oku, M., Komatsu, K., Watanabe, S., & Hanada, S.** (2006). Corrosion behavior of iron-aluminum alloys and its composite steel in sulfuric acid. *Corrosion Science*, *48*(4), 829–839.

[74] **Öncel, S.** (2013). *Alüminyum Katodik Ark Plazması ile Ni-Al Termal Bariyer Bağ Katmanlarının Üretilmesi*. Istanbul Technical University.

[75] **PalDey, S., & Deevi, S. C.** (2003). Cathodic arc deposited FeAl coatings: Properties and oxidation characteristics. *Materials Science and Engineering A*, *355*(1–2), 208–215.

[76] **Sezgin, N.** (2018). *Katodik Ark Elektron Metal İyon İşlemi ile Ni – Ti Sisteminde Difüzyona Bağlı Faz Oluşumlarının İncelenmesi*. İstanbul Teknik Üniversitesi.

[77] **Ding, Z., Hu, Q., Lu, W., Ge, X., Cao, S., Sun, S., Yang, T., Xia, M., & Li, J.** (2018). Microstructural evolution and growth behavior of intermetallic compounds at the liquid Al/solid Fe interface by synchrotron X-ray radiography. *Materials Characterization*, *136*(December 2017), 157–164.

[78] **Tuğba, Ç.** (2020). *Katodik Ark FBB Yöntemi Kullanılarak Çelik Yüzeylerin Alüminyumlanması*. İstanbul Teknik Üniversitesi.

[79] **Hirano, K., & Hishinuma, A.** (1968). Interdiffusion in α-Solid Solution of the Fe-Al System. *Journal of the Japan Institute of Metals*, *32*(6), 516–521.

[80] **NISHIDA, K., YAMAMOTO, T., & NAGATA, T.** (1971). On the interdiffusion in a-solid solution of the Fe-Al system in Al vapor. *Trans Jap Inst Metals*, *12*(5), 310–316.

[81] **Shankar Rao, V.** (2004). A review of the electrochemical corrosion behaviour of iron aluminides. *Electrochimica Acta*, *49*(26), 4533–4542.

[82] **Lai, G. Y.** (1991). High-temperature corrosion: Issues in alloy selection. *Jom*, *43*(11), 54–60.

[83] **Sykes, C., & Bampfylde, J. .** (1934). The physical properties of iron–aluminium alloys. *Journal of Iron and Steel Institute*, *130*, 389–418.

[84] **Tortorelli, P. F., & Natesan, K.** (1998). Critical factors affecting the high-temperature corrosion performance of iron aluminides. *Materials Science and Engineering A*, *258*(1–2), 115–125.

[85] **Sikka, V. K., & Viswanathan, S.** (1992). Fabrication and processing of iron aluminides. *Conference: 6. Annual Fossil Energy Materials Conference*, 195–206.

[86] **Kofstad, P.** (1988). *High temperature corrosion*. Elsevier Applied Science Publishers,.

[87] **Grabke, H. J., & Schütze, M.** (2007). Oxidation of Intermetallics. In *Oxidation of Intermetallics*.

[88] **Prescott, R., & Graham, M. J.** (1992). The oxidation of iron-aluminum alloys. *Oxidation of Metals*, *38*(1), 73–87.

[89] **McKamey, C. G.** (1990). *Proceedings of the Fourth Annual Conference on Fossil Energy Materials*.

[90] **Strafford, K. N., & Datta, P. K.** (1989). Design of sulphidation resistant alloys. *Materials Science and Technology (United Kingdom)*, *5*(8), 765–779.

[91] **Strafford, K. N., & Manifold, R.** (1969). The scaling behavior of an iron-5% aluminum alloy in sulfur vapor. *Oxidation of Metals*, *1*(2), 221–240.

[92] **Setterlund, R. B., & Prescott, G. R.** (1961). Corrosion Characteristics of Iron-Aluminum And Iron-Chromium-Aluminum Alloys In High Temperature Petroleum Applications. *Corrosion the Journal of Science and Engineering*, *17*(6), 277–282.

[93] **Gesmundo, F.** (1994). *Materials for Advanced Power Engineering* (D. Cousouradis (ed.)). Kluwer Academic Publishers.

[94] **DeVan, J. H.** (1988). *Oxidation Sehavior of High-Temperature Intermetallics* (T. Grobstein & J. Doychak (eds.)). The Materials, Metals and Minerals Society.

[95] **Klöwer, J.** (1996). High temperature Corrosion behaviour of iron aluminides and iron-aluminium-chromium alloys. *Materials and Corrosion*, *47*(12), 685–694.

[96] **Strauß, S., Krajak, R., Palm, M., & Grabke, H. J.** (1996). Metal dusting of Fe3Al and (Fe,Ni)3Al. *Materials and Corrosion*, *47*(12), 701–702.

[97] **Natesan, K., & Johnson, R. .** (1995). *Heat-resistant Materials II* (K. Natesan, P. Ganesan, & G. Lai (eds.)). ASM International.

[98] **Saunders, S. R. J., Gohil, D. D., Banks, J. P., Sheriff, M. U., Tortorelli, P. F., De Van, J. H., & Wright, I. G.** (1997). Behaviour of Fecralloy and Iron Aluminides Alloys in Coal Gasification Atmospheres Containing HCI. *Materials Science Forum*, *251–254*, 583–590.

[99] **Kung, S. C., & Bakker, W. T.** (1998). Effects of Sulfur and Chlorine on Furnace Wall Corrosion. In *CORROSION 98* (p. 12). NACE International.

[100] **Gleeson, B., Cheung, W. H., Costa, W. Da, & Young, D. J.** (1992). The hot-corrosion behavior of novel CO-deposited chromium-modified aluminide coatings. *Oxidation of Metals*, *38*(5), 407–424.

[101] **Van Weele, S., & Blough, J. L.** (1991). *Fireside corrosion testing of candidate superheater tube alloys, coatings, and claddings*.

[102] **Tortorelli, P. ., & Bishop, P. .** (1991). *Influnces of compositional modifications on the corrosion of iron aluminides by molten nitrate salt*.

[103] **García-Alonso, M. C., Lopez, M. F., Escudero, M. L., González-Carrasco, J. L., & Morris, D. G.** (1999). Corrosion behaviour of an Fe3Al-type intermetallic in a chloride containing solution. *Intermetallics*, *7*(2), 185–191.

[104] **Shankar Rao, V.** (2004). Repassivation behaviour and surface analysis of Fe 3Al based iron aluminide in 0.25 M H2SO4. *Corrosion Science*, *47*(1), 183–194.

[105] **Milam, E. E., Crow, W. B., & Myers, J. R.** (1977). Anodic Polarization of Iron Aluminum Alloys in Sulfuric Acid Solutions. *Corrosion Nace*, *33*(7), 240243.

[106] **Frangini, S., De Cristofaro, N. B., Lascovich, J., & Mignone, A.** (1993). *On the passivation characteristics of a β-FeAl intermetallic compound in sulphate solutions*. *35*, 153–159.

[107] **Shankar Rao, V., Baligidad, R. G., & Raja, V. S.** (2002). Effect of carbon on corrosion behavior of Fe3Al intermetallics. *Corrosion Science*, *44*(3), 521–533.

[108] **Luu, W. C., & Wu, J. K.** (2001). Influence of aluminium content on retarding hydrogen transport in Fe-Al binary alloys. *Corrosion Science*, *43*(12), 2325–2333.

[109] **Nişancioğlu, K.** (1990). Electrochemical behavior of aluminum-base intermetallics containing iron. *Journal of the Electrochemical Society*, *137*(1), 69–77.

[110] **Huape-Padilla, E., Sánchez-Carrillo, M., Flores-de los Rios, J. P., Espinosa-Medina, M. A., Bautista-Margulis, R. G., Ferrer-Sánchez, M. I., Carbajal-de la Torre, G., Bejar-Gómez, L., Chacón-Nava, J. G., & Martínez-Villafañe, A.** (2015). Corrosion study of Fe-Al intermetallic alloys in simulated acid rain. *International Journal of Electrochemical Science*, *10*(3), 2141–2154.

[111] **Frangini, S., & Lascovich, J.** (1995). *AC Impedance Intermetallic Study of Passive B2 FeAl*. *40*(5), 637–642.

[112] **Seri, O.** (1994). The effect of NaCl concentration on the corrosion behavior of aluminum containing iron. *Corrosion Science*, *36*(10), 1789–1803.

[113] **Ahledel, N.** (2018). *Corrosion Resistance and Electrochemical Behavior of Fe3Al Intermetallic Matrix Composites Reinforced by TiC*. Universitie Laval.

[114] **Choe, H. C., Kim, H. S., Choi, D. C., & Kim, K. H.** (1997). Effects of alloying elements on the electrochemical characteristics of iron aluminides. *Journal of Materials Science*, *32*(5), 1221–1227.

[115] **Birbilis, N., & Buchheit, R. G.** (2005). Electrochemical characteristics of intermetallic phases in aluminum alloys : An experimental survey and discussion. *Journal of the Electrochemical Society*, *152*(4), 140–151.

[116] **Defrancq, J. N.** (1977). Cast Iron with High Al-Content in Sulfuric Acid. *Materials and Corrosion*, *28*(7), 480–483.

[117] **Flores-Chan, J. E., Torres-Islas, A., Patiño-Carachure, C., Rosas, G., & Espinosa-Medina, M. A.** (2016). Corrosion study of Al-Fe (20 wt%) alloy in seawater alkaline solutions. *International Journal of Electrochemical Science*, *11*(9), 7359–7369.

[118] **Choi, Y. S., & Kim, J. G.** (2002). Investigation of passivity and its breakdown on Fe3Al-Cr-Mo intermetallics in thiosulfate-chloride solution. *Materials Science and Engineering A*, *333*(1–2), 336–342.

[119] **Flores-Chan, J. E., Torres-Islas, A., Patiño-Carachure, C., Rosas, G., & Espinosa-Medina, M. A.** (2016). Corrosion study of Al-Fe (20 wt%) alloy in seawater alkaline solutions. *International Journal of Electrochemical Science*, *11*(9), 7359–7369.

[120] **López, M. F., & Escudero, M. L.** (1997). Corrosion behaviour of FeAl-type intermetallic compounds. *Electrochimica Acta*, *43*(7), 671–678.

[121] **Nigam, A. K., Balasubramaniam, R., Bhargava, S., & Baligidad, R. G.** (2006). Electrochemical impedance spectroscopy and cyclic voltammetry study of carbon-alloyed iron aluminides in sulfuric acid. *Corrosion Science*, *48*(7), 1666–1678.

[122] **Arrieta-Gonzalez, C. D., Porcayo-Calderon, J., Salinas-Bravo, V. M., Gonzalez-Rodriguez, J. G., & Chacón-Nava, J. G.** (2011). Electrochemical behavior of Fe3Al modified with Ni in Hank's solution. *International Journal of Electrochemical Science*, *6*(9), 4016–4031.

[123] **Frangini, S., Giorgi, R., Lascovich, J., & Mignone, A.** (1994). XPS study of passive films formed on an iron—aluminium intermetallic compound in acid solution. *Surface and Interface Analysis*, *21*(6-7), 435–441.

[124] **Defrancq, J. N.** (1976). The corrosion behaviour of Al-cast iron in sulfuric acid. *Materials and Corrosion*, *320*, 315–320.

[125] **Escudero, M. L., García-Alonso, M. C., Gonzalez-Carrasco, J. L., Muñoz-Morris, M. A., Montealegre, M. A., Oca, C. G., Morris, D. G., & Deevi, S. C.** (2003). Possibilities for improving the corrosion resistance of Fe-40Al intermetallic strip by prior oxide protection. *Scripta Materialia*, *48*(11), 1549–1554.

[126] **Nachman, J. F., & Duffy, E. R.** (1974). Effect of Alloying Additions on Sea Water Corrosion Resistance of Iron-Aluminum Base Alloys. *Corrosion*, *30*(10), 357–365.

[127] **Osório, W. R., Peixoto, L. C., Goulart, P. R., & Garcia, A.** (2010). *Electrochemical corrosion parameters of as-cast Al – Fe alloys in a NaCl solution*. *52*, 2979–2993.

[128] **García-Alonso, M. C., Lopez, M. F., Escudero, M. L., González-Carrasco, J. L., & Morris, D. G.** (1999). Corrosion behaviour of an Fe3Al-type intermetallic in a chloride containing solution. *Intermetallics*, *7*(2), 185–191.

[129] **Shankar Rao, V., & Raja, V. S.** (2003). Anodic polarization and surface composition of Fe-16Al-0.14C alloy in 0.25 M sulfuric acid. *Corrosion*, *59*(7), 575–583.

[130] **Brito, P., Schuller, É., Silva, J., Campos, T. R., Araújo, C. R. de, & Carneiro, J. R.** (2017). Electrochemical corrosion behaviour of (100), (110) and (111) Fe3Al single crystals in sulphuric acid. *Corrosion Science*, *126*(August), 366–373.

[131] **De Cristofaro, N., Frangini, S., & Mignone, A.** (1996). Passivity and passivity breakdown on a β-FeAl intermetallic compound in sulphate and chloride containing solutions. *Corrosion Science*, *38*(2), 307–315.

[132] **McCafferty, E.** (2010). Thermodynamics of corrosion: Pourbaix diagrams. In *Introduction to Corrosion Science* (pp. 95–117). Springer.

[133] **Vargel, C.** (2004). Corrosion of Aluminium. In *Corrosion of Aluminium*. Elsevier.

[134] **Cabrera, N., & Mott, N. F.** (1949). Theory of the oxidation of metals. *Reports on Progress in Physics*, *12*(1), 163–184.

[135] **Sato, N., & Cohen, M.** (1964). The Kinetics of Anodic Oxidation of Iron in Neutral Solution. *Journal of The Electrochemical Society*, *111*(5), 519.

[136] **Balasubramaniam, R.** (1996). On the role of chromium in minimizing room temperature hydrogen embrittlement in iron aluminides. *Scripta Materialia*, *34*(1), 127–133.

[137] **Wolff, I. M., Iorio, L. E., Rumpf, T., Scheers, P. V. T., & Potgieter, J. H.** (1998). Oxidation and corrosion behaviour of Fe–Cr and Fe–Cr–Al alloys with minor alloying additions. *Materials Science and Engineering: A*, *241*(1), 264–276.

[138] **Fan, D. W., & De Cooman, B. C.** (2012). State-of-the-knowledge on coating systems for hot stamped parts. *Steel Research International*, *83*(5), 412–433.

[139] **Cho, Y.-R., Tai-Ho, K., Sung-Ho, P., & Eung-Ryul, B.** (2010). *Aluminum-Plated Steel Sheet Having Superior Corrosion Resistance, Hot Press Formed Product Using the Same, and Method for Production Thereof* (Patent No. US 20220300407A1).

[140] **Fan, D. W., & De Cooman, B. C.** (2010). Formation of an aluminide coating on hot stamped steel. *ISIJ International*, *50*(11), 1713–1718.

[141] **Fleischanderl, M., Kolnberger, S., Faderl, J., Landl, G., Raab, A.-E., & Brandstatter, W.** (2007). *Method for Producing a Hardened Steel Part* (Patent No. US 20070256808A1).

[142] **Çelikel, T., Kacar, E., Ürgen, M., & Çelikel, Q. T.** (2019). Aluminising of steel with a cathodic arc plasma based method. *Transactions of the IMF*, *97*(3), 140–145.

[143] **American Society for Testing and Materials**. (2014). Standard Reference Test Method for Making Potentiodynamic Anodic Polarization Measurements. *Annual Book of ASTM Standards*, *December 2014*, 1–9.

[144] **Khalifeh, A.** (2020). Stress Corrosion Cracking Behavior of Materials. In K. Thanapala (Ed.), *Engineering Failure Analysis* (Vol. 15, Issue 1, p. 13). IntechOpen.

[145] **Kim, J. G.** (1995). Stress corrosion cracking susceptibilities of Fe3Al-based iron aluminides. *Metals and Materials*, *1*(2), 133–141.

CURRICULUM VITAE

Name Surname : Burcu EROĞLU

Place and Date of Birth :

E-Mail :

EDUCATION :

- **B.Sc.** : 2018, Istanbul Technical University, Faculty of Chemical and Metallurgical Engineering, Metallurgical and Materials Engineering
- **M.Sc.** : 2021, Istanbul Technical University, Graduate School, Materials Engineering